Design and Development of Microwave Patch Antennas using Conductive Polymers

By

Akhilesh Verma

B.E. (Electronics and Telecommunication)
University of Jabalpur, India, 1988

M.Tech (Radar and Communication Engineering)
Indian Institute of Technology, New Delhi, India, 1996

Thesis submitted for the degree of

Doctor of Philosophy

THE UNIVERSITY OF ADELAIDE
AUSTRALIA

The School of Electrical and Electronics Engineering,
The Faculty of Engineering, Computer and Mathematical Sciences
The University of Adelaide, Australia

Aug 2011

Dedicated to my parents

Abstract

Recent advances in the electrical conductivity levels of Conducting Polymers (CP) and impressive improvements in their stability are making these materials very attractive potential alternatives to copper in planar antennas. This is particularly so in applications where light weight, inexpensive and/or wearable/conformal antennas are a consideration. There have been isolated efforts in the past towards using CP as material for antenna and transmission line design. This thesis endeavours to provide a systematic study of key factors that are important for the understanding of these materials, their design and simulation as basis material for building microwave antennas.

The thesis could be considered as made up of two parts. The first part (Chapter 2 and Appendix A) presents a mathematical model of electrical conduction and permittivity in CPs as a function of dopant concentration and frequency. The electrical conduction and permittivity are very dispersive for these materials primarily due to different relaxation times exhibited by the conduction electrons. This part also develops closed-form expressions formulas for rapid estimation of the effective permittivity of microstrip lines on multi-layer substrates. A 2D finite element eigen-mode analysis leading to the effective permittivity for two and three layer microstrip line structures is used as a reference solution and successfully validates the closed-form expressions.

The second part (Chapter 3 and 4) presents the design, simulation and fabrication of microwave antennas using thin CP films. Results on CP based microstrip patch antennas operating at 2 GHz, 4.5 GHz and 6 GHz are presented. This part also presents a systematic study on the impact of CP film thickness, conductivity and fabrication method on antenna performance. An indirect method for determination of the permittivity of non-standard RF substrates and detection of dispersion in the electrical conductivity of CP film has been demonstrated. This part validates the possibility of using CPs as microwave antennas and gives credence to many possibilities in the field of conformal antennas, wearable antennas, sports and medical applications.

The thesis is concluded in chapter 5 by summarising the results and presenting some exciting possibilities that these exotic materials open for future applications in the field of antenna applications.

Declarations

This work contains no material which has been accepted for the award of any other degree or diploma in any university or other tertiary institutions to **Akhilesh Verma** and, to the best of my knowledge and belief, contains no material previously published or written by another person, except where due reference has been made in the text.

I give consent to this copy of my thesis when deposited in the University Library, being made available for loan and photocopying, subject to the provisions of the Copyright Act 1968.

The author acknowledges that copyright of published works contained within this thesis (as listed under publications in this thesis*) resides with the copyright holder(s) of those works.

I also give permission for the digital version of my thesis to be made available on the web, via the University's digital research repository, the Library catalogue and also through web search engines, unless permission has been granted by the University to restrict access for a period of time.

Date: **Aug 2011**

_____

(**Akhilesh Verma**)

Place: **Adelaide**

Acknowledgements

I would like to thank my Supervisor, Professor Bevan D. Bates for his support, guidance and encouragement throughout this work. I am deeply indebted to the efforts of my external supervisor Dr Leigh Powis towards reviewing my work and navigating me through this beautiful experience of research. I cannot present this work without thanking enough, Associate Professor Christophe Fumeaux for his critical review of my ideas and the discussions that helped improve my understanding of microwave devices and antennas.

I would like to thank Defence Science and Technology Organisation (DSTO) and the School of Electrical and Electronics Engineering, University of Adelaide for supporting my research endeavours. I am grateful to these organisations for providing me with a scholarship and the facilities of laboratory and workshop. It goes without saying that this work could not have been completed without the great work environment provided at the Centre for Expertise in Phased Array and Microwave Radar (CEPAMiR). I would also like to thank my fellow “postgrads”, who provided the support when you most needed it. I will miss the discussions on almost everything under the sun in the “postgrad” room.

I would like to thank my wife Dr Roopali Verma and my son Anush Verma; whose constant faith in me and support when the chips were down will ever remain embossed in my memory. I feel blessed to have such a loving and supportive family.

Last but not least I would like to thank Mrs Rashmi Bhansali for ensuring that I complete my thesis and not leave it for the elves to complete. Rashmi is one of the unsung heroes of this thesis whose contribution will ever remain etched in my heart and hidden deep inside the pages of this thesis.

Akhilesh Verma

Aug 2011

Publications

Verma, A. and Bates, B. D.; "Microstrip patch antenna with polypyrrole ground plane," in 2008 *International Conference on Radar*, Adelaide, SA, Australia, 2008, pp. 424-429.

Verma, A., Fumeaux, C., Truong, Van-Tan; Bates, B.D.; "A 2 GHz Polypyrrole microstrip patch antenna on Plexiglas™ substrate," in 2009 *Asia Pacific Microwave Conference, APMC 2009.*Singapore, pp.36-39.

Verma, A., Fumeaux, C., Bates, B.D; "Modified Getsinger's model for accurate determination of effective permittivity dispersion in multilayered microstrip lines," in 2010 *International Conference on Electromagnetics in Advanced Applications (ICEAA)*, Sydney, Australia 2010, pp.325-328.

Verma, A., Weng, B., Shepherd, R., Fumeaux, C., Truong, Van-Tan, Wallace, G. G., Bates, B. D., "6 GHz microstrip patch antennas with PEDOT and polypyrrole conducting polymers," in 2010 *International Conference on Electromagnetics in Advanced Applications (ICEAA)*, Sydney Australia 2010, pp.329-332.

Verma, A., Fumeaux, C., Truong, Van-Tan, Bates, B.D.; "Effect of Film Thickness on the Radiation Efficiency of a 4.5 GHz Polypyrrole Conducting Polymer Patch Antenna," in 2010 *Asia Pacific Microwave Conference, APMC 2010.*Yokohama, Japan pp.95-98.

Contents

List of Figures

List of Tables

List of Symbols

ϕ	Concentration in inclusions (dopants)
ϕ_c	The critical concentration at percolation threshold
ω_p	Plasma frequency
f	Frequency
ϵ	Complex permittivity
ε'	Real part of permittivity
ε''	Imaginary part of permittivity
$\boldsymbol{\tau}$	Relaxation time
$\boldsymbol{\varepsilon_\infty}$	permittivity at very high frequency
$\boldsymbol{\varepsilon_0}$	static permittivity (at frequency=0)
$\sigma_{AC}(\omega)$	Electrical AC conductivity
σ_{DC}	Electrical DC conductivity
ε^*	Complex permittivity ($\varepsilon^* = \varepsilon' - i\varepsilon''$)
E_0	Peak applied electric field
γ	Propagation Constant
δ	Skin depth
e	Electronic Charge
g	The transmission coefficient of chain-links across grains
$N_\perp$	N perpendicular chains
$N_\parallel$	N parallel chains
z	Number of nearest neighbouring grains

R	The mean distance between neighbouring grains
g_c	Critical transmission coefficient
$\tan\delta$	Loss tangent
ϵ_s	The relative dielectric constant of a single layered dielectric in a Microstrip transmission line
ϵ_{e0}	The quasi-static effective dielectric constant
q	The effective filling fraction of the dielectric material
ϵ_{seq}	The equivalent relative dielectric constant
Z_0	Characteristic impedance
η_0	Free space impedance
Z_{0i}	Characteristic impedance of i^{th} layer
ξ	The crystalline domain coherence length

Glossary

List of Acronyms

BW	Band width
CP	Conducting Polymer
CCP	Conjugated Conductive Polymer
CPC	Conductive Polymer Composites
CSA	Camphor Sulphonic acid
EM	Electromagnetic
EMI	Electromagnetic Interference
FSS	Frequency selective surfaces
GEM	General Effective Media
ICP	Intrinsically Conductive Polymers
IMT	Insulator-Metal transition
LSE	Longitudinal Section Electric
MPA	Microstrip Patch Antenna
OEM	Original Equipment Manufacturer
OPC	Organic Polymers Conductors
PA	Polyacetylene
PANi	Polyaniline
PEC	Perfect Electric Conductor
PMC	Perfect Magnetic Conductor
PML	Perfectly Matched Layer

PMT	Poly3-methylthiophene
PPy	Polypyrrole
PSS	Polystyrene Sulphonic acid
PT	Polythiophenes
PU	Polyurethane
PVS	Polyvinyl Sulphonic acid
RF	Radio frequency
RT	Room temperature
SEM	Scanning Electron Microscope
SLR	Single Layer Reduction
SPDR	Split Post Dielectric Resonator
TL	Transmission Line
TR	Transverse Resonance
UDM	Unified Dispersion Model
VLT	Visual Light Transmission

Scope of Thesis

The scope of this thesis is bounded in terms of materials defined as conducting plastics, mechanism of conductivity in such materials and the models ascribed to simulate the conduction mechanism in these materials. This work will not be dwelling in depth into molecular structure of CPs at the quantum level. However, different models for describing conductivity and permittivity variation are discussed in brief in chapter 2. Following salient points defining the scope of this thesis are as follows:

- ❖ A number of materials which are conductive do not necessarily fall in the category of CPs and these are excluded from the scope of this work. Some of such excluded materials are :

  - ➢ Metallo-phthalocyanines (such as copper or cobalt-phthalocyanines etc)

  - ➢ Tetrathiafulvalene/ Tetracyanoquinodimethanide (TTF/TCNQ); such charge-transfer materials that are based on donor-acceptor complexes.

  - ➢ Polysilanes. These materials are quite similar to CPs in properties such as conductivity and non-linear optical properties. They differ essentially in their conjugation structure. They are σ based rather than π based in the case of CPs.

  - ➢ Ion Conductive Polymers; such as Polyethylene oxide impregnated with $LiClO_4^-$ cations. These materials find application as solid electrolyte in dry cells and the mechanism of conduction is through ion exchange process.

  - ➢ Organic polymers such as$(SN)_x$, Polythiazyl. They are very conductive at room temperature (RT) and become super

conductive at temperatures below 0.26^{0}K. The conductivity in these materials is highly directional and is mostly along the polymer chain.

- Polymer materials with conductive fillers such as graphite or metallic powder for introducing conductivity in otherwise non-conductive polymer.

❖ No effort is made in this work to present models for depicting other (physical or chemical) properties of CPs (such as environmental stability, temperature, aging, thermal conduction etc.) and describing a detailed account of the quantum mechanism for observed conductivity in CPs. Further, the research in this work is also constrained to Polypyrrole and PEDOT CPs due to ease of availability and inherent stability of these materials over other CPs such as PA, PT etc.

Chapter 1

Introduction

Interest in Conducting Polymers (CPs) was "jump started" in 1977, with some excellent results reported on electrical conductivity observed in these materials by Shirakawa et al. [1] . A *Doped* Polyacetylene (PA), a type of Conducting Polymer (CP) was used by Shirakawa et al. [1] . This finding opened the flood gates for some very interesting discoveries and inventions into a new domain of materials, whose optical, electrical and mechanical properties could be manipulated in real time. Shirakawa and his team were later awarded the Nobel Prize in chemistry in 2000 for their ground breaking contribution to this exciting new field of exotic materials.

Ever since then, higher and higher levels of conductivities at Room Temperature (RT) are being reported in different types CPs, which are also popularly known as "Conducting Plastics". The interesting feature of CP is that their electrical conductivity (and also electrical permittivity) could be transformed from insulating to metallic and vice versa through the process of electro-chemical doping. This process leads to many different Radio Frequency (RF) applications.

The motivation of this research in very broad terms is to develop considerable understanding of using CP material in microwave antennas. This research is a baseline study for understanding, both the peculiar properties of CPs and also the fabrication issues associated with using it in microwave antennas. This research also lays the foundation for, and validates the modelling of, thin film patch antennas made of CPs using Electromagnetic (EM) simulation software such as CST™ [2] and HFSS™ [3] which would immensely help in exploring the potential of CPs as microwave antennas. This research also focuses on the effect of different fabrication techniques of CPs

on its performance as microwave antennas. The impact of film thickness on antenna performance in conjunction with CP film conductivity needs deeper analysis and understanding. Motivation is also derived from the following questions: how low conductive can a CP film could be or how thin can the CP film could be before no appreciable impact on antenna performance is registered.

Development of re-configurable planar antennas by exploiting the Insulator-Metal Transition (IMT) in CPs could be explored based on the work presented in this research. Re-configurable antennas would provide the possibility of controlling antenna characteristics such as gain, directivity and bandwidth etc. on a real time basis. This research also provides the theoretical basis for developing optically transparent antennas. It also throws open numerous possibilities for developing hybrid antennas and conformal antennas using CPs.

1.1 Introduction to Conducting Polymers

1.1.1 What are Polymers and Conducting Polymers?

Polymers are defined as large chains of repeated carbon-based units that are generally covalently bonded together to form very large molecules. Polymers could be both organic and inorganic in nature and are generally non-conductive. In popular usage, the term “Polymers” is also associated with manmade plastics such as ‘Polyethylene’ or ‘Polyethene’. Some well known naturally occurring polymers are proteins and DNA. Common organic polymers and plastics such as Polyethylene, Polyvinyl Chloride, Polyester, etc. are highly insulating.

In contrast, CPs are polymer materials that exhibit both electrical and thermal conductivity. This property of electrical and thermal conduction is possibly associated with polymer back bone (chain) being impregnated with highly conductive metals or carbon particles. CPs are also referred in literature and commercially as Conjugated Conductive

Polymer (CCP) or Organic Polymers Conductors (OPC) or as Intrinsically Conductive Polymers (ICPs).

Conductivity in CPs is achieved through oxidation and reduction reactions along the polymer back bone. The oxidation and reduction reactions also referred to as ‘Redox’ reactions and are generally conducted electrochemically. Certain anionic or cationic species (or ions) are inserted into the polymeric chain as “dopants”. These impurities cause either oxidation or reduction of the polymeric chain and results in formation of charge centres, which in turn contribute towards the observed conductivity in CPs. The conductivity observed in the CPs is associated with delocalized conjugation due to overlapping of π-electrons in the molecular structure of the polymer molecule [4].

A number of CPs are now popular and have been studied in detail for their properties and possible applications in very diverse engineering disciplines. Some of the CPs are Polyacetylene, Polythiophenes, Polyaniline (PANi), Polypyrrole (PPy), Poly3-methylthiophene (PMT) or PEDOT.

1.1.2 Development of Conducting Polymers over the decades

The earliest reference to CP through oxidative polymerisation is attributed to Letheby in 1862 by Chandrasekhar [4]. This reference further reports that Pyrrole also known as “Pyrrole black” was obtained from spontaneous polymerisation in air and was studied in detail as far back as in 1916. The conductivity of these and subsequent CPs was very low and were often termed as “dirty metals”.

Since 1957, studies on electro-chemical oxidation of aromatic monomers have been reported in the literature as “electro-organic preparations” and/or as “electro-oxidations”. In around 1967, CPs such as Polypyrrole (PPy), Polythiophenes (PT) and Furan were characterized for their electrical conductivity and properties. During this period, literature also reports observations made on Polyaniline (PANi) conductivity.

Many material scientists today are of the opinion that recent interests in CPs are essentially a revisit to already discovered conducting polymers. However, on the issue of “resurgence of interest”, most unanimously agree that it is because of the works of Shirakawa, Heeger, and others that contributed extensively to this field over the following decades. Shirakawa et al. [1] reported very high conductivity in Polyacetylene when exposed to iodine vapours. This cleared a way for creating conductive organic materials; a new field of science with wide applications. In recognition to this ground breaking work, Shirakawa et al. [1] were awarded the 2000 Nobel Prize for chemistry. Chandrasekhar [4] is of the opinion that CP field also received an impetus due to the efforts of the Diaz group at IBM [5, 6].

Amongst all the CPs, Polyacetylene is one of the most studied CPs. Interest in this polymer at present is more academic in nature. Commercial or application oriented interests in this CP have steadily declined due to its inherent chemical instability in air and humidity in the environment. In contrast, interest in other CPs such as Polyaniline,

PPy and Polythiophenes are still alive. In the recent past considerable work has been reported using these CPs in various fields, details of which are presented later in this chapter and also elsewhere in the thesis.

1.1.3 Types of Conducting Polymers

The common electronic feature of un-doped ("pristine") CPs is the conjugated π system, formed by the overlapping carbon P_x orbitals and having alternating carbon-carbon bond lengths as shown in figure 1.1.

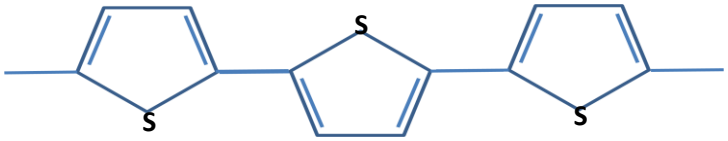

Polythiophene

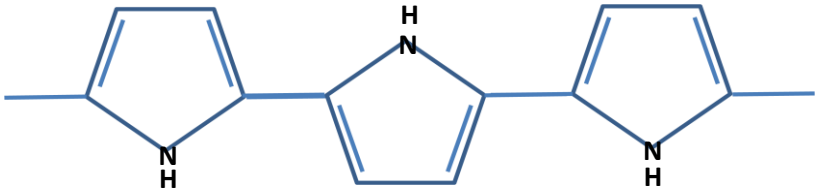

Polypyrrole

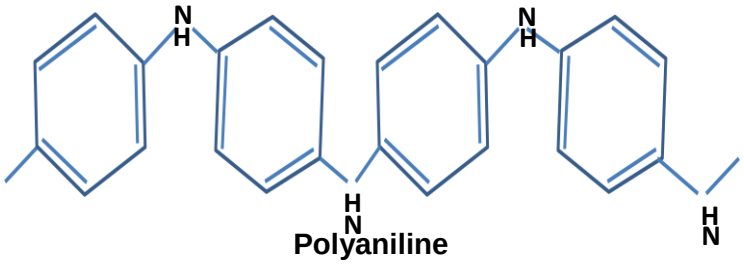

Polyaniline

Polyacetylene

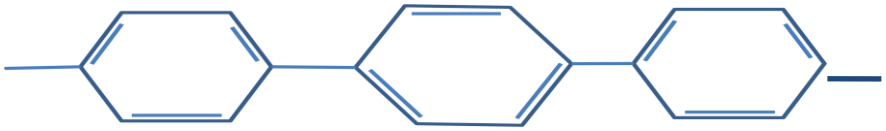

Polyphenylene

Figure 1.1: Chemical structure of some Conducting Polymers

Freund and Deore in their book on self doped CPs [7] state that *"Electronically CPs possess a variety of properties related to their electrochemical behaviour and are therefore active materials whose properties can be altered as a function of their electrochemical potential."* Post the Shirakawa et al. [1] discovery of conductivity in PA, it was found that this sort of analogous behaviour could be introduced in polymers through doping with electron donors (*n*-type dopants). Joo et al. [8] indicates that there is a fundamental difference between semi-conductors and CPs. The semi-conductors have three dimensional (3D) structures; while the morphological unit of CP is a quasi one dimensional (1D) conjugated polymer chain. This chain has covalent bonding along the chain but considerably weak bonding between chains. Further, the dopant ions in CPs are positioned interstitially between polymer chains, while in the case of semiconductors, the dopant is substituted directly in the lattice structure. Manipulation of electronic nature of CPs through introduced dopants lead to an explosion in research activity in a wide range of fields from electronics to medicine.

CPs are often categorised into "Conducting Polymer Composites" (CPC), "Redox polymers", "Ionically" CPs (such as polymer-salt electrolytes; more popularly known as "solid electrolytes") and "doped conjugated polymers" or "Intrinsically CPs" (ICP). Freund et al. [7] defines an ICP as *"An organic polymer that possesses the electrical and optical properties of a metal while retaining its mechanical properties and process ability is an ICP".* The electrical conductivity of a doped CP is distinctly above insulators and semiconductors. It is in fact in the realm of common metals and that is why ICPs are also referred to as "synthetic metals". The common feature of most ICPs is the presence of alternating single and double covalent bonding in its polymer chain. The delocalization or mobility of π-bounded electrons, (which is considered to be responsible for electrical conduction in ICPs), is attributed to this feature (i.e.

alternating single and double covalent bonding) of the ICP polymer chain. This arrangement of the ICP is known to exhibit some very unusual electronic properties such as: low ionization potential, low energy optical transitions, and high electron affinities. ICPs are readily oxidized and reduced at relatively low potentials and interestingly the redox process is reversible.

ICPs are conducting as a consequence of redox reaction between the conjugated semiconducting polymer and an oxidizing or reducing agent, or a protonic acid. This reaction results in delocalization of poly-cations and poly-anions which contribute towards electrical conductivity. The overall conductivity of these materials can be tuned by chemical manipulation of the polymer backbone, by the nature of the dopant, by the degree of doping and by blending with other polymers.

Commercially, ICPs are provided by a number of companies. For example Zipperling Kesseler & Co. [9] produces polyaniline powder suspensions under the name ‘Ormecon’. This product has now been taken over by Enthone, [10]. In Germany Bayer Corporation [11] make a highly transparent and stable poly(3,4-ethylendioxythiophene) PEDOT with variable conductivity under trade name ‘Baytron’, Agfa [12] make conductive coatings of PEDOT (with trade name ‘Orgacon’) on PET or Polyester substrate.

CPCs, in contrast are typically a physical mixture of non-conductive polymer and a conducting material (such as a metal or carbon powder etc. also called as “fillers”) that is distributed uniformly throughout the solution. In some very early experiments for developing CPCs conductive materials such as conductive carbon blacks, short graphite fibres, metal coated glass fibres, and metal particles (or flakes or filings) were mixed (or inserted) in the non-conductive matrix of polymers. The electrical conductivity through such a system of non-conducting and conducting mixture is best described by “percolation

theory". This theory describes the movement of electrons through the metallic phases and the variation in conductivity σ due to variation in dopant concentration in the mixture. A more detailed discussion on this theory is presented subsequently in chapter 2. Despite CPCs attractiveness as a highly conductive composite, it suffers from some inherent drawbacks such as: (i) the composite becomes mechanically unstable when loaded heavily with conducting particles; (ii) an insulating layer is very often formed on the conducting particles and (iii) the overall conductivity of CPC is highly dependent upon the processing conditions. Recent advances in CPCs, particularly with reference to making blends with ICPs are very promising since they impart improved process ability and mechanical properties to CPCs.

Unlike "Conjugated Conducting Polymers" (CCP), redox polymers have localized redox sites on the conjugated π-system. In redox polymers the transport of electrons is through hopping or self-exchange between donor and acceptor sites. The conductivity of redox polymers is lower than that observed in CCP due to slower electron transport or exchange between donor and acceptor sites. More recently, hybrids formed with CCP and redox polymers are attracting more interest. The main feature of this class of CPs is that a metal is directly coordinated or linked to the conjugated backbone of the polymer. This contributes immensely towards increased electronic interaction between electro active metal centres and electro active polymer backbone.

1.1.4 A Brief on "Doping" in Conducting Polymers

Doping of CP depends on injecting charge onto conjugated, semiconducting molecular chains. This process of injecting compatible charge carriers is in fact erroneously called as 'doping'. A number of different methods have been explained by Heeger [13, 14] for achieving this, such as:

(a) Chemical doping consists in doping of the polymeric chain with redox reactions. This method suffers from the problem that once initiated, the process of doping cannot be controlled. The chemical as well as the electro-chemical doping process through redox reaction leads to a charged CP. The accumulated charge remains de-localized over several monomer units in the CP. These charges also cause relaxation of geometry of the polymer. Schematic electro-chemical reactions are represented below:

$PPy + MClO_4 \rightarrow (PPy)^+ClO_4^- + M^+ + e^-$ (oxidation reaction)

$PA + NaA \longrightarrow Na^+PA^- + A^-$ (reduction reaction)

where M is a cation and A is an anion.

Typical dopants used as chemical redox agents are listed in the Table 1.1. Dopants could be small ionic species or large polymer molecules such as the "poly electrolytes" (Polystyrene Sulfonic Acid (PSS) and Polyvinyl sulfonic acid (PVS)). An undoped polymer is called as *"Pristine"* polymer. The concentration of dopant used in a CP is indicated as either volume fraction or in terms of molar concentration. Due to various constraints with polymers, 100% (1:1) concentration of dopant is not possible. Some of the maximum concentrations levels achieved in CPs is listed in Table 1.2.

Table 1.1 : Typical CP Dopants

Dopant	**Formula**
Anionic:	
Chloride	Cl^-
Perchlorate	ClO_4^-
Tetrafluoroborate	BF_4^-
Tos, p-toulene sulfonate	$CH_3\text{-}C_6H_5\text{-}SO_3^-$
Trifl, trifluoromethane sulfonate	$CF_3SO_3^-$

Hexafluorophosphate	PF_6^-
Polystyrene Sulphonate (PSS)	$[-CH_2CH(C_6H_4SO_3)-]_n^{n-}$
Cationic:	
Proton	H_3^+O
Sodium	Na^+

Table 1.2 : Maximum Doping levels (Typical) in CPs

Polymer	Maximum Doping Level (of Dopant)
Polypyrrole (PPy)	33% (ClO_4^-)
Polythiophene	30% (ClO_4^-); 6% (PF_6^-)
Polyaniline (PANi)	42% (Cl^-)
Poly (p-phenylene)	44% (Li^+)

CPs can also be synthesized in a doped condition or alternatively may also be doped from their "pristine" state to a highly doped state through exposure to dopant solution or vapour (such as Iodine or HCl vapour). The change in conductivity due to doping process is permanent and can not be reversed.

(b) Electrochemical doping: Electrical doping allows for achieving intermediate levels of doping. Both chemical and electrochemical doping processes are redox reactions. In electrochemical doping, the electrode supplies the redox charge to the CP, while ions diffuse into (or out of) the polymer structure from the nearby electrolytic solution to compensate the electronic charge. This process of doping is reversible.

In the electro-chemical synthesis process, the radical cations are in far larger concentration at the electrode than the neutral monomers. The seat of generation of dimmer radical cations as a result of radical-radical interaction is at

the electrodes. The effects of this then propagate along the polymer chains. This method is considered to be widely accepted cause of conductive polymerization.

The doping level is determined by the voltage difference between CP and the counter electrode. This voltage difference allows for controlling the depth of doping in the CP. This type of redox reaction follows the well established principles [15] of ionic concentration and redox potential of the material involved in the process. Anionic doping is termed as *p-type doping*, while cationic doping is termed as *n-type doping*. It is pertinent to mention here that during the doping/de-doping process the dopant actually moves in and out of the polymer chain or lattice.

It can be clearly seen that the terms doping and de-doping are misplaced in relation to conduction in CPs. In the case of Si or Ge based semiconductors, the conductivity is dependent on the concentration of impurities (dopants) added to the structure (or lattice) of these materials. The electrons contributed by these dopants in the conduction band, are responsible for observed conductivity. In contrast, CPs are actually formed by chemical redox reactions. The term “doping” and “de-doping” however are used extensively in CP literature and are now considered as acceptable terms.

(c) Photo doping: The semi-conducting polymer is locally oxidized and reduced by photo-absorption and charge separation i.e. creation of electron-hole pairs and thereafter creation of free carriers. This process, like the chemical process of doping is not reversible.

(d) Charge injection doping:- Electrons and holes can be injected from metallic contacts into the π^*- and π-bands, respectively. In the case of charge injection at a metal-semiconductor interface, the polymer is oxidised or reduced since electrons are added to the π^*-band or removed from the π-band. The polymer is not doped in the sense of chemical or electrochemical doping, since there are no counter-ions. This process, like the electro-chemical process is a reversible doping process.

Figure 1.2 below presents the various methods for synthesising CPs and lists some of their application areas or potential applications. The processes indicated in red are non-reversible doping processes while the processes indicated in yellow are reversible doping processes.

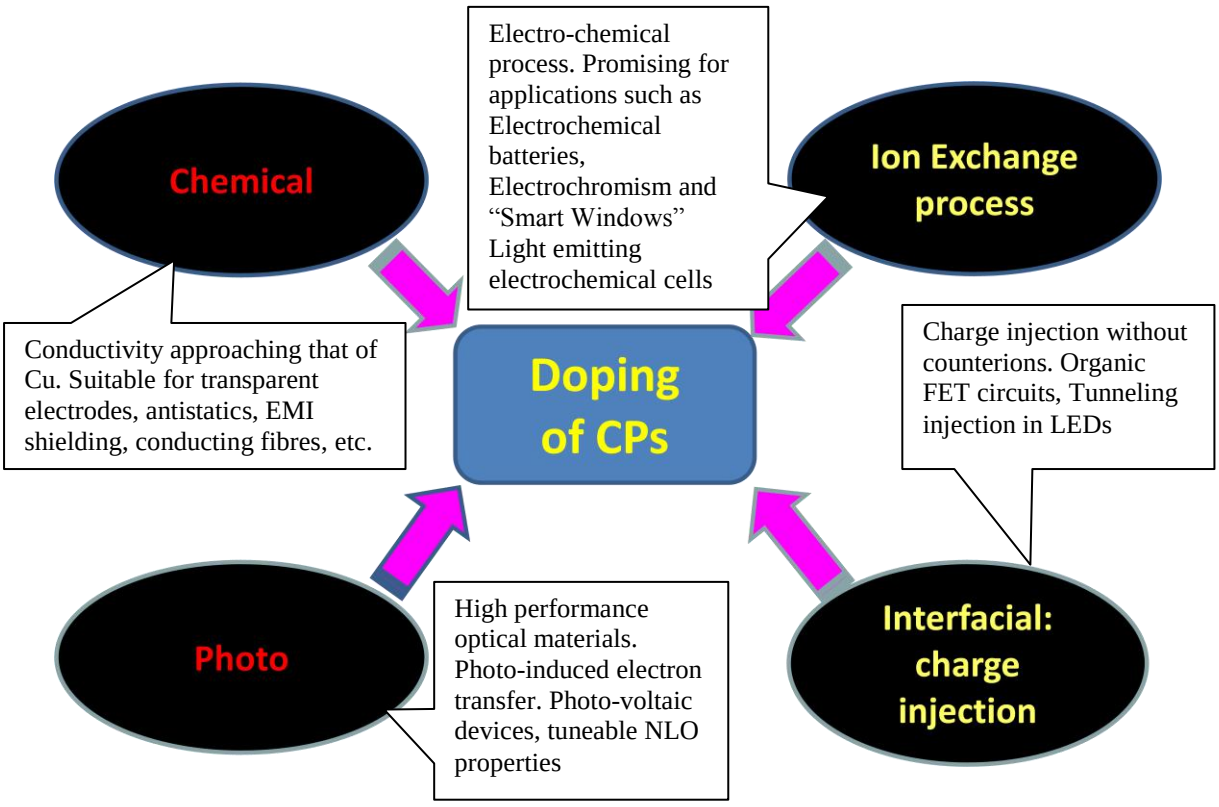

Figure 1.2: Doping methods and related application

1.1.5 Synthesis of Conducting Polymers

Chandrasekhar et al. [4] categorizes synthesis of CPs into two broad categories:

(a) **Condensation Polymerization** (also called as the *step growth polymerization*).

(b) **Addition Polymerization** (also called as the *Chain-growth Polymerization*).

Nearly all electro-chemical syntheses are addition polymerizations, while chemical syntheses are condensation polymerizations. Chandrasekhar et al. [4] has simplistically explained the process of synthesis of CP (in both chemical and electro-chemical methods) in general as:

- Creation of radical cation.
- The radical cation then attacks the monomer molecules available in large amounts in its vicinity. This process generates a “dimmer” radical cation.
- This chain of reaction propagates along the polymer chain till termination.

The electrochemical process is considered to be the method of choice for quickly developing CPs, when well defined polymer structure or morphology is not important. It is also important to understand that the doping process may not be uniform and therefore highly conductive patches (or islands) may be interspersed with insulating patches (or islands). Chandrasekhar et al. [4] indicates that even the best CPs have poor morphology. In the case of fibrous CPs, the length, orientation and thickness of fibres may vary and may also be disconnected. If CPs are globular, then large void spaces may be encountered in its internal structure. Some of the factors affecting synthesis of Polyacetylene have been highlighted by Shirakawa et al. [16] .

1.2 Electrical Conduction in Conducting Polymers

1.2.1 Insulation Metal Transition in Conducting Polymers

The common electronic feature of un-doped CPs is the conjugated π-system that is formed by the overlap of carbon p_z orbitals. The charges introduced into the polymers through the process of doping are stored in such states as solitons, polarons and bi-polarons. Despite strong electron-phonon coupling in CPs, the conductivities of the polymers can be changed from purely insulating to highly metallic states. This transformation is achieved through the process of doping. The transition from insulator to metallic state is called Insulator-Metal Transition (or IMT). Doping process in CPs is known to provide an extraordinary range of DC conductivities, with the highest achieved value (~10^7 S/m) as shown in Figure 1.3.

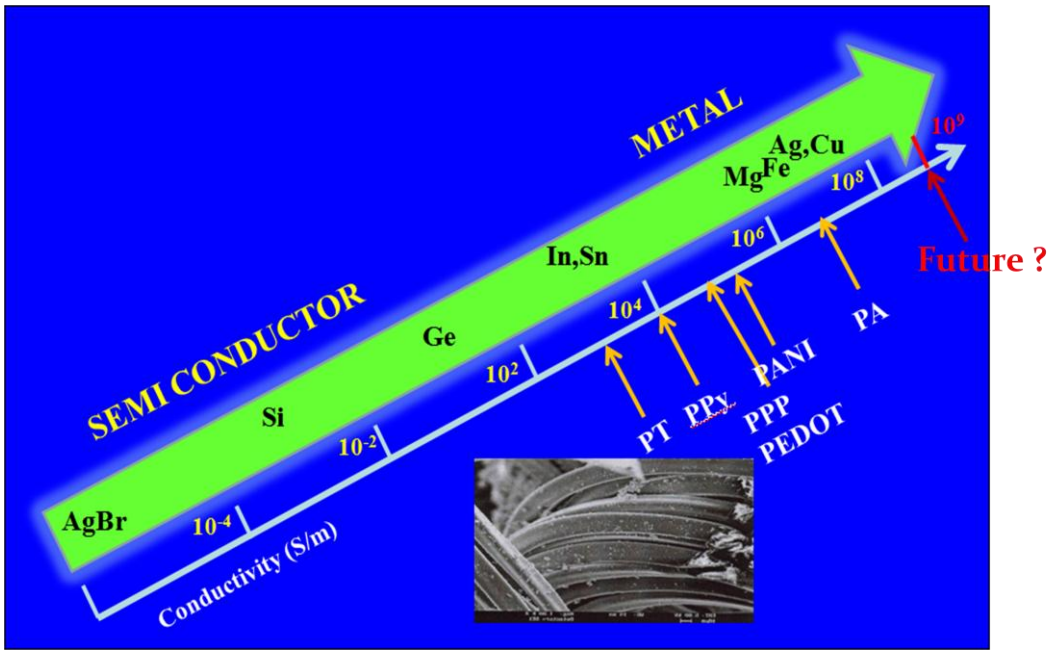

Figure 1.3 : DC Conductivity in CPs

High DC conductivities in CPs often exhibit intrinsic metallic behaviour, which is apparent through negative dielectric constant, a Drude metallic response, temperature independent Pauli's susceptibility and a linear dependence of thermoelectric power on

temperature. However deviations from “typical” metallic behaviour are also observed in some CPs. Reynolds et al. [17] indicates that electrochemically prepared PPy doped with PF_6 are metallic to millikelvin temperatures. However, when PPy is synthesized using different dopants the material exhibits insulating behaviour.

The transport properties of CPs are highly dependent upon the structural disorder arising from sample quality, doping procedure, and aging. The effect of the disorder and the one dimensionality (1D) of polymers on the nature of metallic state or the IMT are strongly debated. It is however a well known fact the disorder and 1D leads ultimately to localization of electron wave function. There is however evidence that metallic state is 3D, though the transport properties are highly anisotropic. Disorder is still a debatable issue and could result in totally different properties if it is homogenous or in-homogenous.

Prigodin et al. [18, 19] have studied the IMT behaviour in CPs. They have proposed a quantum hopping mechanism in metallic polymers to explain frequency dependence of conductivity and dielectric constant of highly CPs. In contrast Effective Medium Theories characterize the frequency dependent transport in systems with large scale in homogeneities such as metal particles dispersed in an insulating matrix. This therefore poses as a percolation problem. MacLachlan et al. [20-23] have proposed the General Effective Medium theory for explaining the IMT behaviour in CPs. In addition some other researchers have also proposed different models for explaining the IMT and metallic behaviour in CPs. These have been described in greater detail in Chapter 2.

The variation of DC conductivity in CPs with temperature is well explained within the band model by the effects of localization caused by disorder. However, the variation of AC conductivity from optical to low frequency and also the variation of dielectric constant are un-explainable through band and hopping models. It has been observed

that at decreasing frequencies the polymers in the dielectric phase exhibit insulator properties and the permittivity is positive (for frequencies ≤0.1 eV).

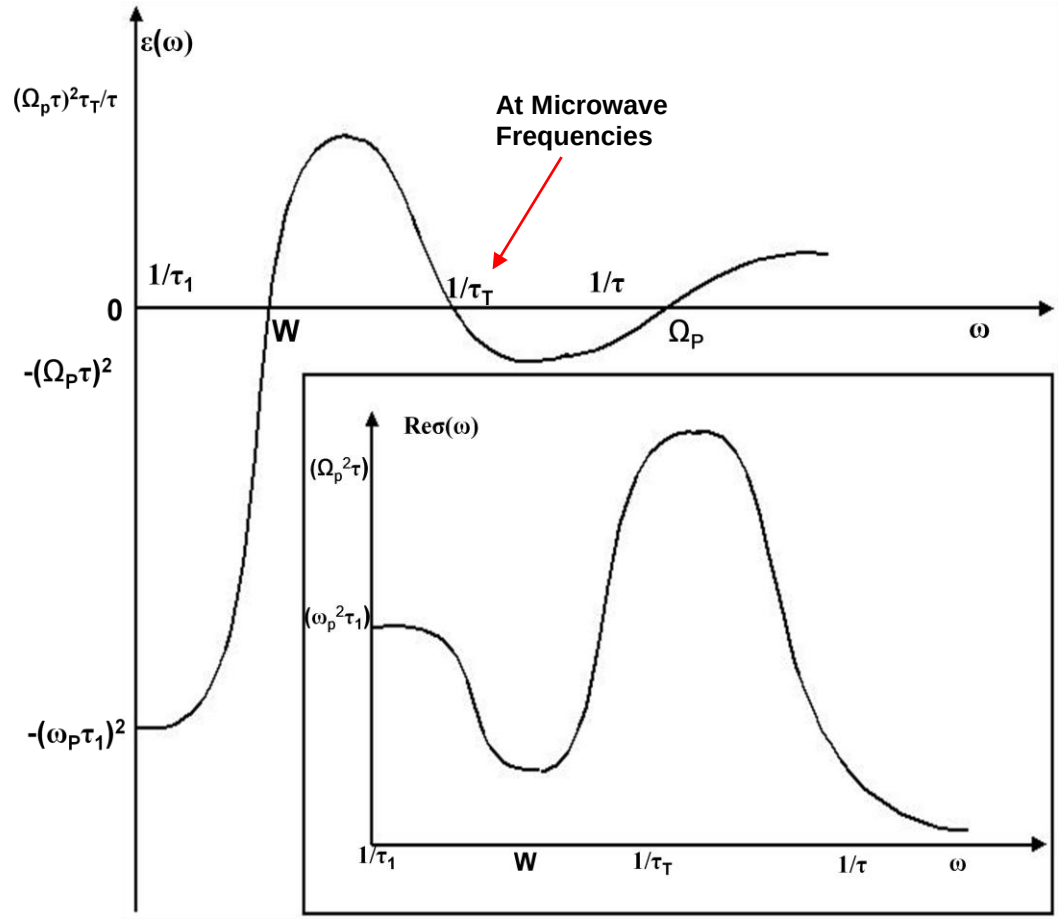

Figure 1.4 : Variation of AC conductivity and Permittivity in CPs. (Figure reproduced and adapted from Prigodin et al. [19].)

At microwave frequencies, permittivity measurements indicate charge localisation lengths of about ~5nm. The permittivity ε changes from negative (metallic value) to positive (dielectric or insulator) value. It is also observed that for metallic samples permittivity ε changes again to a negative value at lower frequencies (i.e. ≤0.01eV). In dielectric phase electrons are bound by fluctuations of the random potential. On the other hand in the metallic side, the free carriers have shorter scattering times. When IMT is approached de-localization first occurs inside crystalline regions. The electron wave functions are strongly localized and therefore these crystalline regions could be considered as nano size metal islands dispersed within poorly

conductive medium. A detailed discussion on IMT and its modelling is presented in Chapter 2.

1.3 Microwave Properties of Conducting Polymers

The properties of CPs in the microwave region are of particular interest as they impact upon a very wide area of applications. These may include (but not restricted to) EMI shielding, stealth technology, radar absorbers, antennas, frequency selective surfaces (FSS) satellite communication links, microchip antennas, sports applications and medical applications.

The physical and chemical properties of different CPs in the microwave region have been extensively studied over the past decade. Most research was focused towards using these materials as EMI Shields [24-26] or as radar absorbent material [26-29]. In the last 5-6 years, with CP's DC conductivity increasing, and stability and aging of the material improving, considerable interest has been shown towards other fields, such as antennas, FSS, etc.

Very few references are available on the work devoted towards use of CPs as microwave absorbers. This may be primarily due to the restrictive or confidential nature of such research with many potential applications in the defence domain. Notwithstanding, we do encounter a number of papers in the material domain where researchers have used microwaves to understand the transport mechanism of these materials. Nalwa et al. [15] in *"Handbook of Organic Conductive Molecules and Polymers"*, indicates that microwave behaviour of CPs such as PPy, Polyparaphenylene, Polythiophene, Poly-p-phenylene-benzobis, etc. have been documented for the frequency range 1 MHz to 20 GHz. These studies have established that CPs as microwave absorbing materials show some sort of corelations between its structural (i.e. crystal structure, counter-anion size, molar mass, length of chain) and electrical properties (such as DC Conductivity σ_{dc} and complex permittivity ε^*). The key parameters affecting the conduction properties of CPs is clearly the interchain distance and the localisation of charge.

Lakshmi et al. [30] has compared the microwave properties of different CPs (PPy, PEDOT, PTH, PPDA and PANi). Their research confirms that the electrical conductivity is not constant along different conducting paths and several relaxation times may co-exist. Lakshmi et al. [30] reconfirms that the distribution of complex conductivity σ leads to dispersion of real part of complex permittivity ε' and σ. Furthermore, microwave conductivity is a direct function of dielectric loss and therefore it exhibits similar variation with frequency as the dielectric loss. In conclusion Lakshmi et al. [30] points that in the S-band region, permittivity, dielectric loss, conductivity, and absorption coefficient, of the studied CPs is higher for highly conductive polymers such as PEDOT (used in the study). However heating coefficient and skin depth show a trend in the reverse order, highly conductive CP have the lowest heating coefficient and skin depth.

A large body of research papers [24, 25, 27-29, 31-38] focus on the utilisation of CPs as RF absorbers in the microwave region. In essence it emerges that:

(a) At low temperatures, the permittivity constant ε is proportional to the square of crystalline domain coherence length ξ. Joo et al. [39] while experimenting with Polyaniline doped with camphor sulphonic acid (PAN-CSA) observed that the variation of permittivity with the square of crystalline domain coherence length ξ^2 is universal for low temperatures, although does show some variation from sample to sample. In contrast, the microwave conductivity of PAN-CSA increases with decreasing temperature.

(b) Wojkiewicz et al. [40] measured the Shielding Effectiveness (SE) of Polyaniline with Polyurethane (PANI-PU) in the microwave band (8.2-18 GHz) and found it to be >80 dB, much above the requirement for commercial applications. Wojkiewicz goes on to highlight the immense advantage these materials have due to their being lightweight, flexible and far less costly than most metals.

(c) Chandrasekhar et al. [41] goes on to explore electrochromics in CPs in the visible, IR and microwave region. They indicate that electrochromism is strongly displayed by CPs right across the visible, near IR, IR and even in microwave spectral regions. Electrochromism could be of great advantage in (i) camouflaging, which is suited for defence applications in this area, (ii) thermal controls of a space craft and (iii) some recreational eye wear.

(d) Similar study on the electrical properties of PPy and its composite over the frequency range 10 kHz to 8 GHz has been undertaken by Mohamed et al. [34]. Mohamed et al. determined the complex permittivity of PPy and polypyrrole-poly(methyl methacrylate) (PPY-PMMA) composite samples over RF 10 kHz to 8GHz.

(e) Jeon et al. [33] uses THz time-domain spectroscopy for characterising the electrical and optical properties of PPy and Poly-3-methylthiophene (PMeT). Jeon concludes that highly conductive PPy and relatively low conductive PMeT polymer films follow the simple Drude and localized-modified Drude theory respectively. Jeon does not dwell on the reasons for such observed differences.

It is evident from the literature that various aspects of CPs and different CPs have been analysed over the entire spectrum and more so in the microwave region. It is also evident that a generalisation of behaviour is hard to make due to a number of parameters controlling the properties of the CP. Furthermore, present fabrication techniques of CP make it hard to get very identical samples or even predict the variation from sample to sample. Notwithstanding, literature does amply prove that suitable CPs could be manufactured that could provide very effective EMI shielding in the microwave region.

1.4 Applications of Conducting Polymers

Polymers are emerging as a group of materials that provide diverse attractive properties, both mechanical and electrical. They are light weight, easy to process, low cost, and environmentally friendly. Furthermore these materials are mechanically and electrically compatible with commonly used conductors such as copper and semiconductors such as silicon. As indicated earlier these materials over the years have improved in electrical conductivity, stability and aging process. It is also emerging that the electrical properties of these materials could be manipulated on a real time basis.

The literature is rich with applications of CPs and also predictions of about what the future could hold. A list of current and future predicted applications is presented in Table 1.3. This list is an indicative list only and is not an exhaustive list of all possible applications that are currently being pursued.

Table 1.3 : Some Applications of CPs

Applications	Developers
Batteries	
• Lithium Polymer (LiPo)	EIG Batteries [42], Nokia [43], Varta [44]
• "Funky" Batteries	IPRI, University of Wollongong [45]
Biomedical Devices	Medtronic [46]
• Coatings for Biomedical devices	SCS Coatings [47], Material Science and Engineering [48]
Capacitors	
• Electrolytic Capacitors	Panasonic [49], HC Starck [50]
• Super capacitors	Crosslink USA [51]
Lighting	
• Flexible Lighting	Crosslink USA [52]
• Organic LEDs	Sony [53], Samsung [54], LG [55], Phillips [56], HC Starck [57]
• Electroluminescent lighting	Agfa [58]
Anti-Static Coatings	Crosslink USA [59], Agfa [60], Groenendaal et al [61], HC Starck [62]
• High Conductive Coatings	HC Starck [63], Enthone [64]
Printed Electronics	
• Printed Wiring Boards	HC Starck [65]
• Organic Thin Film Transistor	HC Starck [66], Barret et al [67], Sirringhaus et al [68], Sandberg et al [69], Okuzaki et al [70], Hsu et al [71]
• FET or OFET	Takshi et al [72], Haddock et al [73], Ashizawa et al [74]
• Schottky Contacts	Takshi et al [75],
• Nano-rectifiers	Majewski et al [76]
• Inexpensive Disposable Electronics	Hohnholz et al [77]
Fabrics	Milliken [78],
Shelf life detectors	Man and Jones [79]
Anti Corrosion	Crosslink USA [80], Panipol [81]
Detoxification	Crosslink USA [82]
Chemical, Biochemical and Biological Sensors	Shim et al [83], Science Daily [84], Sasso et al [85]
Smart Surfaces	
• Smart Skins	Lockheed Martin [86]
• Smart Windows	IPRI [87], Azom [88]
Actuators	EAP [89], Xi [90]
Electric Cables	Rengel [91]

It is evident from the above that in the coming decade CPs are going to impact upon almost all fields of technology. Antenna applications would not remain unaffected. In this study we attempt to systemise the study of CPs purely from the perspective of microwave antenna applications.

1.5 Conducting Polymers and RF Antennas

Recent advances in electrical conductivity and impressive improvements in stability are making conducting polymers (CPs) very attractive as alternatives to copper (Cu) for planar antennas. This is particularly so in applications where light weight [92], inexpensive [93] and/or wearable/conformal antennas [94] are a consideration. There have been isolated or very few efforts in the past towards using CP as material for antenna design. In particular, Solberg Jr. et al. [95] used a conducting polymer (CP) composite to build a non-planar direction-finding antenna operating in the frequency range of 30 MHz to 1 GHz. Cichos et al. [96] have tried using polymeric film with silver flakes for designing low cost RFID coil antennas. Rmili et al. [97] have reported fabricating a rectangular microstrip patch antenna with the radiating element made of polyaniline (PANI), a CP having a bulk DC conductivity of 6000 S/m.

In this research we explore the possibility of using CPs for application at microwave frequencies, in particular as a resonant patch on a planar microstrip patch antenna (MPA). This research is a baseline study and could form as a basis for work on re-configurable antennas using CPs. This investigation is a first step towards a better understanding of the numerical simulation, design and fabrication issues associated with antennas using these materials for various future applications.

1.6 Thesis Outline and Contributions

This thesis looks at the problem of simulation and design of low conducting thin film CPs antennas at different microwave frequencies. The

study dwells in depth on the effect of film thickness and conductivity on antenna performance. It also explores the impact of different film development methods on antenna fabrication and performance.

Use of EM simulation software to accurately simulate very thin conducting films has also been addressed in this work. Furthermore, problems associated with estimating or accurately determining the permittivity constant of a multilayered structure or non-standard substrate has also been taken up in this thesis. A theoretical approach has been provided by suitably modifying the Getsinger model [98] for multilayer structures. In addition use of simulation and actual measurements to estimate substrate permittivity constant has also been demonstrated in the design of 2 GHz microstrip patch antennas.

This thesis provides clear evidence of the fact that CP based thin films fabricated by different methods could be used as microwave antennas. It establishes that if modest radiation efficiencies in antennas are acceptable then such antennas may be considered as an alternative to metal based antennas.

The main original contributions made in this thesis could be summarised as follows:

- Theoretical method for modelling electrical properties of CPs.
- Development of a closed form expression for effective permittivity constant in three and four layered substrates; obtained by modifying the Getsinger's model.
- Simulation of very thin CP films as resonant patch in microstrip patch antennas using commercial EM simulation software.
- Use of indirect methods for estimating the permittivity constant of non-conventional substrates. This method is based on using known design of microstrip patch antenna and refining the simulation to match up with measured results, keeping all other parameters constant.
- Establishment of antenna performance variation with CP film thickness and conductivity. Over here it is pertinent to mention that traditional

design view of resonant patch thickness being at least couple of skin depths thick is desirable property but not essential.

- Providing indirect evidence of increase in AC conductivity of CP film with frequency.

1.7 Chapter Summaries

The work in this thesis is organised into five chapters. These chapters present the different issues that are central to better our understanding of CPs and their subsequent utilisation in microwave antennas.

Chapter 2 - Modelling Electrical Conduction in Conducting Polymers: In this chapter different methods for modelling electrical conduction in Conducting Polymers (CPs) are discussed. It is also highlighted that this study is essential for simulating re-configurable antennas made from these materials. In principle, a re-configurable antenna would utilise the ability of CPs to dynamically transit between insulator state (non-conductive) and metal state (highly conductive) through change in its dopant concentration and/or change in its frequency of operation. It is therefore imperative that an accurate model is available that describes electrical conduction in CPs as a function of dopant concentration and frequency of operation.

The main original contribution in this chapter is to combine two different models on electrical conduction in CPs; with the intention of having one model that describes AC conductivity as a function of dopant concentration and frequency.

Chapter 3 – Building Microstrip Patch Antenna with Polypyrrole: In this chapter we explore the effect of using Polypyrrole (PPy) as the ground plane in a planar microstrip Cu-patch antenna. The possibility of using a CP patch in a planar microstrip microwave antenna is also investigated. The problem of determining the electrical properties of unknown materials is also addressed by deploying indirect methods, such as a microstrip patch antenna for estimating the electrical properties of unknown materials.

The main original contribution of this chapter is an in-depth understanding of EM simulation method that is suitable for design of these antennas. In addition permittivity of unknown substrates is also determined through indirect techniques.

Chapter 4 – Radiation Efficiency in CP based patch Antennas: In this chapter the focus is towards establishing a good understanding of the effect of CP patch thickness and its conductivity on overall antenna efficiency. The purpose is to clearly understand the relationship between patch thickness, its conductivity and radiation efficiency. This would help in predicting *a priori,* conductivity levels needed for a given thickness of polymer film to be able to radiate as an antenna with acceptable efficiency. Alternatively, determining the required film thickness and conductivity needed for an acceptable antenna performance.

The main original contribution of this chapter is a good understanding of thin film simulation; estimation of permittivity of substrates through indirect antenna design-simulation cycle; variation of AC conductivity in CPs with frequency and observed trend of variation in antenna gain and efficiency with film thickness and conductivity.

Chapter 5 – Quo Vadis?: This chapter summarises the main results from the thesis and also presents some interesting possibilities for future research in this field.

Appendix A – Determination of Effective Permittivity of Multi-layer Microstrip lines using a Modified Getsinger's Model: In this Appendix, the possibility of applying multilayered dielectric microstrip line structures directly to the Getsinger model is explored and the performance of this model is evaluated against Unified Dispersion Model (UDM) and a reference solution obtained using 2D finite-element eigenmode analysis from the port solution in Ansoft's HFSS^{TM}.

The main original contribution of this Appendix is development of closed form expressions of effective permittivity for two and three layer substrates in microstrip lines. The proposed closed form expressions are more accurate than similar expressions provided by other methods.

Appendix B – In this appendix additional result of 4.5 GHz PPy patch antennas of different patch thicknesses is presented.

Appendix C – In this Appendix, the technical data sheets of Dimatix DMP 2800 inkjet printer and Clevios P™ are placed for reference.

Appendix D – This Appendix presents additional results on 6 GHz PPy and PEDOT patch antennas, used for studying the effect of patch thickness, conductivity and CP on antenna performance.

References

[1] H. Shirakawa, E. Louis, A. G. MacDiarmid, C. K. Chiang, and A. J. Heeger, "Synthesis of electrically conducting organic polymers: halogen derivatives of polyacetylene, (CH)x," *Journal of the Chemical Society, Chemical Communications* pp. 578-580, 1977.

[2] CST. (17 May 2011). Available: http://www.cst.com/

[3] Ansoft. (17 May 2011). Available: http://www.ansoft.com/products/hf/hfss/

[4] P. Chandrasekhar, *Conducting Polymers, Fundamentals and Applications: A practical Approach*. Boston: Kluwer Academic Publishers, 1999.

[5] A. Diaz, K. Kanazawa, and G. Gardini, "Electrochemical polymerization of pyrrole," *Journal of Chemical Society: Chemistry Communication*, pp. 635-636, 1979.

[6] A. Diaz and J. A. Logan, "Electroactive polyaniline films," *Journal of Electroanalytical Chemistry*, pp. 111-114, 1980.

[7] M. S. Freund and B. A. Deore, *Self-Doped Conducting Polymers*: John Wiley & Sons Ltd, 2007.

[8] J. Joo, J. K. Lee, J. S. Baeck, K. H. Kim, E. J. Oh, and A. J. Epstein, "Electrical, Magnetic and Structural Properties of Chemically and Electrochemically Synthesised Polypyrroles," *Synthetic metals*, vol. 117, pp. 45-51, 2001.

[9] Z. K. Co. (17 May 2011). Available: http://www.zipperling.de/

[10] Enthone. (17 May 2011). Available: http://www.enthone.com

[11] Bayer. (17 May 2011). Available: http://www.bayercoatings.de

[12] Agfa. (17 May 2011). Available: http://www.agfa.com

[13] A. J. Heeger, "Semiconducting and metallic polymers: the fourth generation of polymeric materials," *The Journal of Physical Chemistry B,* vol. 105(36), pp. 8475-8491, 2002.

[14] A. J. Heeger, P. Smith, A. Fizazi, J. Moulton, K. Pakbaz, and S. Rughooputh, "Recent Progress in Conducting Polymers: Opportunities for Science and Opportunities for Technology," *Synthetic Metals,* vol. 41-43, pp. 1027-1032, 1991.

[15] H. S. Nalwa, *Handbook of Organic Conductive Molecules and Polymers* vol. 3: John Wiley & Sons Ltd, 1997.

[16] H. Shirakawa, Y.-X. Zhang, T. Okuda, K. Sakamaki, and K. Akagi, "Various factors affecting the synthesis of highly conducting polyacetylene," *Workshop on the Metallic Phase of Conducting Polymers,* vol. 65, pp. 93-101, 1994.

[17] T. A. Skotheim, R. L. Elsenbaumer, and J. R. Reynolds, *Handbook of Conducting Polymers*, 3rd ed.: Marcel Dekker, 2007.

[18] V. N. Prigodin and A. J. Epstein, "Nature of Insulator-metal transition and novel mechanism of charge transport in the metallic state of highly doped electronic polymers," *Synthetic Metals,* vol. 125, pp. 43-53, 2002.

[19] V. N. Prigodin and A. J. Epstein, "Quantum Hopping in metallic Polymers," *Physica B,* vol. 338, pp. 310-317, 2003.

[20] D. S. MacLachlan, "An equation for the conductivity of binary mixtures with anisotropic grain structures," *Journal of Physics: Solid State Physics,* vol. 20, pp. 865-877, 1987.

[21] D. S. MacLachlan, "Analytical functions for the DC and AC conductivity of Conductor-Insulator Composities," *Journal of Electroceramics,* vol. 5:2, pp. 93-110, 1999.

[22] D. S. MacLachlan, K. Cai, C. Chiteme, and W. D. Heiss, "An analysis of dispersion measurements in percolative metal-insulator systems using analytic scaling functions," *Physica B,* vol. 279, pp. 66-68, 2000.

[23] D. S. MacLachlan, C. Chiteme, C. Park, K. E. Wise, S. E. Lowther, P. T. Lillehei, E. J. Siochi, and J. S. Harrison, "AC and DC Percolative Conductivity of Single Wall Carbon Nanotube Polymer Composites," *Journal of Polymer Science: Part B: Polymer physics,* vol. 43, pp. 3273-3287, 2005.

[24] E. Hakansson, A. Amiet, and A. Kaynak, "Electromagnetic shielding properties of polypyrrole/polyester composites in the 1-18 GHz frequency range," *Synthetic Metals,* vol. 156, pp. 917-925, 2006.

[25] J. Joo and A. J. Epstein, "Electromagnetic radiation shielding by intrinsically conducting polymers," *Applied Physics Letters,* vol. 65, pp. 2278-2280, 1994.

[26] T. C. P. Wong, B. Chambers, A. P. Anderson, and P. V. Wright, "Large area conducting polymer composites and their use in microwave absorbing material," *Electronics Letters,* vol. 28, pp. 1651-1653, 13 Aug 1992.

[27] T. C. P. Wong, B. Chambers, A. P. Anderson, and P. V. Wright, " Fabrication and evaluation of conducting polymer composites as radar absorbers," *Antennas and Propagation, 1993., Eighth International Conference on,* vol. 2, pp. 934-937, 1993.

[28] T. C. P. Wong, B. Chambers, A. P. Anderson, and P. V. Wright, "Characterisation of conducting polymer loaded composite materials at oblique incidence and their application in Radar absorbers," *Antennas and Propagation, 1995. ICAP '95. Ninth International Conference on (Conf. Publ. No. 407),* vol. 1, pp. 441-444, 4-7 Apr 1995.

[29] V. T. Truong, S. Z. Riddell, and R. F. Muscat, "Polypyrrole based microwave absorbers," *Journal of Materials Science,* vol. 33, pp. 4971-4976, 1998.

[30] K. Lakshami, H. John, R. Joseph, K. E. George, and K. T. Mathew, "Comparison of Microwave and Electrical Properties of Selected Conducting Polymers," *Microwave and Optical Technology letters,* vol. 50, pp. 504-508, 2007.

[31] T. C. P. Wong, A. Barnes, B. Chambers, A. P. Anderson, and P. V. Wright, "Microwave Characterisation of smart materials based on Conducting Polymer Composite Materials," *10th International Conference on Antennas and Propagation,* pp. 1478-1482, 1997.

[32] V. T. Truong, A. R. Codd, and M. Forsyth, "Dielectric properties of conducting polymer composites at microwave frequencies," *Journal of Materials Science,* vol. 29, pp. 4331-4338, 1994.

[33] T.-I. Jeon, D. Grischkowsky, A. K. Mukherjee, and R. Menon, "Electrical and optical characterization of Conducting Polymers by THz time-domain spectroscopy," *Applied Physics Letters,* vol. 79, pp. 451-452, 2003.

[34] A. B. H. Mohamed, J. L. Miane, and H. Zangar, "Radiofrequency and Microwave (10KHz - 8 GHz) Electrical Properties of Polypyrrole and Polypyrrole-Poly(Methyl Methacrylate) Composites," *Polymer International,* vol. 50, pp. 773-777, 2001.

[35] V. T. Truong and J. G. Ternan, "Complex conductivity of a conducting polymer at microwave frequencies," *Polymer,* vol. 36, pp. 905-909, 1995.

[36] K. Naishadham and P. K. Kadaba, "Measurement of the Microwave Conductivity of Polymeric material with Potential Applications in Absorbers and Shielding," *Transactions on Microwave Theory and Techniques*, vol. 39, pp. 1158-1164, 1991.

[37] J. Joo, J. P. Pouget, E. J. Oh, and A. J. Epstein, "Microwave Dielectric response of Mesoscopic metallic regions and the intrinsic metallic state of Polyaniline," *Physical Review B*, vol. 49, 1994.

[38] C. Y. Lee, H. M. Kim, J. W. Park, Y. S. Gal, J. J. Jin, and J. Joo, "AC Electrical Properties of conjugated polymers and Theoretical High-Frequency behaviour of Multilayer Films," *Synthetic metals*, vol. 117, pp. 109-113, 2001.

[39] J. Joo, Z. Oblakowski, G. Du, J. P. Pouget, E. J. Oh, J. M. Wiesinger, Y. Min, A. G. MacDiarmid, and A. J. Epstein, "Microwave dielectric response of mesoscopic metallic regions and the intrinisic metallic state of polyaniline," *Physica Review B*, vol. 49, pp. 2977-2980, 15 Jan 1994.

[40] J. L. Wojkiewicz, S. Fauveaux, N. Redon, and J. L. Miane, "High electromagnetic shielding effectiveness of polyaniline-polyurethane composites in microwave band," *International Journal of Applied Electromagnetics and Mechanics*, vol. 19, pp. 203-206, 2004.

[41] P. Chandrasekhar, B. J. Zay, T. McQueeney, G. C. Birur, V. Sitaram, R. Menon, M. Coviello, and R. L. Elsenbaumer, "Physical, Chemical, theoretical aspects of Conducting Polymer electrochromics in the visible, IR and microwave region," *International Conference on Synthetic Metals*, pp. 649-653, 2005.

[42] EIG. (31 December 2010)). *ePLB*. Available: http://www.eigbattery.com/eng/technology/about_epb.htm

[43] Nokia. (31 December 2010)). *Ultra thin Lithium Polymer Batteries*. Available: http://press.nokia.com/PR/199909/775937_5.html

[44] Varta. (31 December 2010)). *Rechargable Lithium Polymer Batteries*. Available: http://www.varta-microbattery.com/en/oempages/product_data/poductdata_types.php?output=typedata&segment=RechLiFlatPoly

[45] W. IPRI. (31 December 2010). *Funky Batteries*. Available: http://www.electromaterials.edu.au/flyers/UOW087809

[46] Medtronics. (31 December 2010)). *Biomedical Devices*. Available: http://www.medtronic.com.au/

[47] SCS. (31 December 2010)). *Coatings for Biomedical devices*. Available: http://www.scscoatings.com/parylene_applications/medical.aspx?gclid=CIe3o42XlqYCFcQ3pAodFlONnA

[48] M. S. a. Engineering. (31 Dec 2010)). *Conducting Polymers in Biomedical Devices*. Available: http://www.mse.engin.umich.edu/research/projects/67

[49] Panasonic. (31 December 2010)). *Electrolytic Capacitors*. Available: http://www.panasonic.com/industrial/electronic-components/capacitive-products/sp-cap-polymer-aluminum.aspx

[50] H. Starck. (31 December 2010). *Capacitors*. Available: http://www.clevios.com/index.php?page_id=1533&prod_service_id=&anw_id=95&operate=&suchstart=938&prodselect_5=0&suchstart=938&anwselect_14=95&suchfeld=

[51] C. USA. (31 December 2010)). *Supercapacitors*. Available: http://www.crosslinkusa.com/energy-storage-materials.html

[52] C. USA. (31 December 2010)). *Flexible Lighting using electroactive poplymers*. Available: http://www.crosslinkusa.com/flexible-lighting.html

[53] Sony. (31 December 2010). *OLED Television*. Available: http://www.sony.com.au/pressrelease/asset/311392/section/consumerproducts pressreleases

[54] Samsung. (31 December 2010)). *OLED Television*. Available: http://www.samsung.com/global/business/lcdpanel/newsView.do?news_id=408

[55] CNET. (31 December 2010)). *LG Unveils thinnest OLED TV*. Available: http://www.cnet.com.au/lg-unveils-world-s-thinnest-3d-oled-tv-339305645.htm

[56] S. Kirchmeyer and L. Brassat. (2005, May 2007). *Intrinsically Conductive Polymers*. Available: http://www.clevios.com/medien/dokumente/document_ConductiveCoating.Instrinsicallyconductivepolymers.pdf

[57] H. Starck, "OLED-Displays and Solar Cells," 31 December 2010.

[58] Agfa. (31 December 2010)). *Electroluminescent Lighting*. Available: http://www.agfa.com/en/sp/solutions/orgacon_electronic_materials/applications_orgacon/el_lamps/index.jsp

[59] C. USA. (31 December 2010)). *Anti-Static coatings*. Available: http://www.crosslinkusa.com/anti-static-coatings.html

[60] Agfa. (31 December 2010)). *Coating Solutions*. Available: http://www.agfa.com/en/sp/solutions/orgacon_electronic_materials/orgacon_products/coating_solutions/index.jsp

[61] L. B. Groenendaal, F. Jonas, D. Freitag, H. Pielartzik, and J. R. Reynolds, "Poly(3,4-Ethylenedioxythiophene) and Its Derivatives: Past, Present, and Future," *Advanced Materials*, vol. 12, pp. 481-494, 2000.

[62] H. Starck. (31 December 2010). *Antistatic Coatings*. Available: http://www.clevios.com/index.php?page_id=1533&prod_service_id=&anw_id

=93&operate=&suchstart=938&prodselect_5=0&suchstart=938&anwselect_14=93&suchfeld=

[63] H. Starck. (31 December 2010). *Highly Conductive Coatings*. Available: http://www.clevios.com/index.php?page_id=1533&prod_service_id=&anw_id=94&operate=&suchstart=938&prodselect_5=0&suchstart=938&anwselect_14=94&suchfeld=

[64] Enthone. (31 December 2010)). *Conductive Coatings*. Available: http://www.enthone.com/ormecon/ormecon-conductive.aspx

[65] H. Starck. (31 December 2010). *Printed Wiring Boards*. Available: http://www.clevios.com/index.php?page_id=1533&prod_service_id=&anw_id=96&operate=&suchstart=938&prodselect_5=0&suchstart=938&anwselect_14=96&suchfeld=

[66] H. Starck. (31 December 2010). *Organic Thin Film Transistors*. Available: http://www.clevios.com/index.php?page_id=1533&prod_service_id=&anw_id=99&operate=&suchstart=938&prodselect_5=0&suchstart=938&anwselect_14=99&suchfeld=

[67] M. Barret, S. Sanaur, and P. Collot, "Inkjet-printed polymer thin film transistors: Enhancing performances by contact resistances engineering," *Organic Electronics,* vol. 9, pp. 1093-1100, 2008.

[68] H. Sirringhaus, T. Kawase, R. H. Friend, T. Shimoda, M. Inbasekaran, W. Wu, and E. P. Woo. (2000, 15 December) High-Resolution Inkjet Printing of All-Polymer Transistor Circuits. *Science* 2123-2126.

[69] H. G. O. Sandberg, T. G. Backlund, R. Osterbacka, and H. Stubb, "High Performance All Polymer Transistor Utilizing a Hygroscopic Insulator," *Advanced Materials,* vol. 16, pp. 1112-1115, 2004.

[70] H. Okuzaki, M. Ishihara, and S. Ashizawa, "Characteristics of Conducting Polymer transistors prepared by line patterning," *Synthetic metals,* vol. 137, pp. 947-948, 2003.

[71] F. Hsu, V. N. Prigodin, and A. J. Epstein, "Electric Field controlled conductance of metallic polymers in a transistor structure," *Physical Review B,* vol. 74, pp. 235219-1 - 235219-12, 28 Dec 2006.

[72] A. Takshi, A. Dimopoulos, and J. D. Madden, "Simulation of a dual gate organic transistor compatible with printing methods," *Solid State Electronics,* vol. 52, pp. 107-114, 2008.

[73] J. N. Haddock, X. Zhang, S. Zheng, Q. Zhang, S. R. Marder, and B. Kippelen, "A comprehensive study of short channel effects in organic field effect transistors," *Organic Electronics,* vol. 7, pp. 45-54, 2006.

[74] S. Ashizawa, Y. Shinohara, H. Shindo, Y. Watanabe, and H. Okuzaki, "Polymer FET with a conducting channel," *Synthetic metals,* vol. 153, pp. 41-44, 2005.

[75] A. Takshi, M. Mohammadi, and J. D. Madden, "Study the effect of Distribution of density of states on the depletion width of organic Schottky contacts," *Solid State Electronics*, vol. 52, pp. 1717-1721, 2008.

[76] L. A. Majewski, C. Balocco, R. King, S. Whitelegg, and A. M. Song, "Fast Polymer nanorectifiers for inductively coupled RFID tags," *Materials Science and Engineering B*, vol. 147, pp. 289-292, 2008.

[77] D. Hohnholz and A. G. MacDiarmid, "Line patterning of Conducting Polymers: New horizons for inexpensive, disposable electronic devices," *Synthetic metals*, vol. 121, pp. 1327-1328, 2001.

[78] Milliken. (31 December 2010)). *Fibers*. Available: http://www.milliken2.com/MFT/MFThtml.nsf/page/home.htm

[79] C. M. D. Man and A. A. Jones, *Shelf Life Evaluation of Foods*: Springer, 2000.

[80] C. USA. (31 December 2010)). *Corrosion Prevention*. Available: http://www.crosslinkusa.com/corrosion-prevention.html

[81] Panipol. (31 Dec 2010)). *Panipol*. Available: http://www.panipol.com/index29ff.html?option=content&task=view&id=10&Itemid=34

[82] C. USA. (31 December 2010)). *Detoxification*. Available: http://www.crosslinkusa.com/detoxification.html

[83] Y. B. Shim. (2007). *Electrochemical Sensors based on Conducting Polymers*. Available: http://www.mdpi.org/sensors/specialissues/conducting-polymer-ec-sensors.htm

[84] S. Daily. (2005). *New Gas Sensor patterned with Conducting Polymer*. Available: http://www.sciencedaily.com/releases/2005/04/050421235954.htm

[85] L. Sasso, P. Vazquez, I. Vedarethinam, J. Costillo-Leon, J. Emneus, and W. E. Svendsen, "Conducting Polymer 3D Microelectrodes," *Sensors*, vol. 10, pp. 10986-11000, 2010.

[86] L. Martin. (31 December 2010)). *Smart Surfaces*. Available: http://www.lockheedmartin.com/data/assets/ssc/atc/LMSeminarChang2010.pdf

[87] W. IPRI. (31 Dec 2010)). *Electro-chromism*. Available: http://www.electromaterials.edu.au/commercialisation/UOW087807

[88] azom. (31 Dec 2010)). *Polyaniline Smart Windows*. Available: http://www.azom.com/Details.asp?ArticleID=1197

[89] E. Hub. (31 Dec 2010)). *Artificial Muscle*. Available: http://eap.jpl.nasa.gov/

[90] B. Xi, "Novel Conducting Polymer structures for Electrochemical Actuators," Doctor of Philosophy, Department of Chemistry, University of Wollongong, Wollongong, 2005.

[91] U. R. Rengel, "Energy Cables 2050: A Futuristic View," *IEEE Power Engineering Review,* p. 18, October 2000.

[92] BY. Bayram, Y. Zhou, B.S. Shim, J. Z. S. Xu, N.A. Kotov, and J. L. Volakis, "E-Textile Conductors and polymer composites for conformal lightweight antennas," *IEEE Transactions on Antennas and propagation,* vol. 58, Aug 2010.

[93] A. Rida, Y. Li, R. Vyas, and M. M. Tentzeris, "Conductive inkjet-printed antennas on flexible low-cost paper-based substrates for RFID and WSN applications," *IEEE Antennas and Propagation Magazine,* vol. 51, pp. 13-22, 2009.

[94] J.J. Adams, E.B. Duoss, T.F. Malkowski, M.J. Motala, B.Y. Ahn, R.G. Nuzzo, J.T. Bernhard, and J.A. Lewis, "Conformal printing of electrically small antennas on three-dimensional surfaces," *Advanced Materials,* vol. 23, pp. 1335-1340, 2011.

[95] R. F. Solberg Jr and P. J. Siemsen, "Development of a conductive polymer composite direction finding antenna," *Antennas and Propagation Society International Symposium,* vol. 3, pp. 1966-1969, 11 Jul 1999.

[96] S. Cichos, J. Haberland, and H. Reichl, "Performance analysis of polymer based antenna-coils for RFID," in *IEEE Polytronic conference,* 2002, pp. 120-124.

[97] H. Rmili, J. L. Miane, H. Zangar, and T. Olinga, "Design of microstrip fed proximity-coupled conducting polymer patch antenna," *Microwave and Optical Technology letters,* vol. 48, pp. 655-660, Apr 2006.

[98] W. J. Getsinger, "Microstrip Dispersion Model," *IEEE Transactions on Microwave Theory and Techniques,* vol. 21, pp. 34-39, 1973.

Chapter 2

Modelling Electrical Conduction in Conducting Polymers

2.1 Introduction

Modelling electrical conduction in Conducting Polymers (CPs) is essential for simulating re-configurable antennas made from these materials. In principle, a re-configurable antenna would utilise the ability of CPs to dynamically transit between insulator state (non-conductive) and metal state (highly conductive) through change in its dopant concentration and/or change in its frequency of operation. It is therefore highly desirable that an accurate model is available that describes electrical conduction in CPs as a function of dopant concentration and frequency of operation. In this chapter different methods for modelling CPs are described and an attempt is also made to develop a model that suits re-configurable antenna applications.

Polymers are essentially made up of repeating units (or groups) predominantly made of carbon. Polymers are electrically non-conducting, since they are formed from covalent bonding between the carbon and other atoms of the polymer chain. This type of bonding does not leave any free valency electrons that could contribute towards electrical or thermal conductivity. In contrast, in the case of metals, we observe high thermal and electrical conductivities due to the availability of a sea of loosely held free valence electrons. Heeger et al. [1] through their discovery demonstrated that it was possible to add or remove an extra charge carrier from a polymer chain, either chemically or electro-chemically. The interest in CP has also grown due to profound increase in their room temperature conductivities and environmental stability.

The improvements in synthesis and processing of CP have steadily increased the magnitude of electrical conductivity and reduced the dependence on temperature. Variation of electrical conductivity of CPs with respect to temperature and frequency vs. that exhibited in metals, has been a field of intense study in recent times. Metals exhibit band transportation method of electrical conduction where the electrical conductivity steadily decreases with increasing temperature and frequency [1, 2]. In contrast "hopping transport" is a general mechanism for low temperature electrical conductivity in disordered materials with localized states, such as doped semiconductors. Prigodin et al. [2] have shown that conductivities due to hopping and band transport have a very different frequency dependence. Both these transport mechanisms do not fully explain the frequency dependence of conductivity in CP. Prigodin et al. [2] therefore have proposed a new mechanism of conduction in highly CP to be based on quantum resonance hopping between adjacent metal grains.

In contrast, variation of AC conductivity and permittivity of CPs with frequency and temperature has also been rigorously studied from the percolation of aggregates point of view. The percolation theory was developed by Stauffer [3] and is based on seven critical power laws of $(\phi - \phi_c)$, where ϕ and ϕ_c are respectively the concentration in inclusions (dopants) and the critical concentration at percolation threshold. MacLachlan et al. [4] studied the conductivity of binary mixtures with anisotropic grain structures and proposed a dynamic General Effective Media (GEM) equation for describing complex permittivity and conductivity of such binary mixtures.

As is evident from the above, GEM-percolation theory is general in nature for describing the electrical properties of any percolating system. However Prigodin's proposed quantum resonance hopping mechanism is specific to CPs and their electrical properties. This model described at [2] presupposes a fixed concentration of the dopant in the CP composite. In applications where dynamic change of CP's electrical properties is envisaged due to variation in dopant concentration, application of GEM alone may not be able to accurately model electrical conduction in CP.

In this chapter an attempt is made to combine the GEM and quantum resonance hopping mechanism to model dynamic changes in dopant concentration in a CP and its effect on the electrical conduction with changes in frequency of operation. This chapter first describes the percolation theory and then the quantum resonance hopping mechanism and finally develops a model that is able to describe the electrical conduction in CPs as a function of dopant concentration and frequency of operation.

2.2 Various Models on Electrical Conductivity in CPs

Pristine (undoped) CPs have the common electronic feature of conjugated π-system, formed by overlapping of carbon p_z orbitals forming alternating single and double bonds. The chemical repeat units of the pristine forms of several families of CPs are shown in Figure 2.1.

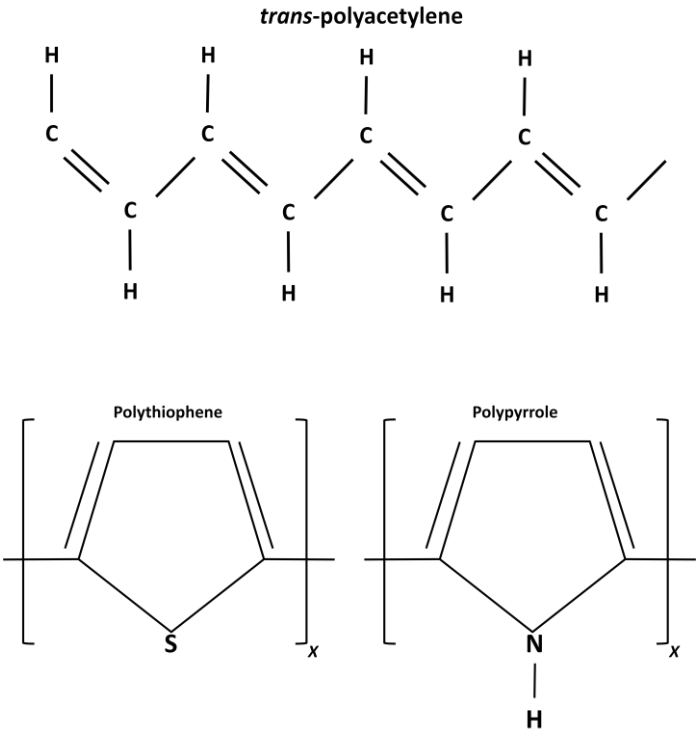

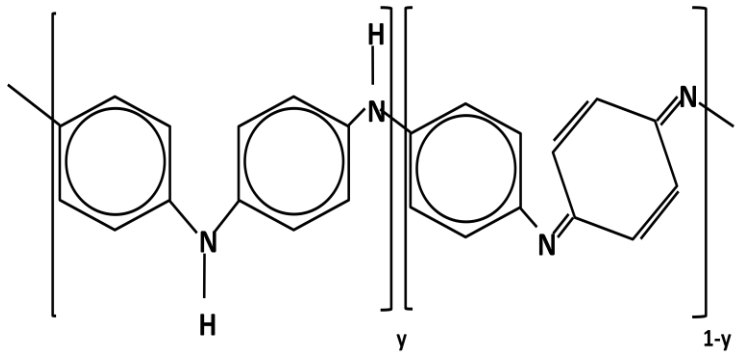

Polyaniline: leucoemeraldine (y=1), emeraldine (y=0.5) and pernigraniline (y=0) base forms

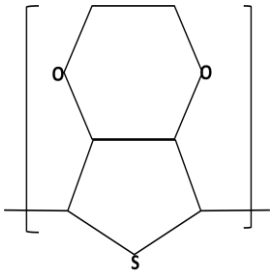

Poly(ethylenedioxy)-thiophene (PEDOT)

Figure 2.1: Schematic chemical structures of CPs

The one dimensional CP chains are vulnerable due to Peierls [5] and Jahn-Teller distortions [6] of the energy bands. Charges introduced into the polymer chain through doping are stored in novel states such as “solitons”, “polarons” and “bipolarons”, which includes a charge and a lattice distortion that surrounds it. The electrical conductivities of pristine CPs can be altered from insulating to metallic levels through the process of doping. The electrical conductivity increases with doping concentration. Both n-type (electron donating), p-type (electron accepting) and protonic acid doping have been used to change the electrical conduction in CPs from insulating to metallic states (also referred to as Insulator-Metal transition (IMT)).

The transport properties of CPs are highly dependent upon the structural disorder arising from sample quality, doping procedure and aging. The effect of the disorder and the one-dimensionality of the polymer on the nature of the metallic state and the IMT are still strongly debated and are beyond the scope of this thesis. In this section we summarise different models that have been proposed for electrical conductivity and permittivity of CPs.

2.2.1 Relaxation Effect

An induced dipole moment is observed in a material subjected to an external electrical field. This dipole moment is attributed to non-homogeneous repartition of the electrical charges in the material. Repartition of the electrical charges could correspond to electronic polarisation, atomic polarisation, dipolar polarisation or interfacial polarisation. It has been observed that the dispersion of the complex permittivity is affected by the different polarisations which in turn are dependent upon the frequency and hence the relaxation time. The molecular origins of the relaxation time have been well established for dipolar molecular liquids by Debye [7]. It has been shown that an applied electric field perturbs the orientation distribution of the dipolar molecules resulting in static relative permittivity $\boldsymbol{\varepsilon}_0$ greater than n^2, where n is the optical refractive index. In this section, very brief details of classical models used for describing relaxation time and dispersion of permittivity are presented.

2.2.1.1 Drude's Model

Drude's [8] model is based on free charges and their collisions. This model is particularly used when delocalised electronic states are involved in electrical transport of charges as is observed in metals. Polyaniline (PA), a type of CP is known to present this kind of metallic behaviour. In Drude's model beyond the plasma frequency ω_p of the compound, the dielectric constant becomes positive and remains constant. In contrast, the imaginary part of the dielectric constant continues to decrease and exhibits inverse proportionality to frequency (i.e.$\propto {}^{1}/_{f}$).

2.2.1.2 Diffusive Type Transport Model

This mechanism of electrical conduction is observed in ionic conductors. A gradient of ionic charges is essential for this method of transportation. Jonscher [9] predicts the real and imaginary part of permittivity to be:

$$\varepsilon' \propto \omega^{-1/2}$$
$$\varepsilon'' \propto \omega^{-1/2} \quad \textbf{(2.1)}$$

2.2.1.3 Debye Model

Debye's model was developed for dilute solutions of polar molecules. In this model a dipole with different possible orientations is considered. A dipole which is displaced from its equilibrium state, takes time '$\boldsymbol{\tau}$' (known as the relaxation time) to revert to its state of equilibrium. It has been shown that the complex dielectric constant complies by the law of the type:

$$\varepsilon'(\omega) = \varepsilon_\infty + \frac{\varepsilon_0 - \varepsilon_\infty}{1 + \omega^2\tau^2}$$
$$\varepsilon''(\omega) = (\varepsilon_0 - \varepsilon_\infty)\frac{\omega\tau}{1 + \omega^2\tau^2} \quad \textbf{(2.2)}$$

where $\boldsymbol{\varepsilon_\infty}$ is the permittivity at very high frequency, $\boldsymbol{\varepsilon_0}$ is the static permittivity (at frequency=0), ω is the pulsation frequency and $\boldsymbol{\tau}$ is the relaxation time. A plot between ε' and ε'' is referred to as Cole-Cole diagram [7], where ε' is the real and ε'' is the imaginary part of the complex dielectric constant. The relationship $\varepsilon'' = f(\varepsilon')$ is represented by a semi-circle with the peak indicating the relaxation frequency.

A number of models are derived from the Debye model and some of the best known ones are shown in Table 2.1. The formulas essentially take into account charge hops, probability, relaxation time etc. A complete review on this is available in [9].

Table 2.1: Models derived from Debye's model

Cole and Cole (1941)	$\varepsilon^*(\omega) = \varepsilon_\infty + \frac{\varepsilon_S - \varepsilon_\infty}{1 + (i\omega\tau)^{1-\alpha}}$
Cole and Davidson (1951)	$\varepsilon^*(\omega) = \varepsilon_\infty + \frac{\varepsilon_S - \varepsilon_\infty}{(1 + i\omega\tau)^{1-\beta}}$
Havriliak and Negami (1966)	$\varepsilon^*(\omega) = \varepsilon_\infty + \frac{\varepsilon_S - \varepsilon_\infty}{(1 + (i\omega\tau)^{1-\alpha})^{1-\beta}}$

The models mentioned in Table 2.1 provide majority of dispersion curves for real ε' and imaginary ε'' part of the dielectric constant in insulators. The observed deviation between the ideal curve and those described by these models is often explained by relaxation time or probability jump distribution. The values of α and β in these models are primarily for curve fitting and therefore describe the curve and are not related to material's physical features. The other limitation of these models is that they ignore interactions between dipoles.

2.2.1.4 Dissado Hill model

This model is comparatively more general and takes into account the nature of relaxation phenomena [9]. The salient features of this model are that no parameter distribution function is needed. The model does take into account inter-dipole interactions. Details of the model are beyond the focus of this thesis and could be obtained at [10].

2.2.2 Relaxation Effect in Conducting Polymers

Pioneering work has been done by Jonscher [9] while studying electrical relaxation in dielectrics. This study seeks to analyse the dispersion of conductivity and permittivity by distinctly separating the effects that are attributed to static conditions (DC) from those due to dynamic (AC) conditions. In other words the total conductivity is expressed as:

$$\sigma(\omega) = \sigma_{DC} + \sigma_{AC}(\omega) \quad \textbf{(2.3)}$$

In a similar manner the complex permittivity ($\varepsilon^* = \varepsilon' - i\varepsilon''$) could be considered as having contributions from the conduction and polarisation mechanisms.

$$\varepsilon''(\omega) = \varepsilon''_{conduction} + \varepsilon''_{polarisation} \quad \textbf{(2.4)}$$

where $\varepsilon''_{conduction} = \frac{\sigma_{DC}}{\varepsilon_0 \omega}$ over the whole frequency range, ω is the angular frequency and ε_0 is the free space permittivity. The $\varepsilon''_{polarisation}$ is effected by dipole rotation (or orientation), space charge relaxation and hopping of confined charges.

In real disordered materials such as CPs, conductivity is not constant along the conducting paths and also several relaxation times co-exist. The decay of electric field therefore cannot be described by simple exponential decay function and is given as:

$$E(t) = E_0 \varphi(t) \quad \textbf{(2.5)}$$

where E_0 is the peak applied electric field and the decay function:

$$\varphi(t) = \int_0^\infty exp\left(\frac{-t}{\tau_\sigma}\right) g(\tau_\sigma) d\tau_\sigma \quad \textbf{(2.6)}$$

$g(\tau_\sigma)$ is the normal distribution function for the several relaxation times. William and Watts [11] have used a decay function φ :

$$\varphi(t) = exp\left(\left(\frac{-t}{\tau_0}\right)^\beta\right) \quad \textbf{(2.7)}$$

where τ_0 and β are the relaxation parameter and β a constant with value between $0 \leq \beta \leq 1$ respectively. This function has been extensively used by several authors for describing electric relaxation in ionic conductors and also in polymers.

2.2.3 Skin depth in Conducting Polymers

It is well known that an electromagnetic wave rapidly attenuates in a conducting medium. The depth of penetration of the electric field is of considerable interest in applications such as antennas where the

performance of an antenna is affected by the thickness of the material selected for patch or ground plane. A good understanding of this depth of penetration could be developed by analysing a wave equation in E_y for a plane electric wave in a conducting medium. A solution of this equation, enables determination of depth of penetration in the conducting medium. Using Maxwell's curl equations as a starting point, it is possible to show that for a linearly polarised harmonic wave ($E_y = E_0 e^{i\omega t}$) travelling in the x direction with electric field $\vec{E}$ in the y direction, the governing equation is given by:

$$\frac{\partial^2 E_y}{\partial x^2} - \gamma^2 E_y = 0 \tag{2.8}$$

where γ is the propagation constant and is given by:

$$\gamma^2 = i\omega\mu\sigma - \omega^2\mu\varepsilon^* \qquad \varepsilon^* = \varepsilon' - i\varepsilon'' \tag{2.9}$$

where ε^* is complex permittivity: Hence, (2.9) could be written as:

$$\gamma^2 = i\omega\mu(\sigma + \omega\varepsilon'') - \omega^2\mu\varepsilon' \tag{2.10}$$

The sum of σ and $\omega\varepsilon''$ could be referred to as *equivalent conductivity* σ' [12]. For a conducting medium, where $\sigma' \gg \omega\varepsilon'$ (2.10) reduces to:

$$\gamma^2 \approx i\omega\mu\sigma' \tag{2.11}$$

Therefore:

$$\gamma \approx (1+i)\sqrt{\frac{\omega\mu\sigma'}{2}} \tag{2.12}$$

The skin depth is defined as the $1/e$ depth of penetration and since:

$$E_y = E_0 e^{-\gamma x} \tag{2.13}$$

The attenuation factor is given by:

$$exp\left(-x\sqrt{\frac{\omega\mu\sigma'}{2}}\right) \quad \textbf{(2.14)}$$

Therefore the skin depth δ in the case of CP (or similar conductive materials) may be given by:

$$\delta = \sqrt{\frac{2}{\omega\mu\sigma'}} = \sqrt{\frac{2}{\omega\mu(\sigma + \omega\varepsilon'')}} = \sqrt{\frac{2}{\omega\mu\left(\sigma + \omega\varepsilon''_{polarisation}\right)}} \quad \textbf{(2.15)}$$

where $\varepsilon''_{polarisation}$ could be modelled by Debye model or similar other models. Furthermore, σ in (2.15) is a representation of $\varepsilon''_{conduction} = \sigma_{DC}/\varepsilon_0\omega$. Hence it emerges that the skin depth in the case of CPs with no magnetic losses could be estimated by accurate measurement of DC conductivity and by developing an accurate model of $\varepsilon''_{polarisation}$. As indicated earlier that $\varepsilon''_{polarisation}$ is effected by dipole rotation (or orientation), space charge relaxation and hoping of confined charges. Hence dispersion of AC conductivity and $\varepsilon''_{polarisation}$ are highly dependent on the internal structure and meshing of the polymer chains inside the CPs.

2.3 General Effective Media (GEM): Percolation Theory

The AC and DC conductivity of a large number of conductor-insulator composites have been shown to be a function of volume fraction and frequency [13]. MacLachlan et al. [14], has shown that in a universal percolating system the composite conductivity and volume fraction are given by Two Exponent Phenomenological Percolation Equation (TEPPE):

$$(1-\varphi)\frac{\sigma_i^{1/s} - \sigma_m^{1/s}}{\sigma_i^{1/s} + A\sigma_m^{1/s}} + \varphi\frac{\sigma_c^{1/t} - \sigma_m^{1/t}}{\sigma_c^{1/t} + A\sigma_m^{1/t}} = 0 \quad \textbf{(2.16)}$$

$$A = (1-\varphi_c)/\varphi_c$$

where the composite complex conductivity (σ_m^*) is given by $\sigma_m^* = \sigma_{mr} + i\sigma_{mi}$, the dopant (or conducting component) complex conductivity (σ_c^*) is $\sigma_c^* = \sigma_{cr} +$

$i\sigma_{ci}$ and the polymer matrix (or insulating component) complex conductivity (σ_i^*) is $\sigma_i^* = \sigma_{ir} + i\sigma_{ii}$, φ is the conducting component's volume fraction and φ_c is the critical volume fraction at which the medium (or composite) would undergo an Insulator-Metal Transition (IMT). The exponents s and t best describe the experimental results for the percolation systems. Following two limits are obtained from (2.16):

$$|\sigma_c| \to \infty : \sigma_m = \sigma_i \left(\frac{\varphi_c}{\varphi_c - \varphi}\right)^s \; for\; \varphi < \varphi_c \qquad \textbf{(2.17)}$$

$$|\sigma_i| \to 0 : \; \sigma_m = \sigma_c \left(\frac{\varphi - \varphi_c}{1 - \varphi_c}\right)^t \; for\; \varphi > \varphi_c \qquad \textbf{(2.18)}$$

Equation (2.17) describes the case of a pure conductor with infinite conductivity in the percolating system composite. Likewise Equation (2.18) describes the case where the insulator is perfect insulator with $\sigma_i \to 0$. For the condition $\varphi > \varphi_c$, $\sigma_{mr} > \sigma_{mi}$, while for the condition, $\varphi < \varphi_c$, $\sigma_{mr} \ll \sigma_{mi}$. The typical value of t indicated in [15] is taken to be 1.7 for three dimensional conductivity. However, MacLachlan also states in [13] that factors determining the values of s, t, and percolation threshold φ_c are still being researched for more accurate formulation.

2.4 Prigodin's Resonant Quantum Tunnelling Model

The structure of CP is very complex. As shown in Figure 2.2, it is an inter-woven mesh of polymer fibres. In polyaniline (PANI) and polypyrrole (PPy) these polymer chains are arranged in a complex manner, forming crystalline regions (metallic islands) where these chains are regularly and densely packed. Elsewhere in the CP, it is a mesh of randomly running polymer fibres. These metallic islands are nanometres in size and are coupled to each other through twisted and tangled polymer fibres with low or nil conductivity. Prigodin et al. [1] states that due to high molecular weight, a single polymer chain at best can cross only a few crystalline regions. Further it is the inter-chain coupling within the crystalline domains that is important rather than the overall arrangement of such domains for the transport property of the material as a whole. It is important to distinguish this structure from a

"metallic grains in an amorphous poorly conducting matrix structure". The peculiarities of CP structure have been listed in [1] and are reproduced here for better understanding of the Prigodin et al. [1] proposed transportation mechanism: (i) The polymer chains running between various metal dots (or islands) is essentially of quantum size. Hence energy levels within the grains are quantized. (ii) Shape of the grain cannot be described in simple geometric terms. (iii) The coupling between the metal islands is due to their interconnections through polymer chains. This implies that coupling is not restricted to "field of view" type but could also include the affects of far off connected metal islands. (iv) The shape and size of the metal grains and their coupling fluctuates over the system.

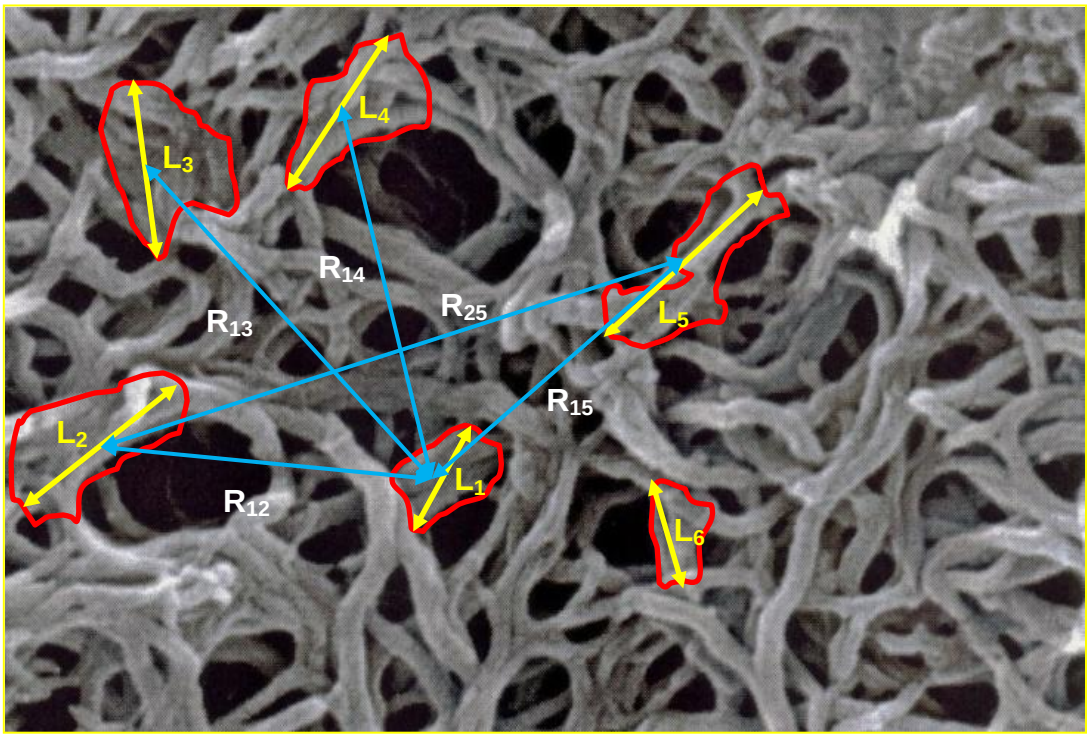

Figure 2.2: Complex inter-woven structure of CP with metallic grains. Where L_i (i=1,2,3 etc) indicates the size of a metal island or grain (typically L~5nm) and R_{ij} (i=1,2 j=1,2,3,etc) indicates the distance between the centers of neighbouring grains.

Prigodin et al. [1] also states that the fraction of crystalline region is strongly dependent on the synthesis method and is generally found to vary from a few percent to up to about 50%. It therefore emerges that in the region of weak inter-grain coupling the system is in the insulator phase and when inter-grain coupling is strong the system is in the metallic phase. Hence there exists a

critical coupling between grains for the system to undergo Insulator-Metal Transition (IMT).

2.4.1 Computation of AC and DC Conductivity in CP

The present discussions on AC and DC conductivities will be restricted to very low frequencies such as $\omega\tau_T \ll 1$ where τ_T is the "Thouless" time of diffusive spreading over a metallic grain. In addition, it will also be assumed that the CP system is in the metallic phase and the system is far away from the IMT($\varphi > \varphi_c$). Based on Einstein's charge mobility equation, the macroscopic DC conductivity given by [2] in the metallic phase is:

$$\sigma_m(0) = (e^2 g)\left(\frac{N_\perp}{z}\right)\left(\frac{1}{R}\right) \qquad \textbf{(2.19)}$$

where, in a broad sense, the first brackets indicates conductivity of a single polymer chain-link, the second bracket indicates the total number of such chain links between neighbouring grains and the third bracket indicates the periodicity of such grains over the entire network. The electrical charge of an electron is indicated by e, the transmission coefficient of chain-links across grains is g, and it is assumed that the grains have $N_\perp$ chains densely packed over $N_\parallel$ repeat units yielding $N_\perp \times N_\parallel$ units cells in each grain. In other words $\frac{N_\perp}{z}$ indicates the number of chains interconnecting two neighbouring grains, where the number of nearest neighbouring grains is z. The mean distance between neighbouring grains is R. The critical transmission coefficient resulting in IMT is given by g_c and is defined by the following condition:

$$2N_\perp g_c = 1 \qquad \textbf{(2.20)}$$

Further it is pertinent to mention here that if the chain link transmission coefficient 'g' is such that $g < g_c$, the CP system behaves like a dielectric and if the CP is in the metallic phase then $g > g_c$. In certain CPs the critical transmission coefficient g_c is of the order of 10^{-2}. In the metallic phase of the CP, the electrons are delocalised over the

network of grains and is a quantum process described by the mean transition frequency W. Furthermore, the anticipated resonance tunnelling in metallic polymers shows a delay determined by the resonance level width γ. For resonance tunnelling the frequency dependent transmission coefficient $g = g(\omega)$ is based on the generalisation of Bright-Wigner formula [16]:

$$g(\omega) = \left[1 - {}^{i\omega}/_{\gamma}\right]^{-1} \qquad \textbf{(2.21)}$$

The low frequency relaxation time τ_1 is related to the width of resonance level γ by $\tau_1 = {}^{1}/_{\gamma}$. In the region where $\omega \ll W$ (since inter-grain hopping is a quantum process, W is the mean hopping frequency), the AC conductivity is expressed by the standard Drude's formula:

$$\sigma_m(\omega) = \frac{1}{4\pi}\left(\frac{\omega_p^2 \tau_1}{1 - i\omega\tau_1}\right) \qquad \textbf{(2.22)}$$

where ω_p is the plasma frequency, determined by quantum inter-grain hops. Figure 2.3 shows the variation of $g(\omega)$ with frequency. The variation shown in this figures is restricted to $\omega \ll W$ region. Prigodin et al. [1] also goes on to show that in the low frequency region described above, CP behaves like a Drude metal with anomalously long relaxation times and very small plasma frequency. The permittivity of the CP in this region is negative.

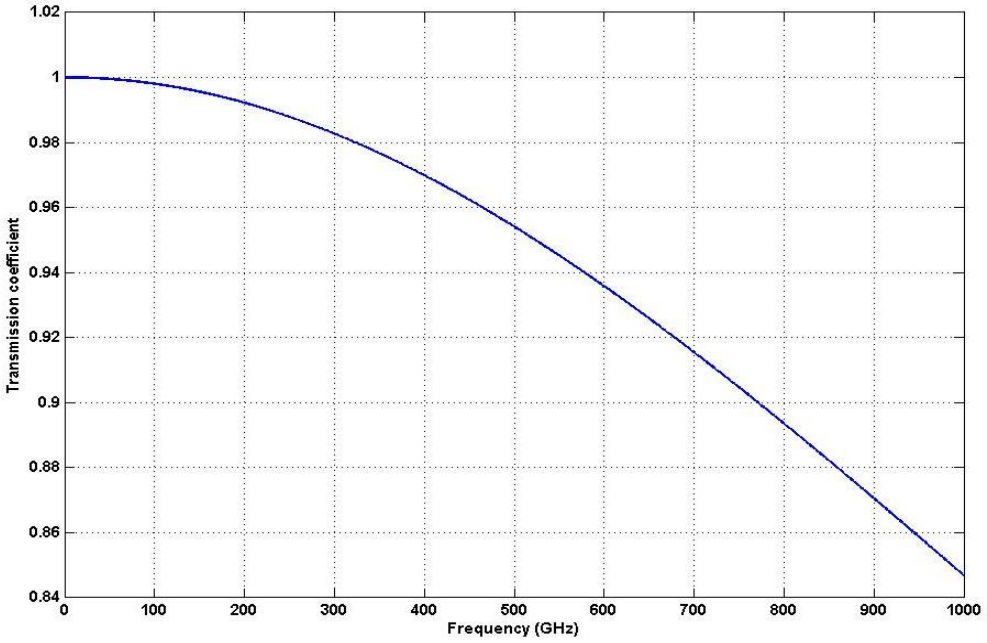

Figure 2.3: Variation of transmission coefficient ($g(\omega)$) with frequency

2.5 Proposed Model for CP conductivity and permittivity

In the design of re-configurable CP based antennas, it is envisaged that dynamic changes in the electrical conductivity of CP components (such as patches, shorting wires etc) are essentially going to contribute towards overall changes in antenna performance. These changes in the CP conductivity at the lowest level would be due to changes in dopant concentration and the frequency of operation. Interestingly, material science literature associated with electrical conductivity in CPs describes the variation in electrical conductivity with dopant concentration and with frequency as two different phenomena. This is understandable from the perspective of material science where variation in electrical conductivity with frequency for a fixed dopant concentration in CP or variation in electrical conductivity for a "*given frequency*" of operation with different dopant concentrations, appear to be more likely practical scenarios. In this section therefore an attempt is made to propose a model that could describe the variation in electrical conductivity in CPs with respect to both the frequency and the dopant concentration. This

model would therefore be more suitable to applications associated with re-configurable planar antennas.

CPs are essentially binary percolating system, where the polymer backbone acts as the path along which the dopant ions ride and provide for the interesting electrical properties. The quantum size of the polymer chains and the inclusion of dopant do indeed affect the quantized energy states of the polymer. The interactions are at the quantum level and manifest at the macroscopic level in the form of bulk properties of conductivity and permittivity.

In order to develop a model that is consistent both at the macroscopic and the quantum level, it is essential certain assumptions are made for its relevance. To that extent, if we are to consider (2.18) of the GEM theory, we need to accept that: (i) the insulator component is a perfect lossless insulator and (ii) the binary composite mixture is far away from IMT. This means that the polymer matrix is such that it has no intrinsic conductivity. Next, considering (2.19) within the above mentioned constraints, the resonance quantum tunnelling model also describes the DC bulk conductivity of such a composite binary mixture. It is assumed here that: (i) the number of inter-grain chain links and metallic grains are dependent on the process of synthesis. (ii) They do not change with change in volume fraction of dopant concentration. It therefore emerges that (2.18) and (2.19) both are describing the same DC bulk conductivity, which implies that:

$$g = \frac{\sigma_c}{e^2}\left(\frac{\varphi - \varphi_c}{1 - \varphi_c}\right)^{1/t}\left(\frac{N_\perp}{z}\right)^{-1}\left(\frac{1}{R}\right)^{-1} \qquad \textbf{(2.23)}$$

The frequency dependent transmission coefficient $g = g(\omega)$ for resonance tunnelling is given by a generalisation of the Bright-Wigner formula:

$$g(\omega) = \left[1 - \frac{i\omega}{\gamma}\right]^{-1} \qquad \textbf{(2.24)}$$

It could be deduced from Bright-Wigner formula (2.24) that under the limiting condition $\omega \to 0$ or in the region where $\omega\tau_1 \ll 1$, the transmission coefficient g is such that:

$$\lim_{\omega \to 0} g(\omega) = 1 \qquad \textbf{(2.25)}$$

If this limiting value of transmission coefficient g is applied to the DC conductivity $\sigma(0)$ equation at (2.19), it would imply that:

$$\sigma(0) = e^2 \left(\frac{N_\perp}{z}\right)\left(\frac{1}{R}\right) \qquad \textbf{(2.26)}$$

Equation (2.26) indicates that the DC conductivity is independent of the dopant concentration, which implies that for any given volume fraction of dopant concentration, the bulk DC conductivity of the composite mixture will remain the same. The only possible way it could vary would be by changing the synthesis process. This is contrary to results shown in [13, 17]. Hence it would not be wrong to consider the transmission coefficient g to be a function of both dopant concentration and the frequency of operation $g = f(\varphi, \omega)$.This implies that transmission coefficient under a given process of synthesis of CP does vary with volume fraction concentration of the dopant and also with the frequency of operation. Hence it emerges that (2.) needs to be reconsidered as:

$$\sigma_m(0) = \left(e^2 g(\varphi, 0)\right)\left(\frac{N_\perp}{z}\right)\left(\frac{1}{R}\right) \qquad \textbf{(2.27)}$$

From (2.23) and (2.24) it may be conjectured (with a degree of approximation and purely for mathematical simplicity) that the transmission coefficient g is affected independently by both dopant concentration and frequency. In other words:

$$g(\varphi, \omega) = g(\varphi)g(\omega) \qquad \textbf{(2.28)}$$

where $g(\varphi), g(\omega)$ are not the same functions and are also not same as $g(\varphi, \omega)$. It is important to mention here that this needs to be validated against suitable experimentation. From (2.23), (2.24) and (2.28) it follows that:

$$g(\varphi, \omega) = \frac{\sigma_c}{e^2}\left(\frac{\varphi - \varphi_c}{1 - \varphi_c}\right)^{1/t}\left(\frac{N_\perp}{z}\right)^{-1}\left(\frac{1}{R}\right)^{-1}\left(1 - \frac{i\omega}{\gamma}\right)^{-1} \qquad \textbf{(2.29)}$$

In the region where $\ll W$, $\sigma_m(\omega)$ could be written in the standard Drude form:

$$\sigma_m(\omega) = \left(\frac{1}{4\pi}\right)\left(\frac{\omega_p^2\tau_1}{1 - i\omega\tau_1}\right) = \left(\frac{1}{4\pi}\right)\omega_p^2\tau_1 g(\omega) \qquad \textbf{(2.30)}$$

with ω_p being *"the plasma frequency"*, which is determined by the frequency of intergrain hops W. The relaxation time $\tau_1 = {}^1/_\gamma$ is determined by the Wigner transmission time. It emerges from the discussion above that assuming constant temperature, the transmission coefficient of the inter-grain chain links is a function of both frequency and volume fraction of the percolating component $= f(\varphi, \omega)$. This implies that:

$$g(\varphi, \omega) = \kappa\frac{\sigma_c}{e^2}\left(\frac{\varphi - \varphi_c}{1 - \varphi_c}\right)^{{}^1/_t}\left(\frac{N_\perp}{z}\right)^{-1}\left(\frac{1}{R}\right)^{-1}\left(1 - \frac{i\omega}{\gamma}\right)^{-1} \qquad \textbf{(2.31)}$$

where κ the constant of proportionality and its value needs to be ascertained from experimentation. Finally, the DC and AC bulk conductivities of the binary composite mixture could be expressed as:

$$\sigma_m(0) = \left(e^2 g(\varphi, 0)\right)\left(\frac{N_\perp}{z}\right)\left(\frac{1}{R}\right) \qquad \textbf{(2.32)}$$

and

$$\sigma_m(\omega) = \left(\frac{1}{4\pi}\right)\omega_p^2\tau_1 g(\varphi_0, \omega) \qquad \textbf{(2.33)}$$

where φ_0 is the fixed dopant concentration in the CP complex.

2.6 Conclusion

We consider Prigodin's resonance tunneling model to be specific to CP and it appears very attractive for modelling the AC and DC conductivities of doped polymer materials. However, in situations where there is dynamic doping and de-doping process of the polymer system, the suggested model is inadequate. In contrast GEM-percolation theory has general applicability for any percolating systems. We have shown that integration of the two models could be achieved, under certain constraints of reasonable assumptions. The

integrated model provides good understanding of AC and DC conductivities of CP, both at the quantum and the macro level. Furthermore, the proposed model promises to provide a method of predicting the conductivity of the CP based on variation in dopant concentration and frequency of operation. The final applicability of model would depend on validation against extensive experimentation. This could not be achieved in this thesis; however it is an important task for succeeding in developing reconfigurable CP based planar antennas.

References

[1] V. N. Prigodin and A. J. Epstein, "Nature of Insulator-metal transition and novel mechanism of charge transport in the metallic state of highly doped electronic polymers," *Synthetic Metals,* vol. 125, pp. 43-53, 2002.

[2] V. N. Prigodin and A. J. Epstein, "Quantum Hopping in metallic Polymers," *Physica B,* vol. 338, pp. 310-317, 2003.

[3] D. Stauffer, *Introduction to Percolation Theory*. London: Taylor and Francis, 1985.

[4] D. S. MacLachlan, "An equation for the conductivity of binary mixtures with anisotropic grain structures," *Journal of Physics: Solid State Physics,* vol. 20, pp. 865-877, 1987.

[5] R. Peierls, *Quantum Theory of Solids*: Oxford: Clarendon Press, 1955.

[6] H. A. Jahn and E. Teller, "Stability of Polyatomic molecules in degenerate electronic states. I. Orbital degeneracy," *Proceedings of Royal Society of London Series-A-Mathematical and Physical Sciences,* vol. 161, pp. 220-235, Jul 1937.

[7] A. R. Von Hippel, *Dielectrics and Waves*. New York: John Wiley, 1954.

[8] P. Drude, "Zur Elektronentheorie der Metalle," *Annalen der Physik,* vol. 306, pp. 566-613, 1900.

[9] A. K. Jonscher, *Dielectric Relaxation in Solids*. London: Chelsea Dielectrics Press, 1983.

[10] L. A. Dissado and R. M. Hill, "Non-Exponential Decay in Dielectrics and Dynamics of Correlated Systems," *Nature,* vol. 279, pp. 685-689, 1979.

[11] G. William and D. C. Watts, "Non-symmeterical Dielectric Relaxation Behaviour arising from a simple Empirical Decay Function," *Transactions of the Faraday Society,* vol. 66, p. 80, 1970.

[12] J. D. Kraus and K. R. Carver, *Electromagnetics*. Tokyo: McGraw Hill, 1981.

[13] D. S. MacLachlan, C. Chiteme, C. Park, K. E. Wise, S. E. Lowther, P. T. Lillehei, E. J. Siochi, and J. S. Harrison, "AC and DC Percolative Conductivity of Single Wall Carbon Nanotube Polymer Composites," *Journal of Polymer Science: Part B: Polymer physics,* vol. 43, pp. 3273-3287, 2005.

[14] D. S. MacLachlan, G. Sauti, and C. Chiteme, "Static Dielectric Function and scaling of the AC conductivity for Universal and non-universal percolation systems," *Physica Review B,* vol. 76, pp. 014201-1-014201-13, 06 Jul 2007.

[15] D. S. MacLachlan, "The Complex Permittivity of Emulsions: An Effective Media-percolation Equation," *Solid State Communications,* vol. 72, pp. 831-834, 1989.

[16] C. S. Bolton-Heaton, C. J. Lambert, V. I. Falko, V. N. Prigodin, and A. J. Epstein, "Distribution of time constants for tunneling through a one-dimensional disordered chain," *Physics Review B,* vol. 60, p. 10569, Oct 1999.

[17] T. A. Ezquerra, F. Kremer, M. Mohammadi, J. Ruhe, G. Wegner, and B. Wessling, "AC Conductivity measurements in Polymeric insulator conductor systems," *Synthetic metals,* vol. 28, pp. 83-88, 1989 1989.

Chapter 3

Building Microstrip Antennas with Polypyrrole

3.1 Introduction

Microstrip antennas have been extensively studied because they have the advantages of low cost and weight, design maturity and robustness, reproducibility, and ease of construction and installation. The performance of the antenna depends to a great extent on the intrinsic properties of the fabrication materials. In the past, numerous attempts have been made to fabricate microstrip antennas using alternative materials to copper. These efforts have been focused towards using materials for the top radiating element that have high conductivity. Solberg Jr. et al. [1], [2] used a Conducting Polymer (CP) composite to build a non-planar direction finding antenna operating in the frequency range of 30 MHz to 1 GHz. Chen [3] has used polyester foil as the substrate for a microstrip antenna. Rmili et al. [4] have reported fabricating a rectangular microstrip patch antenna with the radiating element made of Polyaniline (PANI), a CP having a bulk DC conductivity of 6000 S/m. Cichos et al. [5] have tried using polymeric film with silver flakes for designing low cost RFID coil antennas.

As indicated before, conductive polymers are emerging as one of the most important materials with very interesting optical, electrical and mechanical properties. Their conductivity lies between that of an insulator and known metallic conductors such as copper. CPs are usually classified as the cation salts of highly conjugated polymers, which are obtained by electrochemical oxidation and electro-chemical polymerization or chemical redox reactions. The most interesting feature of CPs is their ability to transit from an insulating state to a highly conductive state on external stimulus.

Furthermore it was also mentioned, that unlike metals, polymers do not have free conduction electrons to contribute towards very high electrical conductivities as observed in metals. Most electrical conduction in polymers is through overlapping π molecular orbits, when one or more π electrons are removed from the polymer chain. Trends in the available literature on CPs are suggestive of very high bulk conductivity. A number of technologies are feeling the impact of these new materials, such as: polymeric batteries [6, 7], photovoltaics [8], electro-chromic devices [7] and ion selective membranes [9], EMI shields [10-13], radar absorbers [14-16], electrical wires [17], corrosion inhibitors [7, 8], bio-sensors [9], and electrochemical actuators (or artificial muscles) [18].

In this chapter we explore the possibility of using polypyrrole (PPy) as the ground plane in a planar microstrip Cu-patch antenna. The possibility of using a CP patch in a planar microstrip microwave antenna is also investigated. The problem of determining the electrical properties of unknown materials is also addressed by deploying indirect methods, such as through identification of the resonance of a microstrip patch antenna, for estimating the electrical properties of unknown materials. Further, the research in this work is also constrained to Polypyrrole and PEDOT CPs due to ease of availability and inherent stability of these materials over other CPs such as PA, PT etc.

3.2 Polypyrrole Free standing Film Preparation

The PPy film for the antenna patch was obtained from The Defence Science and Technology Organization (DSTO) in Melbourne, Australia. It was prepared in accordance with the procedure indicated by Truong et al. [19]; i.e. by conducting electrochemical polymerization in an aqueous solution. Sodium *p*-toluene sulphonate (*p*-TS) was used as the dopant. The polymerization solution contained freshly distilled pyrrole (0.1 M) and the above-mentioned dopants (0.1 M) in distilled water. Electrodes of stainless steel were used for growing the film in a nitrogen environment. A current density of 2.8 mA/cm^2 was passed through the solution for about 2 hours. The films obtained by the above procedure were 120 μm thick and were washed in acetonitrile/water (1:1 solution) to remove excess dopant. The films were then allowed to dry. Using the four-probe technique, the DC conductivity of the film sample was

measured as 2000 S/m. PPy films obtained from this process were used in the ensuing studies on PPy ground plane and patches for microwave microstrip patch antennas.

3.3 A Polypyrrole Ground-plane for 11 GHz Patch Antenna

3.3.1 Antenna Design

The configuration of the rectangular microstrip antenna used in this study is shown in Figure 3.1. The antenna was fabricated on a FR-4 substrate of thickness 0.8 mm (h1). FR-4 is an epoxy substrate with reinforced glass (Manufacturer: Satcam). Instead of a metallic ground plane, a film of PPy with conductivity of 2000 S/m was pasted on the under-surface of another FR-4 substrate of thickness 1.6mm (h2). The film was pasted by using epoxy adhesive. The thickness of the PPy film was about 330 μm, which is far greater than the skin depth (δ~107.3 μm) at 11 GHz for a conductivity of 2000 S/m. The top radiating element of copper and therefore there is no problem in attaching a direct co-axial feed for the patch. A picture of the fabricated 11 GHz patch antenna is shown in Figure 3.2.

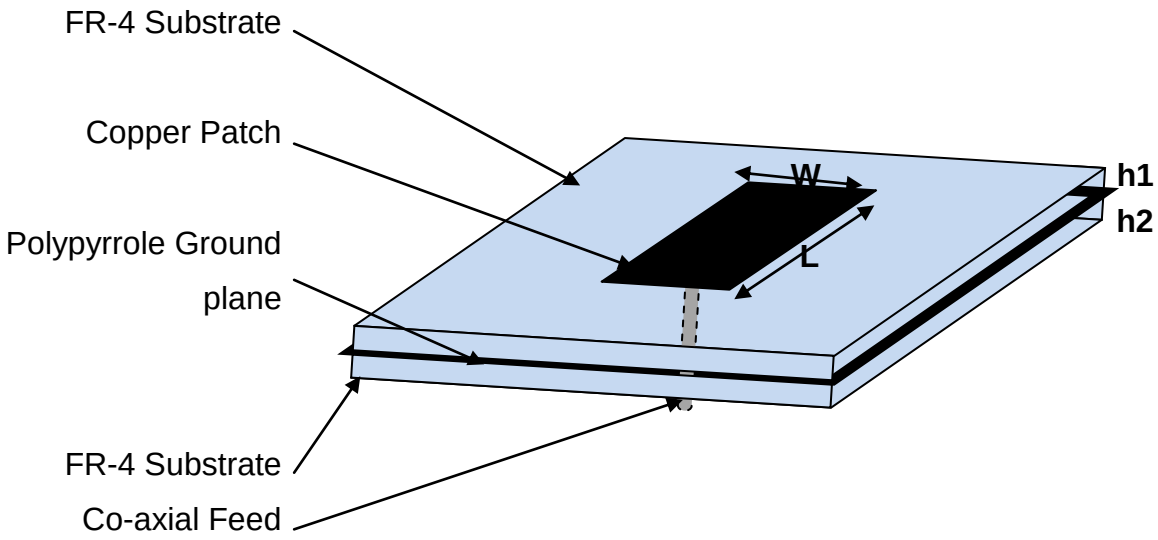

Figure 3.1: Schematic layout of MPA with Polypyrrole ground plane

Figure 3.2: Photograph of 11 GHz patch antenna with polypyrrole ground plane

The centre pin of the SMA connector was soldered to the radiating patch, while the jacket of the SMA connector was pasted to the PPy ground plane by using silver-loaded epoxy adhesive. The design was realised using CST™ Microwave Studio to optimize the length, width of the antenna and the location of the co-axial feed for good impedance matching. The design data are indicated at Table 3.1. The CST™ optimised 11 GHz MPA parameters are indicated at Table 3.2.

Table 3.1: Design Data for Substrate and PPy Ground plane

Parameters	Values
Substrate	**FR-4**
➢ Substrate Thickness	0.8mm
➢ Permittivity ϵ_r	4.9
➢ Loss Tangent (tanδ)	Assumed loss free
Ground Plane	**Polypyrrole (PPy) Film**
➢ Film thickness	330μm
➢ Conductivity (S/m)	2000
➢ Permittivity ϵ_r	10-j10

Table 3.2: Design Data for 11 GHz Rectangular Microstrip Patch Antenna

Parameters	Values
Patch Length 'L'	11.74 mm
Patch Width 'W'	5.96mm
Co-axial feed location (from centre of patch)	2.27mm

A similar microstrip antenna with copper ground plane was fabricated for comparison of performance. However, some differences with respect to the PPy ground plane antenna are notable, viz.:

- The copper cladding of FR-4 board, used for ground plane is about 17 μm thick, as against the PPy ground plane of 330 μm thickness.
- The copper ground plane did not require any pasting on the board.
- The SMA connector was soldered at both points, i.e. at the centre pin and at the grounded jacket. This resulted in superior electrical connectivity than pasting with conductive adhesive.

3.3.2 Modelling Polypyrrole for Simulation

The accuracy of the results presented by the simulated design depends greatly on the accuracy of material simulation. In this case, it was important to be able to simulate the dispersion properties of PPy film over 8 to 16 GHz (the frequency range of excitation signal for the simulated antenna with PPy ground plane).

3.3.3 Simulation Results

CST™ Microwave Studio was used for simulating a rectangular microstrip antenna with PPy as the ground plane. Electrical parameters such as relative permittivity and AC conductivity of PPy material were modelled based on equations (3.1) and (3.2).

$$\sigma(\omega) = \left(e^2 g(\varphi, \omega)\right)\left(\frac{N_\perp}{z}\right)\left(\frac{1}{R}\right) \qquad \textbf{(3.1)}$$

$$\varepsilon(\omega) = 1 - a\frac{\Omega_p^2\tau^2}{1+(\omega\tau)^2} \quad \textbf{(3.2)}$$

Equation (3.1) has been derived by combining two different models viz. General Effective Media (GEM)-percolation theory [20-22] and Prigodin's quantum resonance tunnelling model [23]. The details of the proposed model are described in section 2.5, chapter 2 (as equation (2.27)). In equation (3.1) σ is the AC conductivity, e is the electronic charge of an electron, $g(\phi,\omega)$ is the transmission coefficient, $N_\perp$ is the number of chains densely packed over repeat units of the polymer,$\frac{N_\perp}{z}$ indicates the number of chains interconnecting two neighbouring grains, and R is the mean distance between neighbouring grains. In (3.2) $\varepsilon(\omega)$ is permittivity, a is a factor whose value depends on the frequency of operation (a is generally 1 for $\omega\tau > 1$), Ω_p is the unscreened plasma frequency, τ is the relaxation time and ω is the angular frequency. Marten et al. [24], through experimentation has shown that for $\omega \ll \Omega_p$, the complex permittivity is negative and could be approximated as $\varepsilon(\omega) \approx -a\left(\frac{\Omega_p}{\omega}\right)^2$.

The planar antenna simulation used 0.8 mm thick FR-4 substrate for building the antenna. Copper cladding on the under-surface of the substrate was totally removed. A PPy layer of thickness 330 μm with DC conductivity of 2000 S/m was used as the ground plane instead. It is pertinent to mention here that the pasting of PPy layer to the substrate (FR-4) was not simulated. The relative permittivity of the PPy layer was measured at 11 GHz to be 10-j10, ($\epsilon_r = 10$) using a Split Post Dielectric Resonator (SPDR). The SPDR measurements were undertaken at James Cook University. Since no data on dispersion of conductivity was available, measured DC conductivity of 2000 S/m was used as conductivity of PPy sample at 11 GHz.

A similar design was used for simulating a copper-based microstrip antenna. The copper ground plane was of 17 μm. In both the cases, a coaxial feed was used. The comparison of the simulated return loss between PPy and copper ground plane against frequency is presented in Figure 3.3. The maximum return loss for the PPy-ground plane antenna with conductivity of 2000 S/m is about 14.21 dB at 10.65 GHz, while that of a copper ground plane

($\sigma = 5.8 \times 10^7$ S/m) is about 11.53 dB at 10.88 GHz. Interestingly, a broadening of bandwidth (at - 10dB, S11) is observed in the microstrip antenna whilst using PPy as the ground plane. The Q factor for PPy antenna is observed to be smaller than that of Cu antenna. This is because PPy is lossier than Cu.

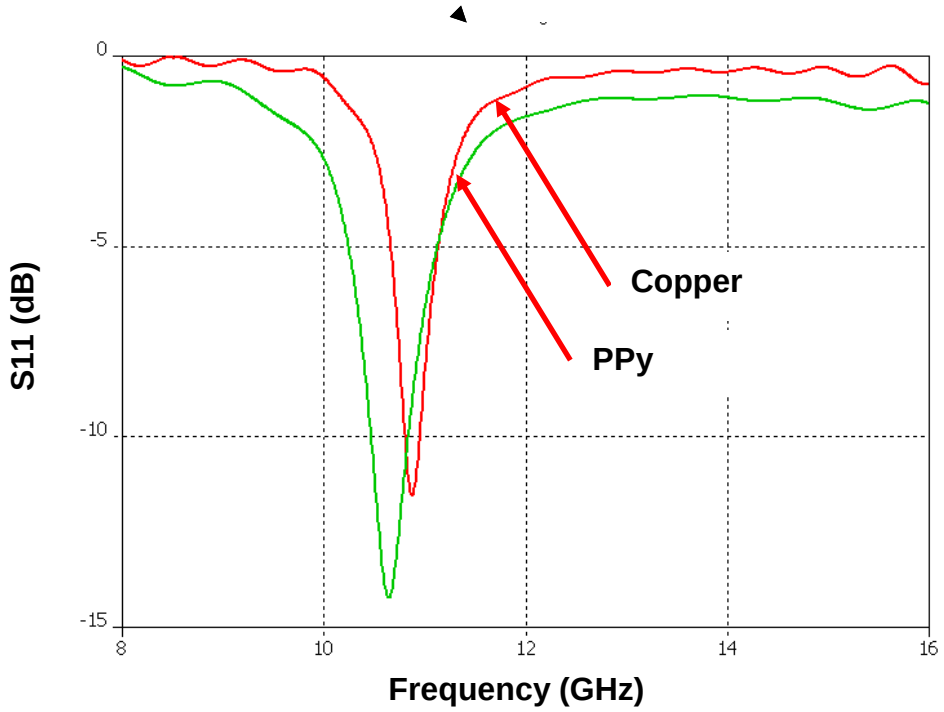

Figure 3.3: Simulated return loss versus frequency for PPy and copper ground

3.3.4 Preliminary Trials

3.3.4.1 Microstrip patch antenna with PPy ground plane

Some preliminary trials with a microstrip antenna on FR-4 substrate with PPy film as ground plane have been undertaken at 6 GHz. The results of these initial trials were very discouraging because of high substrate losses and suspected low conductivity of PPy film. However the trials showed that skin depth is an important consideration for effective utilization of CPs in antennas at microwave frequencies. Experimental results at 11 GHz were also fraught with fabrication errors and it was hard to conclusively accept or reject the possibility of using CPs such as Polypyrrole, Polyaniline and PEDOT as antennas in the microwave region.

3.3.4.2 Optically transparent microstrip patch antenna with Orgacon™ films

An optically transparent Microstrip Patch Antenna (MPA) operating at 2 GHz has been built using Orgacon™ Conducting Polymer (CP) films from Agfa. These films have a coating of PEDOT (Poly 3, 4-ethylenedioxthiophene), a type of conducting polymer on PET substrate of thickness 125 μm. Orgacon™ films [25] used for building this antenna, have a DC conductivity of 50000S/m (skin depth at 2GHz: 89.2μm; surface resistance <347Ω/sq; Orgacon film data [25]). Interestingly these films provide about 85.44% Visual Light Transmission (VLT) at 550 nm. Simons and Lee [26] have previously reported building an optically transparent MPA for 2.3 and 19.5 GHz. Their work is based on using a thin sheet of polyester as substrate with AgHT-8 (conductive silver) as an optically transparent conductive coating on the substrate. The reported surface resistance of the AgHT-8 is about 6-10Ω/sq and the AgHT-8 coated polyester film has about 82% VLT at 600nm[27]. The picture of the constructed optically transparent antenna is shown in Figure 3.4

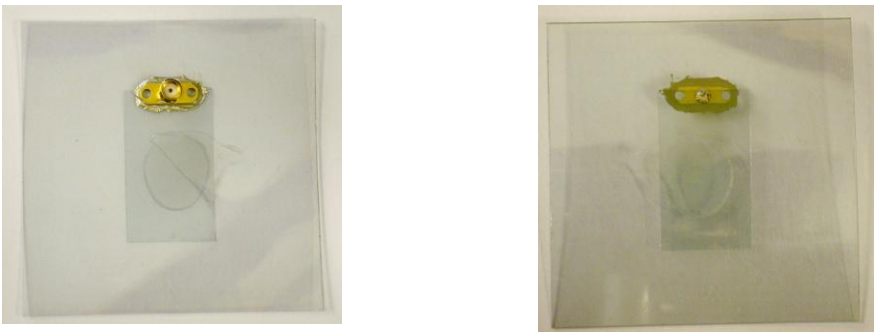

Figure 3.4 Orgacon™ film based 2 GHz microstrip patch antennas. Bottom and top views of the antenna and its SMA connector.

The initial trial results were not very encouraging due to a number of possible reasons. The Orgacon™ film was very thin (~100 nm) despite its conductivity being relatively high. The PET substrate was not perfectly flat and that made electrical integrity of SMA connector doubtful. Furthermore, the samples obtained from the OEM were too limited in quantity. It was therefore decided that further experimentation with the material should be undertaken later after refining our simulation ability of the material.

3.3.5 Sumary

The initial experimental results were inconclusive in regards to whether PPy-based ground plane in a microwave antenna could be realized and also on the possibility of developing an optically transparent antennas. However, these initial experiments highlighted the fabrication and measurement difficulties this project was likely to face. Furthermore, low conductivity (2000 S/m) of the PPy stand alone film being used as ground plane, was also a matter of concern for frequencies below 6 GHz. Accurate measurement of AC conductivity of the PPy film at 6 and 11 GHz and permittivity of the multi-layer antenna structure were pertinent design issues that needed resolving. The results were not very successful due to a number of issues such as: (a) Difficulty in modelling thin films in EM simulation software; (b) Getting good impedance matching due to actual fabrication issues, especially at 11 GHz; (c) Establishing a good comparison between designs with different metal ground planes and their fabricated antennas.

Despite the setback, the PPy materials currently being developed (in the lab environment) have conductivities as high as 20,000 S/m [9]. In our opinion this greatly enhances the possibility of using these materials for making bio-degradable organic antennas for various radar, bio-medical and communications applications.

3.4 A 2 GHz polypyrrole Patch antenna on Plexiglas™ Substrate

In this section we explore the possibility of using Polypyrrole (PPy) film as a radiating patch for antenna application at microwave frequencies, in particular as the resonant patch of a planar Microstrip Patch Antenna (MPA). This investigation is a first step towards a better understanding of the numerical simulation, design and fabrication issues associated with antennas using these materials for various future applications.

3.4.1 Antenna Design

The selection of Plexiglas™ as a substrate for this antenna was on the premise that a successful antenna design on Plexiglas™ could lead to development of some interesting low-cost conformal and planar future designs, including optically transparent microwave antennas. The fabricated Cu and PPy-patch MPA are shown in Figure 3.5.

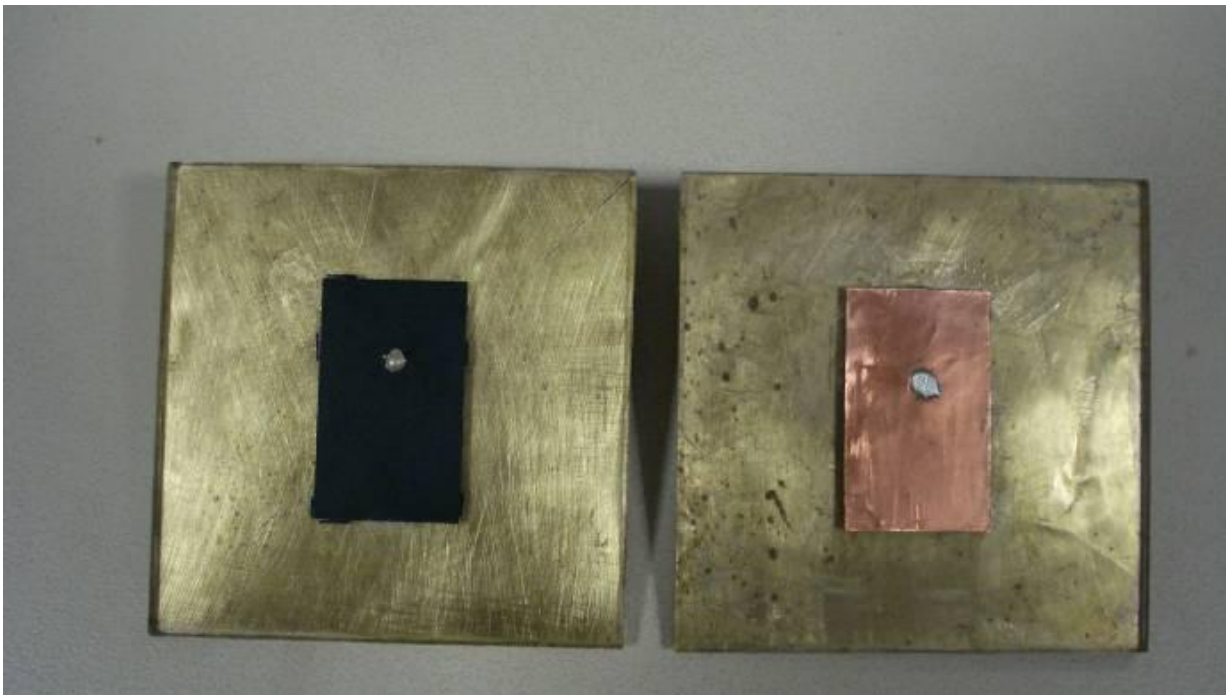

Figure 3.5: PPy (left) and Cu (right) MPAs on Plexiglas™ substrate

The permittivity of Plexiglas™ substrate at microwave frequencies is not accurately available from the manufacturer's data sheets and therefore an indirect approach for determining permittivity was adopted [28]. The schematic

diagram in Figure 3.6 shows the configuration of the patch antenna used in this study. An identical Cu-patch antenna was fabricated as reference.

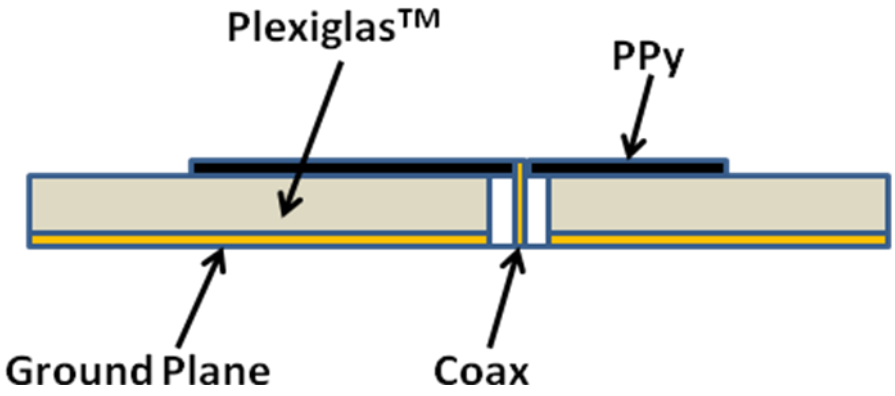

Figure 3.6: A cross sectional view of the MPA.

3.4.1.1 Determination of permittivity of Plexiglas™

The relative permittivity value of Plexiglas™ indicated in the literature varies from 2.4 to 3.7. As the material library of the electromagnetic simulation tool CST™ indicates a relative permittivity value of 3.4 for Plexiglas™, initial design and simulations were made using this value. Actual measurements on a reference Cu-MPA indicated a large discrepancy between the resonance frequencies of the simulated and measured results (as shown in Figure 3.7). Adjustment to permittivity and loss tangent (tan δ) value of Plexiglas™ used in simulations was undertaken towards matching of the measured Cu-MPA results. Through this process, which involved the first two resonances of the patch, the Plexiglas's permittivity was estimated to be 2.5, with a loss tangent of 0.001. This permittivity value for the substrate was taken as a basis for the design of the PPy-MPA. The accurate match of simulated and measured results subsequently obtained for the designed PPy-MPA (as shown in Figure 3.8) further validated the permittivity value of 2.5 and $\tan\delta$ = 0.001 for the Plexiglas™ substrate.

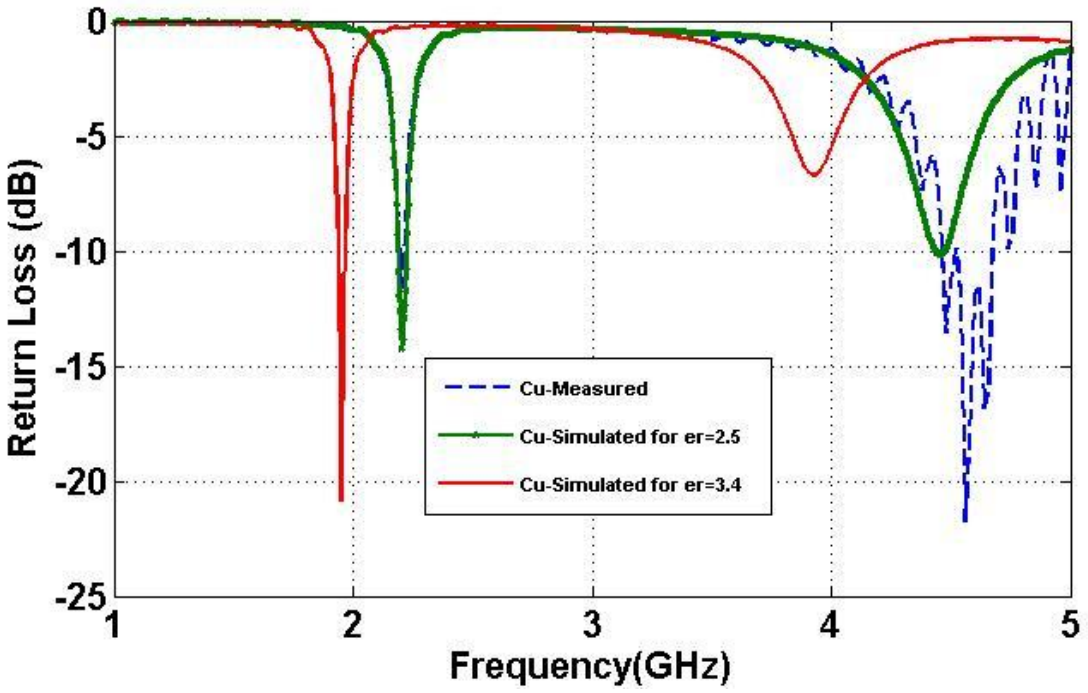

Figure 3.7: Simulated (CST™) and measured return loss of Cu MPA on Plexiglas™ substrate for different permittivity values.

3.4.1.2 Simulation and Design optimisation

The effect of the patch thickness for less conductive material (such as PPy) is an important consideration in this design. Most antenna designers would consider a couple of skin depths thickness for PPy (or similar less conductive material) patch as essential. However, two key questions that need to be considered here are: (1) How to simulate thin materials using EM simulators (such as CST^{TM} and HFSS^{TM}); (2) what is the minimum fraction of skin depth for the patch (of less conductive material) that could be used for acceptable antenna performance. An in-depth investigation of these questions will be the focus of further study. At present, it is important to state that initial simulations in this work were undertaken by assuming zero thickness of the patches. PPy was simulated as a sheet with finite conductivity of 2000 S/m. This approach is in contrast to the earlier approach in section 3.3.2 to simulate the CP permittivity over a range of frequencies. MPAs are high Q resonators and therefore at the frequency of interest, the material properties could be assumed as constant. Furthermore at this stage of research, it was

exploratory work to determine whether a PPy antenna at microwave frequency is feasible.

The Cu and PPy MPA designs were separately optimized for good impedance matching using CST^{TM} and HFSS^{TM}. The optimized design parameter values are indicated in Table 3.3.

Table-3.3: Design data for Copper and PPy Microstrip Patch Antenna

Parameters	Copper-MPA	PPy-MPA
Substrate		
• **Thickness**	3mm	3mm
• **Estimated ϵ_r**	2.5	2.5
• **Estimated tanδ**	0.001	0.001
• **Dimensions**	80x80mm	80x80mm
Patch		
• **Length**	40.1mm	40.1mm
• **Width**	24.46mm	24.46mm
Coaxial Feed		
• **Off center**	4.0mm	6.67mm

3.4.2 Experimental Results

The return loss measured on the PPy antenna is presented in Figure 3.8 together with the predicted curves from both simulation tools used. The good agreement in terms of resonant frequencies and associated bandwidths validate the design procedure, including the determination of the material parameter of the Plexiglas™ substrate.

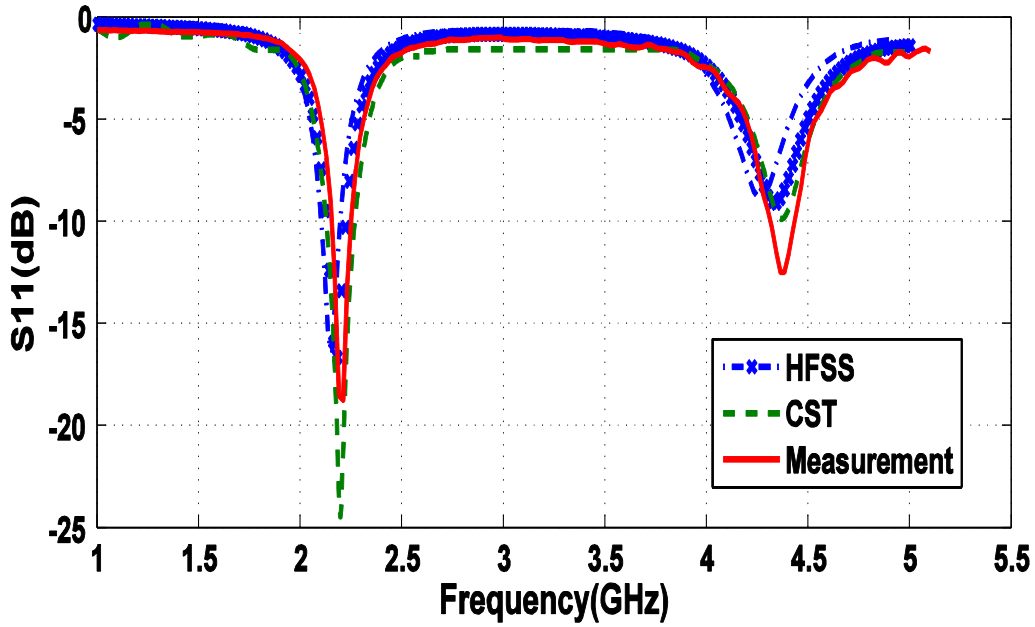

Figure 3.8: Simulated and measured return loss for PPy-MPA.

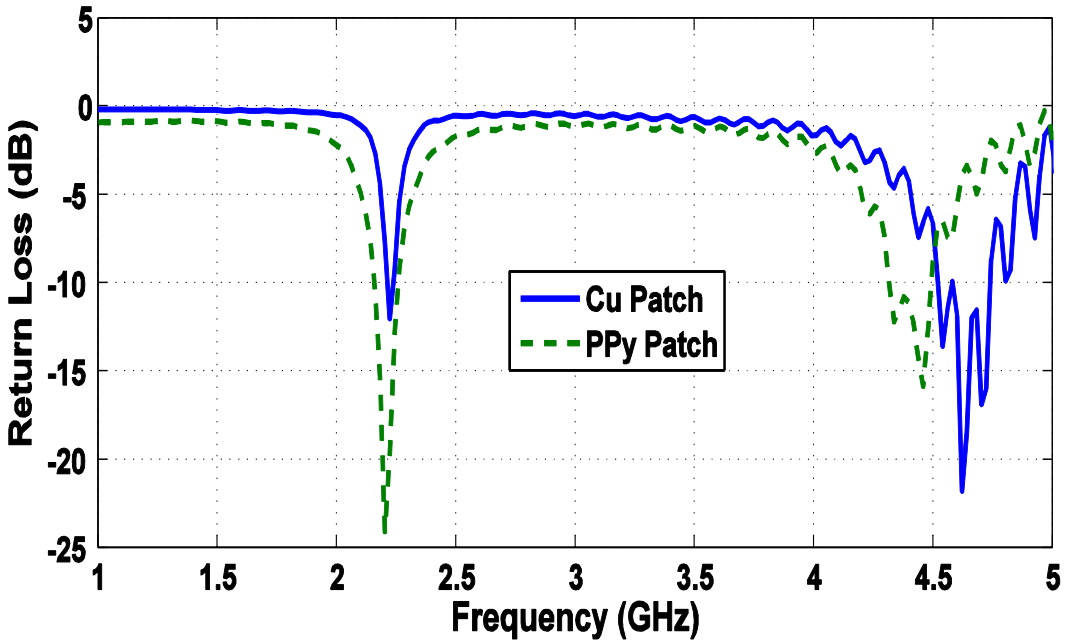

Figure 3.9: Comparison between measured return loss for Cu and PPy-MPA.

A direct comparison of the return loss from the PPy antenna and the Cu antenna is shown in Figure 3.9. The observed differences in the S11 plots of PPy in Figure 3.8 and 3.9 are due to number of points used for plotting the measurements. The Cu-patch MPA is resonant at 2.2 GHz, while the PPy-patch MPA has a resonance frequency of 2.18 GHz with a -10 dB BW of about 100 MHz or 4.5%. Considering that the Cu-MPA

was designed using an inaccurate substrate permittivity, and that it was primarily used as tool for estimating permittivity of Plexiglas™, it is clear that the high return loss observed in Cu-MPA (Figure 3.7 and Figure 3.9) is due to a poor input impedance match. The consistency of the results is further validated by the comparison of the shape of the measured and simulated radiation pattern of Cu-MPA shown in Figure 3.10. The discrepancy between the curves is attributed to fabrication imperfections.

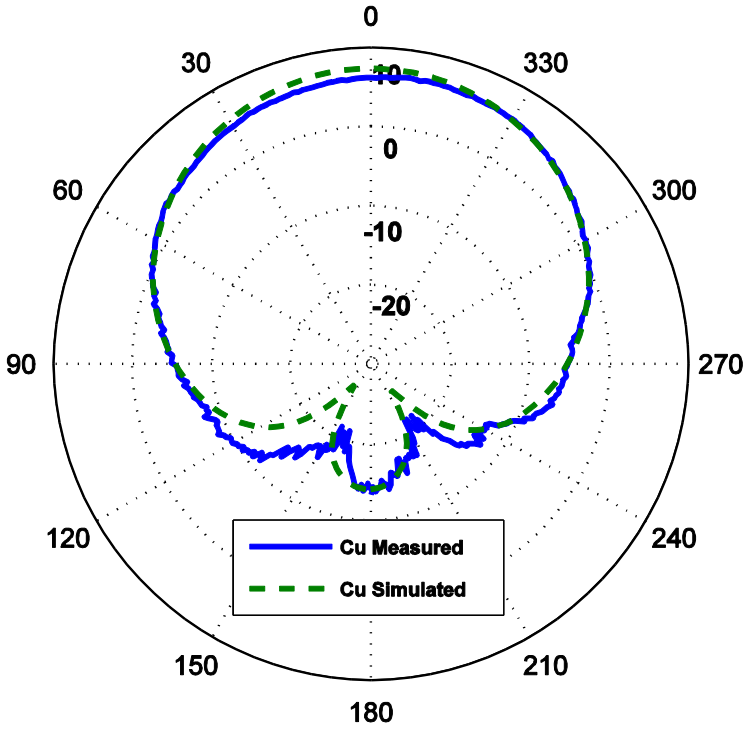

Figure 3.10: Simulated (CST™) and measured E-plane radiation pattern for 2 GHz Cu-MPA.

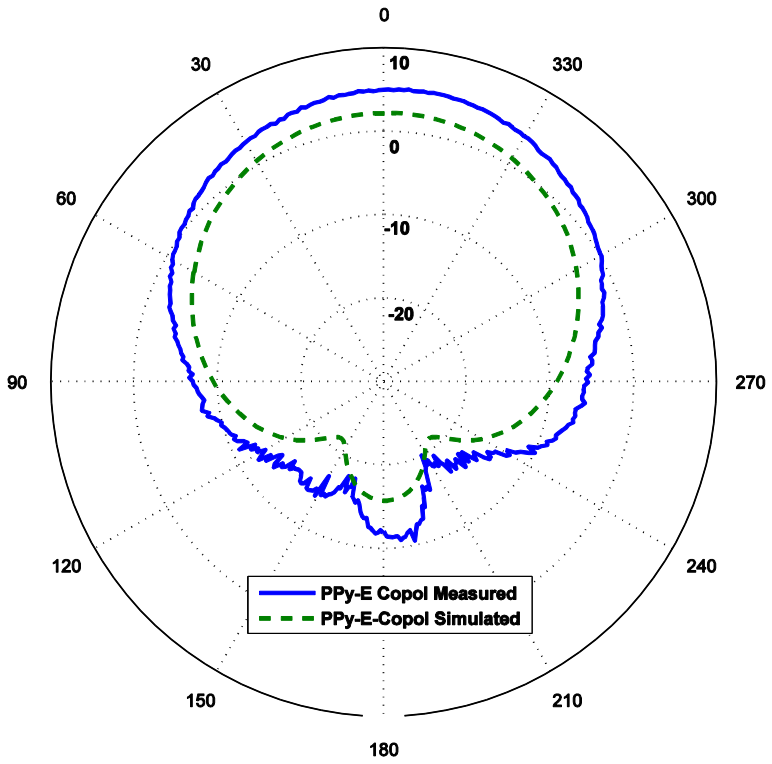

Figure 3.11: Simulated (CST™) and measured E-plane radiation pattern for 2 GHz PPy-MPA.

Results for the PPy-MPA as presented in Figure 3.11 indicate that the simulated results are quite consistent with measured results in terms of the overall shape of the radiation patterns. However, measured results shown in Figure 3.11 indicate a higher overall gain as against those indicated by simulation. It is suspected that this may be due to higher actual conductivity of the PPy patch at 2 GHz as against DC conductivity of 2000 S/m used in simulation.

The measured E and H-plane co- and cross-polarized patterns of the Cu and PPy patch antenna are presented in Figure 3.12 and Figure 3.13 respectively.

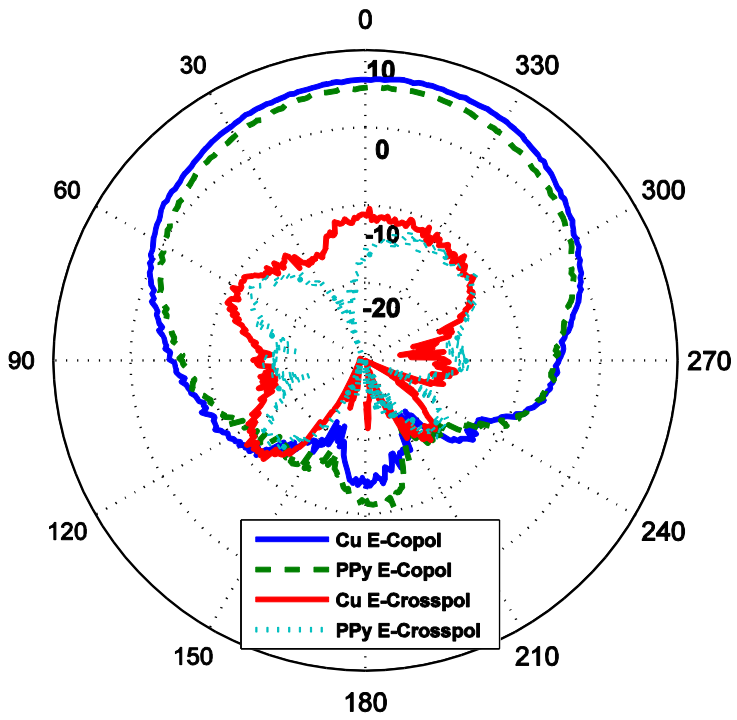

Figure 3.12: E-plane Co-pol and Cross-pol radiation pattern measurements for 2 GHz Cu and PPy MPA.

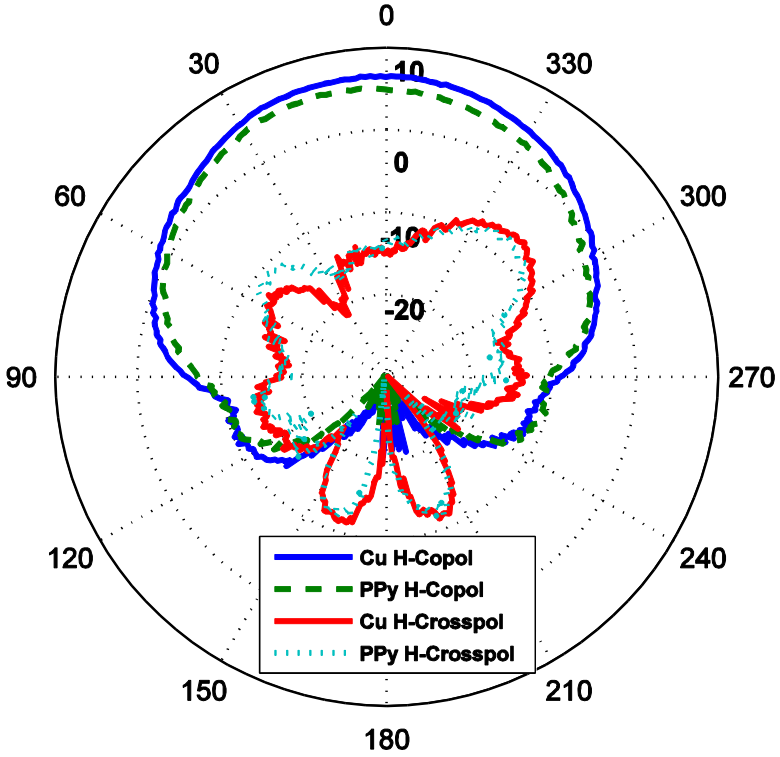

Figure 3.13: H-plane Co-pol and Cross-pol radiation pattern measurements for 2 GHz Cu and PPy MPA.

On the basis of above measurement data, the simulated radiation efficiency of the Cu MPA is estimated to be around 80%, most of the losses being attributed to the dielectric losses in the substrate. The efficiency is reduced to a value of around 62% by replacing the Cu patch by the less conductive PPy material.

3.4.3 Discussions

Construction of a MPA using a less conductive material (such as PPy) on a non-standard substrate (such as Plexiglas™) has some interesting design aspects from the point of view of patch thickness (e.g. skin depth), fabrication issues and characterization of permittivity of substrate.

The computed value of skin depth for a patch with a DC conductivity of 2000 S/m at 2 GHz is 251.6 μm, which is about twice the thickness of the PPy patch used in the MPA. However, it is important to consider that the mechanism of electrical conduction and dispersion of electrical conductivity in CPs is different from that of metals [29]. Epstein et al. [29] has also described in detail the mechanism of conduction and its dispersion with frequency in CPs. The observed performance of the PPy-MPA in this work is suggestive of an increase in bulk AC conductivity of the patch with frequency.

Current literature [30] on PPy indicates DC conductivities up to 20,000 S/m, which would noticeably improve the performance reported in this section. Furthermore, other CPs such as PEDOT, PANI and PA can provide much higher conductivity than PPy and therefore may be used as good alternatives. However, designs techniques with relatively low-conductivity materials and their associated fabrication issues need further investigation.

3.4.4 Summary

In this section, results of a CP based MPA on a non-standard substrate such as Plexiglas™ have been presented. The results of PPy patch were compared with an identical Cu MPA used as reference. The obtained performances indicate that a PPy based microwave antenna is feasible. It is further emphasized that the MPA design, as a resonant structure, provides a good tool for understanding exotic materials.

Enhancement in our understanding of the microwave properties of CP materials could eventually lead to their usage in a range of passive microwave circuits in the future.

3.5 Conclusions

In this chapter we have investigated the possibility of using Polypyrrole (PPy) film as a ground plane and also as a radiating patch for antenna application at microwave frequencies. The results clearly indicate that, despite the PPy film having low conductivity (2000 S/m) and its thickness (120 μm) being less than the desired skin depth thickness (251.6 μm) at 2 GHz, it is possible to realize adequate microwave antennas with these materials.

In the next chapter, we shall investigate further on the effect of CP patch thickness and conductivity on the microwave antenna performance. We will seek answers for questions such as: what is the minimum patch thickness and conductivity for acceptable performance of a microwave planar antenna?

References

[1] R. F. Solberg Jr and P. J. Siemsen, "Development of a conductive polymer composite direction finding antenna," *Antennas and Propagation Society International Symposium*, vol. 3, pp. 1966-1969, 11 Jul 1999.

[2] R. F. Solberg Jr, S. P. Saulnier, D. D. Winnie, C. K. Baker, P. J. Siemsen, and C. H. Parr, "Polymer composite direction finding antenna," USA Patent, 2001.

[3] Chen and Yung-Shun, "Conducting antenna structure consisting of a thin plastic polyester foil substrate.," Germany Patent DE 20 2006 016 626 U1, 2006.

[4] H. Rmili, J. L. Miane, H. Zangar, and T. Olinga, "Design of microstrip fed proximity-coupled conducting polymer patch antenna," *Microwave and Optical Technology letters*, vol. 48, pp. 655-660, Apr 2006.

[5] S. Cichos, J. Haberland, and H. Reichl, "Performance analysis of polymer based antenna-coils for RFID," in *IEEE Polytronic conference*, 2002, pp. 120-124.

[6] C. Pratt. (30 Nov 2006). *Applications of conducting polymers* [Internet]. Available: http://homepage.ntlworld.com/colin.pratt/appleap.htm

[7] J. D. Stenger-Smith, "Intrinisically electrically conducting polymers, synthesis, characterization, and their applications," *Progress in Polymer Science*, vol. 23, pp. 57-79, 1998.

[8] S. Kirchmeyer and L. Brassat. (2005, May 2007). *Intrinsically Conductive Polymers*. Available: http://www.clevios.com/medien/dokumente/document_ConductiveCoating.Instrinsicallyconductivepolymers.pdf

[9] N. Gomez and E. S. Christine, "Conducting Polymers in Biomedical Engineering," *Progress in Polymer Science*, vol. 32, pp. 876-921, 2007.

[10] J. Joo and A. J. Epstein, "Electromagnetic radiation shielding by intrinsically conducting polymers," *Applied Physics Letters*, vol. 65, pp. 2278-2280, 1994.

[11] J. L. Wojkiewicz, S. Fauveaux, N. Redon, and J. L. Miane, "High electromagnetic shielding effectiveness of polyaniline-polyurethane composites in microwave band," *International Journal of Applied Electromagnetics and Mechanics*, vol. 19, pp. 203-206, 2004.

[12] A. Barnes, A. Despotakis, P. V. Wright, T. C. P. Wong, B. Chambers, and A. P. Anderson, "Control of microwave reflectivities of polymer electrolyte-silver-polyaniline composite materials," *Electrochimica Acta*, vol. 43, pp. 1629-1632, 1998.

[13] E. Hakansson, A. Amiet, and A. Kaynak, "Electromagnetic shielding properties of polypyrrole/polyester composites in the 1-18 GHz frequency range," *Synthetic Metals*, vol. 156, pp. 917-925, 2006.

[14] V. T. Truong, S. Z. Riddell, and R. F. Muscat, "Polypyrrole based microwave absorbers," *Journal of Materials Science*, vol. 33, pp. 4971-4976, 1998.

[15] T. C. P. Wong, B. Chambers, A. P. Anderson, and P. V. Wright, " Fabrication and evaluation of conducting polymer composites as radar absorbers," *Antennas and Propagation, 1993., Eighth International Conference on*, vol. 2, pp. 934-937, 1993.

[16] T. C. P. Wong, B. Chambers, A. P. Anderson, and P. V. Wright, "Large area conducting polymer composites and their use in microwave absorbing material," *Electronics Letters*, vol. 28, pp. 1651-1653, 13 Aug 1992.

[17] M. Rabinowitz, "Power Systems of the Future (Part 3)," *IEEE Power Engineering Review May 2000*, pp. 21-24, May 2000.

[18] B. Xi, "Novel Conducting Polymer Structures for Electrochemical Actuators," PhD, Department of Chemistry, University of Wollongong, Wollongong, 2005.

[19] V. T. Truong and J. G. Ternan, "Complex conductivity of a conducting polymer at microwave frequencies," *Polymer*, vol. 36, pp. 905-909, 1995.

[20] D. S. MacLachlan, C. Chiteme, C. Park, K. E. Wise, S. E. Lowther, P. T. Lillehei, E. J. Siochi, and J. S. Harrison, "AC and DC Percolative Conductivity of Single Wall Carbon Nanotube Polymer Composites," *Journal of Polymer Science: Part B: Polymer physics*, vol. 43, pp. 3273-3287, 2005.

[21] D. S. MacLachlan, G. Sauti, and C. Chiteme, "Static Dielectric Function and scaling of the AC conductivity for Universal and non-universal percolation systems," *Physica Review B*, vol. 76, pp. 014201-1-014201-13, 06 Jul 2007.

[22] D. S. MacLachlan, "The Complex Permittivity of Emulsions: An Effective Media-percolation Equation," *Solid State Communications*, vol. 72, pp. 831-834, 1989.

[23] V. N. Prigodin and A. J. Epstein, "Nature of Insulator-metal transition and novel mechanism of charge transport in the metallic state of highly doped electronic polymers," *Synthetic Metals*, vol. 125, pp. 43-53, 2002.

[24] H. C. F. Martens, J. A. Reedijk, H. B. Brom, D. M. de Leeuw, and R. Menon, "Metallic state in disordered quasi-one-dimensional conductors," *Physical Review B*, vol. 63, pp. 073203-1-073203-4, 2001.

[25] Agfa. (2008, 23 Oct 2008). *Orgacon™ Electronic Materials* [Internet]. Available: http://www.agfa.com/en/sp/solutions/orgacon_electronic_materials/index.jsp

[26] N. R. Simons and R. Q. Lee, "Feasibility study of optically Transparent Microstrip Patch Antenna," *Antennas and Propagation Society International Symposium 1997*, vol. 4, pp. 2100-2103, 1997.

[27] I. P. Ltd. (23 Oct 08). *Conductive Silver Coated Films AgHT* [Internet]. Available: http://www.instrumentplastics.co.uk/products_cscf.php

[28] M. Bogosanovich, "Microstrip patch sensor for measurement of the permittivity of homogenous dielectric materials," *IEEE Transactions on Instrumentation and Measurement*, vol. 49, pp. 1144-1148, Oct 2000.

[29] A. J. Epstein and V. N. Prigodin, "Low-dimensional Variable Range Hopping in Conducting Polymers," *Synthetic Metals*, vol. 117, pp. 9-13, 2001.

[30] P. Chandrasekhar, *Conducting Polymers, Fundamentals and Applications: A practical Approach*. Boston: Kluwer Academic Publishers, 1999.

Chapter 4

Radiation Efficiency in Conducting Polymer based Patch Antennas

4.1 Introduction

In this chapter the focus is towards establishing a good understanding of the effect of CP patch thickness and its conductivity on overall antenna efficiency. The purpose is to clearly understand the relationship between the patch thickness, its conductivity and the achievable radiation efficiency. This will help in predicting *a priori*, conductivity levels needed for a given thickness of polymer film to be able to radiate as an antenna with acceptable efficiency, or alternatively, determining the required film thickness for the available conductivity needed for an acceptable antenna performance.

The study presented in this chapter has been undertaken in two phases. In the first phase four different PPy based antennas were fabricated on FR-4 substrate to operate in the 4.5 GHz region. These antennas have been made from films developed using the same manufacturing process and with 2000 S/m DC conductivity, but have four different thicknesses. In the second phase of the study, PPy and PEDOT based patch antennas were fabricated on Roger's Ultralam™ 2000 substrate to operate at 6 GHz. These antennas have patches that are made from different CPs and are based on different fabrication techniques. In addition the patches have different thicknesses and conductivities. The PPy patches have DC conductivity of 2000 S/m while PEDOT based patches have 10000 S/m DC conductivity.

In the previous chapter it was established that CP based films provided acceptable antenna performance despite the patch film thickness being lesser than one skin depth. In this chapter, the intention is also to explore the

limitations associated with patch thickness for a given level of conductivity on the overall antenna performance.

4.2 A Study of Radiation Efficiency in PPy based 4.5 GHz MPA

In this section, the first stage of the study, based on 4.5 GHz microstrip patch antenna is presented. Four microstrip patch antennas were fabricated on FR-4 substrate, using patches made from PPy stand-alone film of different thicknesses. The DC conductivity of all the PPy based patches was 2000 S/m. The thicknesses of the PPy films range between 40 and 140 μm and were accurately determined by using a Scanning Electron Microscope (SEM).

The PPy film for the antenna patch was obtained from The Defence Science and Technology Organization (DSTO) in Melbourne, Australia. It was prepared in accordance with the procedure indicated by Truong et al. [1]; i.e. by conducting electrochemical polymerisation in an aqueous solution. Sodium *p*-toluene sulphonate (*p*-TS) was used as dopant.

4.2.1 Antenna Design

Four PPy patch and one equivalent Cu-patch antenna were fabricated on FR-4 substrate. Examples of fabricated Cu and PPy-patch MPA are shown in Figure 4.1.

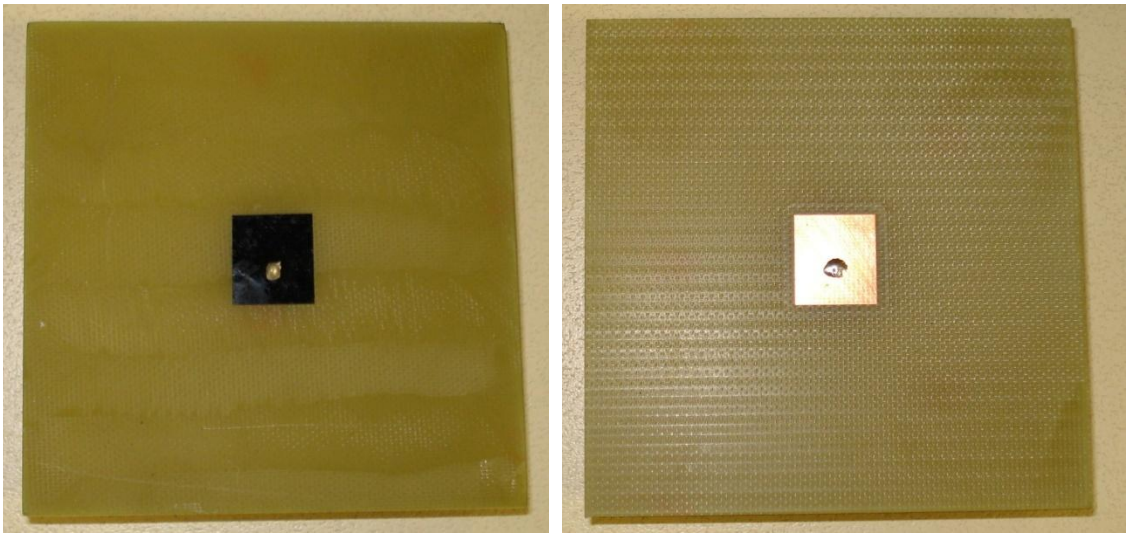

Figure 4.1: (a) PPy Patch Antenna (b) Cu-Patch Antenna on FR-4 substrate

The permittivity of FR-4 substrate at microwave frequencies is not accurately available from the manufacturer's data sheets and it varies from panel to panel of FR-4. An indirect approach was therefore applied for determining the permittivity of FR-4 at the frequency of interest (i.e. 4.5 GHz). The schematic diagram in Figure 4.2 shows the configuration of the probe-fed patch antenna used in this study. An identical Cu-patch antenna was also fabricated for reference.

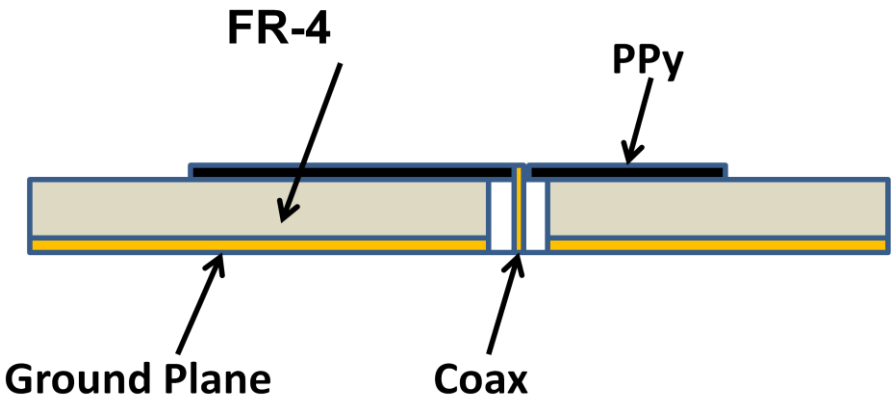

Figure 4.2: A cross sectional view of MPA

4.2.1.1 Determination of permittivity of FR-4 substrate

The relative permittivity value of FR-4 indicated in the literature varies from 4.0 to 4.9. The material library of the electromagnetic simulation tool CST^{TM} indicates the relative permittivity value of FR-4 to be 4.9, while the HFSS simulation material library indicates a value of 4.4. Initial design and simulations were made using this latter value. Actual measurements on a reference Cu-patch antenna indicated a large discrepancy between the resonance frequencies of the simulated and measured results. As described earlier in chapter 3, an adjustment to permittivity and loss tangent (tan δ) value of FR-4 used in simulations was undertaken towards matching of the measured reference Cu-patch antenna results. Through this process, the FR-4's permittivity was estimated to be 4.1, with a loss tangent of 0.001(Figure 4.3).

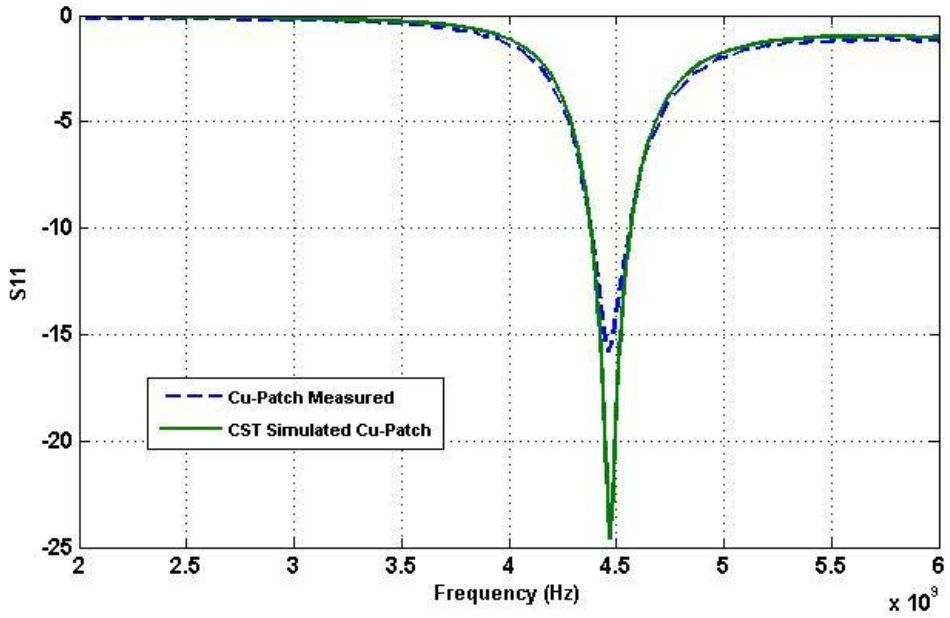

Figure 4.3: Simulated and measured S11 for a Cu-Patch antenna on a FR-4 substrate with permittivity ε_r = 4.1

This permittivity value for the substrate was taken as a basis for the design of the four PPy-patch antennas on FR-4 substrate. The accurate match between simulation and measurement results for the designed PPy-patch antennas (Figure 4.4) further validated the permittivity value of 4.1 and tanδ = 0.001 for the FR-4 substrate. Minor discrepancies observed are due to inaccuracies of hand fabrication. Similar further simulations and measured results are placed in Appendix B.

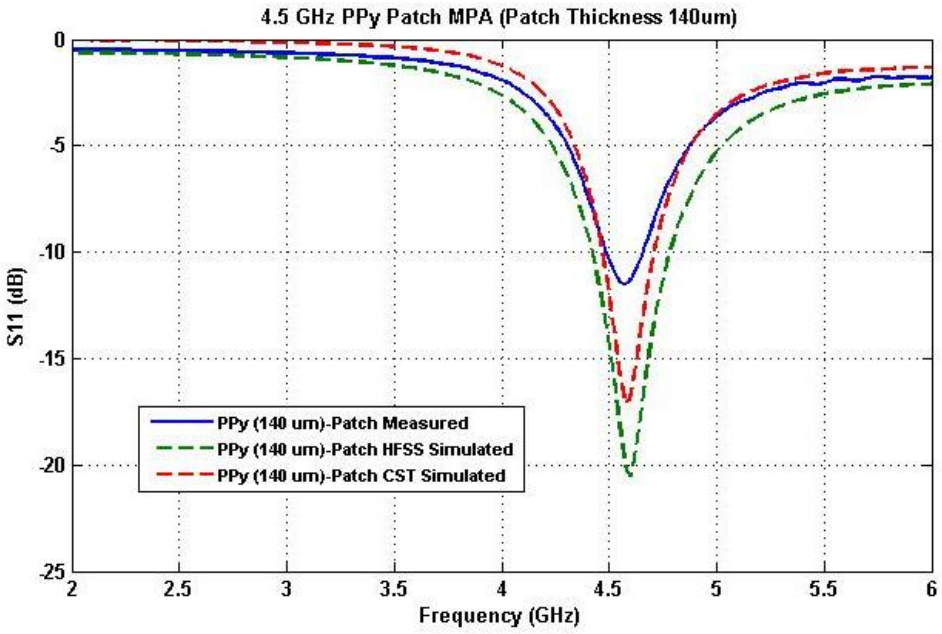

Figure 4.4: Simulated and measured S11 for a PPy (140 μm) -Patch antenna on a FR-4 substrate with permittivity ε_r = 4.1

Four different thickness of PPy film were used in the fabrication of the PPy-patch antenna on FR-4 substrate of 3.2 mm thickness. The Scanning Electron Microscope (SEM) Philips XL 30 (shown in Figure 4.5) was used for accurate determination of the thickness of the stand-alone PPy films. The SEM pictures of the PPy samples used in this study are shown in Figure 4.6.

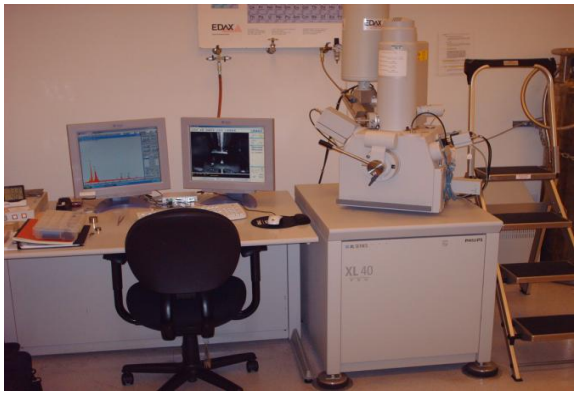

Figure 4.5: Philips XL 30 Scanning Electron Microscope

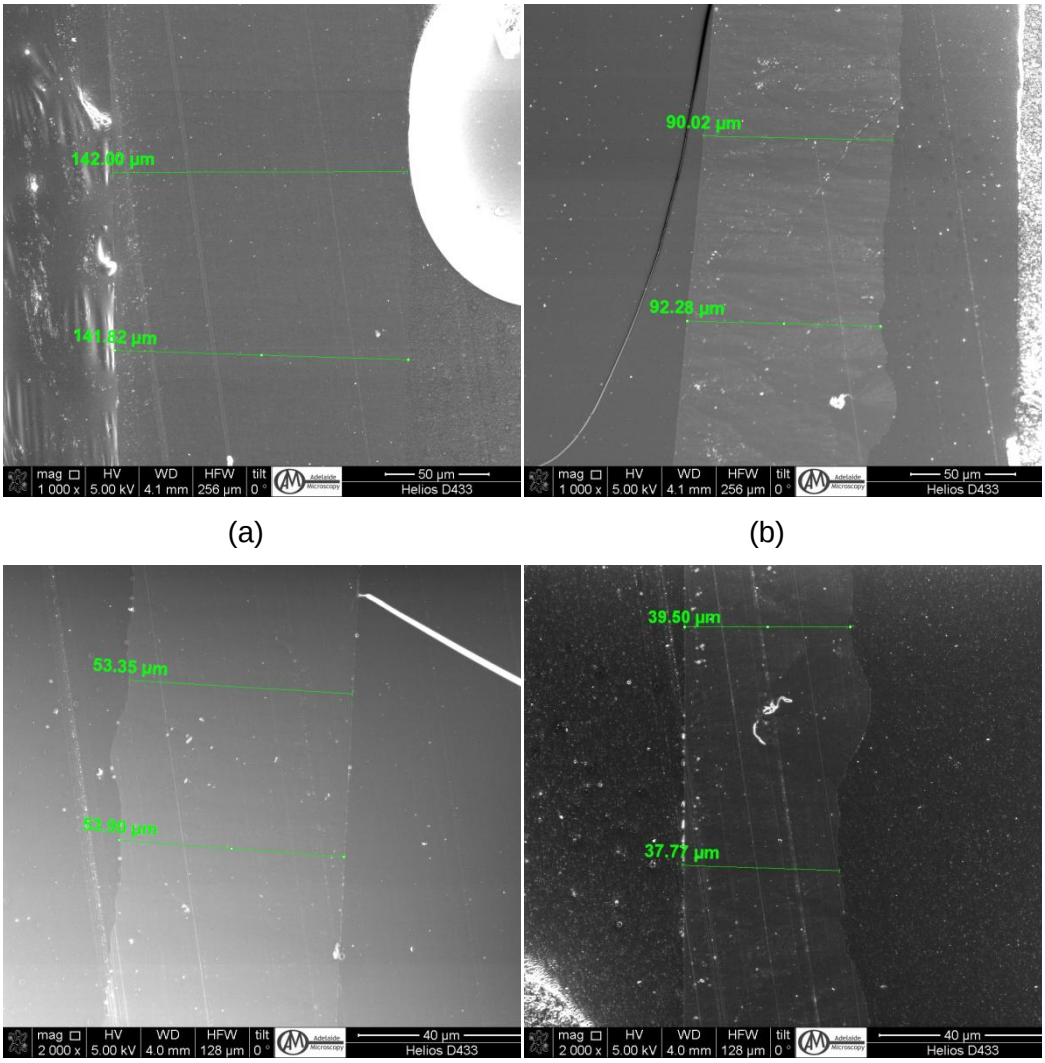

(a) (b)

(c) (d)

Figure 4.6: PPy Stand-alone film cross section SEM pictures; thicknesses: (a) 140µm (b) 90 µm (c) 50 µm and (d) 40 µm

All the above films had a DC conductivity of 2000 S/m, which translates into a volume resistivity of $5x10^{-2}\Omega cm$. The relationship between sheet resistance, film thickness and volume resistivity is given by:

$$Sheet\ resistance\ \left(in\frac{\Omega}{\square}\right) \times\ thickness\ of\ material\ (in\ cm)$$
$$= Volume\ resistivity\ (in\ \Omega\ cm)$$

Using this relationship, the computed values for the DC sheet resistances for the different PPy samples is as indicated in Table 4.1.

Table 4.1: Sheet Resistance of PPy film samples

Sno.	PPy Sample Type	Sheet Resistance (in $\frac{\Omega}{\square}$)
(a)	140 µm (sample 'A')	3.6
(b)	90 µm (sample 'B')	5. 6
(c)	50 µm (sample 'C')	10.0
(d)	40 µm (sample 'D')	12.5

The optimized design parameters for the microstrip patch antenna are indicated in Table 4.2.

Table 4.2: Microstrip Antenna design data

Parameters	Copper	PPy (140 µm)	PPy (90 µm)	PPy (50 µm)	PPy (40 µm)
Substrate					
• FR-4	$\varepsilon_r = 4.1$				
• Thickness	3.2 mm				
• Dimension	80x80 mm				
Radiating Patch dimensions					
• Length	14.26 mm	14.16 mm	14.16 mm	14.16 mm	14.16 mm
• Width	12.9 mm	12.9 mm	12.9 mm	12.9 mm	12.9 mm
Feed point (off set from centre)	2.09 mm	2.53 mm	2.53 mm[1]		

4.2.2 Simulations and Experimental Results

The effect of the patch thickness for less conductive material (such as PPy) is an important consideration in this design. In this section the PPy patches have been simulated as impedance sheets with finite thickness using both CST™ and HFSS™ as EM simulators. It is pertinent to mention here that the EM solvers, while simulating the CP material (or any other material with finite thickness and conductivity), take into account its thickness only in the

[1] The PPy (140 µm) antenna feed point location has been used for all other PPy patch thicknesses. This is primarily to isolate the effect of patch thickness on antenna performance.

frequency-domain solution and discard the effect of thickness in the time-domain solution. The microstrip antenna with CP material was therefore simulated in the frequency domain.

The material's thickness and conductivity are both taken into account by simulating the material as an impedance sheet with a finite sheet resistance (expressed in $\frac{\Omega}{\square}$ *Ohms per square*). In contrast, in the time domain, CST™ discards the thickness of the material and simulates it as a sheet with finite conductivity. The inherent assumption made by CST™ is that the film thickness is well above the required skin depth for the frequency and conductivity under consideration. This approach was adopted while simulating the 2 GHz PPy-patch (in chapter 3), where the thickness of the patch was assumed to be zero and the material was represented as a sheet with finite conductivity of 2000 S/m. The basic advantage of simulating the CP as an impedance sheet in the frequency-domain is that the effect of film thickness can be taken into account.

The Cu and PPy MPA designs were separately optimized for good impedance matching using CST^{TM} and HFSS^{TM}. The optimized design parameter values are indicated in Table 4.2. The E-Copol and H-Copol radiation plots of the PPy patch antennas and equivalent Cu-patch antenna are shown above in Figure 4.7 and Figure 4.8. Additional plots on measured and simulated antenna pattern for various thickness of PPy patch are placed in Appendix B.

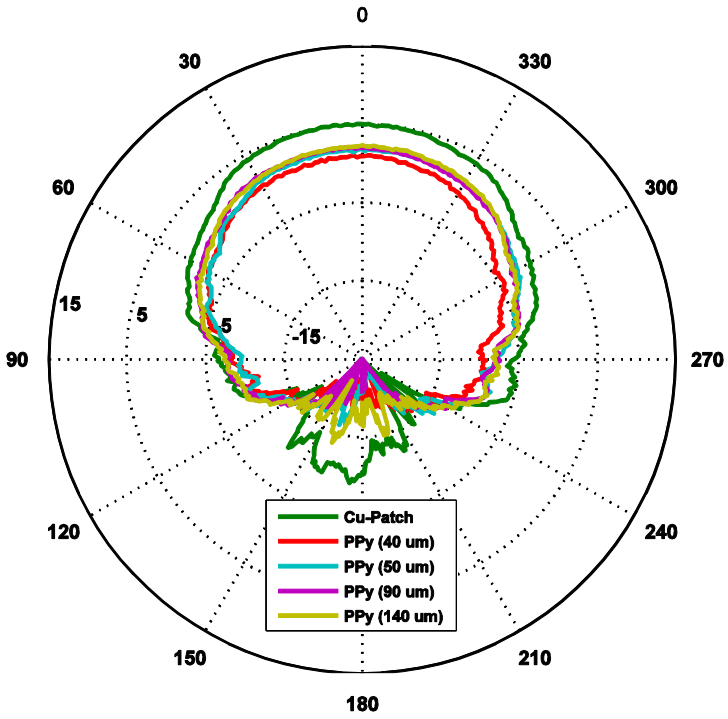

Figure 4.7 : 4.5 GHz E-Copol radiation pattern measurement

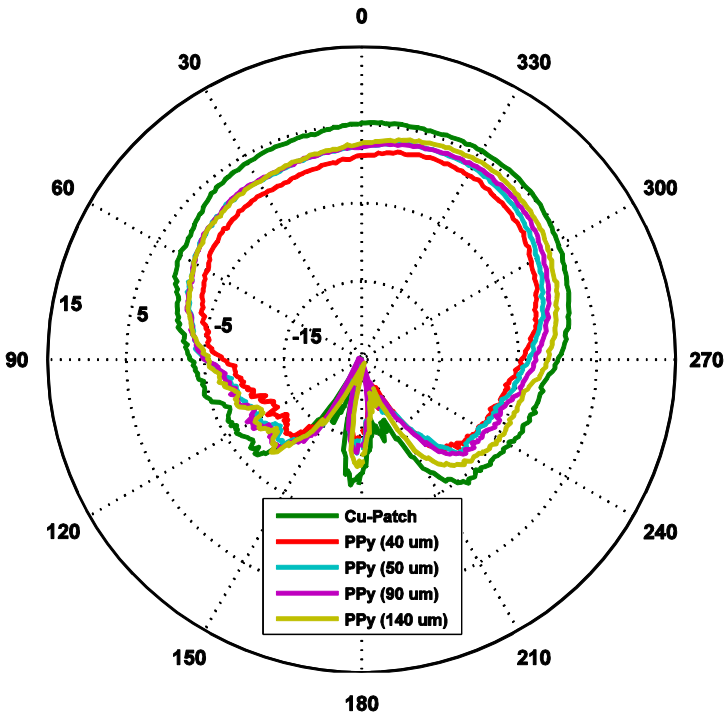

Figure 4.8: 4.5 GHz H-Copol radiation pattern measurement

The IEEE gain and estimated radiation efficiency of PPy and Cu patch antennas are placed in Table 4.3. The radiation of the PPy patch antennas was estimated by comparing measured gain against that of the equivalent Cu

patch antenna. The radiation efficiency of the copper patch antenna was determined from measurement and simulation.

The Cu patch antenna is resonant at 4.46 GHz with a -10 dB bandwidth of about 300 MHz or 6.7%. The resonant frequencies of the PPy patch antennas are with 1% of 4.5 GHz. The consistency of the results is further validated by the comparison of the shape of the measured and simulated radiation pattern of the Cu patch antenna (considered as reference) and PPy patch antennas.

Table 4.3: Gain and Radiation Efficiency measurement

Patch Thickness (μm)	Gain (dB)	Radiation Efficiency (%)
40	2.42	38.5
50	3.41	47.8
90	3.80	52.3
140	4.63	64.8
Cu	5.45	100[2]

The classical antenna design approach requires that the patch thickness should be at least couple of skin depth thick, for materials with low conductivity. However, if the patch thickness needs to be off-set then this is achieved by having a patch with very high conductivity (e.g. Cu or any other highly conductive metal/material) or increasing the frequency of operation. Interestingly, from the above experimentation we could make the following observations

- The skin depth is computed from the expression

$$\delta = \sqrt{\frac{2}{\omega\mu\sigma}} \qquad \textbf{(4.1)}$$

Where δ is the skin depth (also known as $1/e$ penetration depth), ω is the angular frequency, μ is the permeability constant and σ is the conductivity. The skin depth required at 4.5 GHz, while using a

[2]Copper patch antenna is taken as reference antenna

2000 S/m conducting patch is: 168 μm. The thickness of PPy patches used in the experiment is below this thickness.

- The antenna resonance is observable with corresponding performance for as low as quarter of a skin depth (i.e. 40 μm).

- The gain and radiation efficiency of the antenna increases with PPy patch thickness.

The variation in gain and radiation efficiency for a 2000 S/m conducting PPy patch is shown in Figure 4.9 and 4.10. Similarly in the Figures 4.11 and 4.12, the variation of gain and radiation efficiency with surface resistance of the patch film is presented.

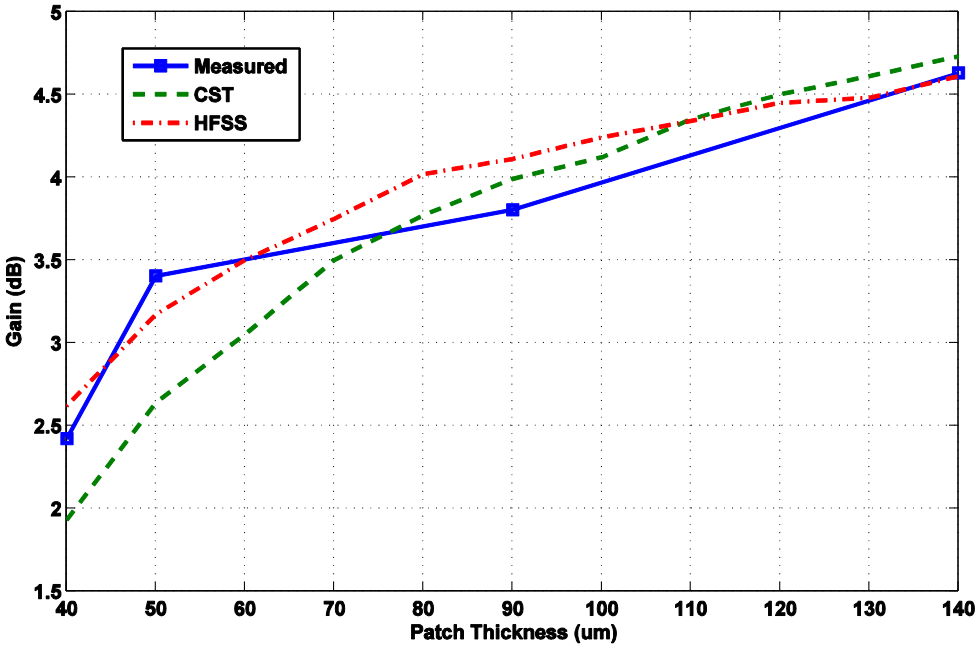

Figure 4.9: Variation of antenna gain with patch thickness

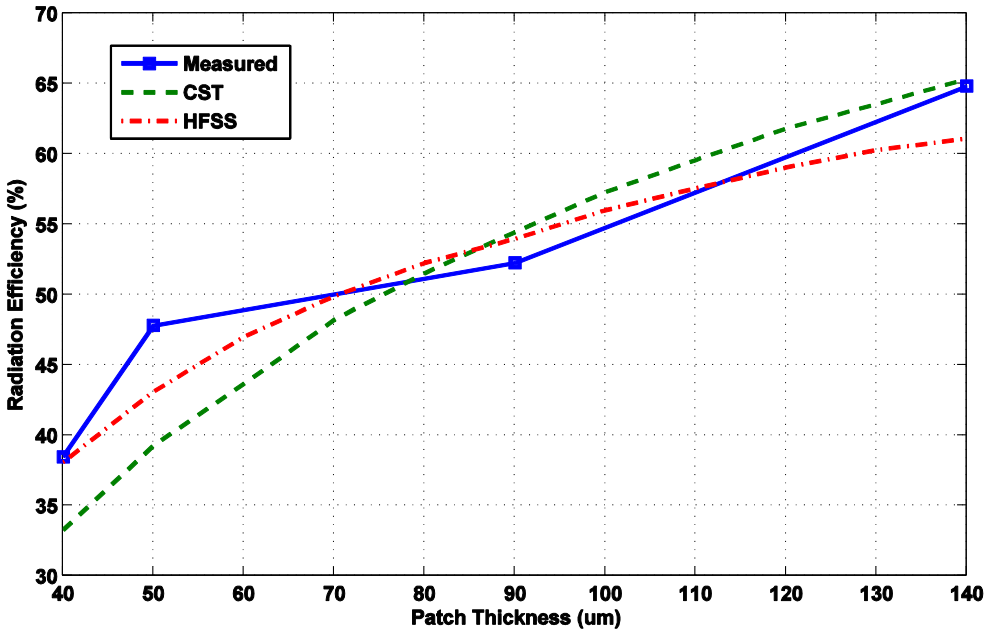

Figure 4.10: Variation of radiation efficiency with patch thickness

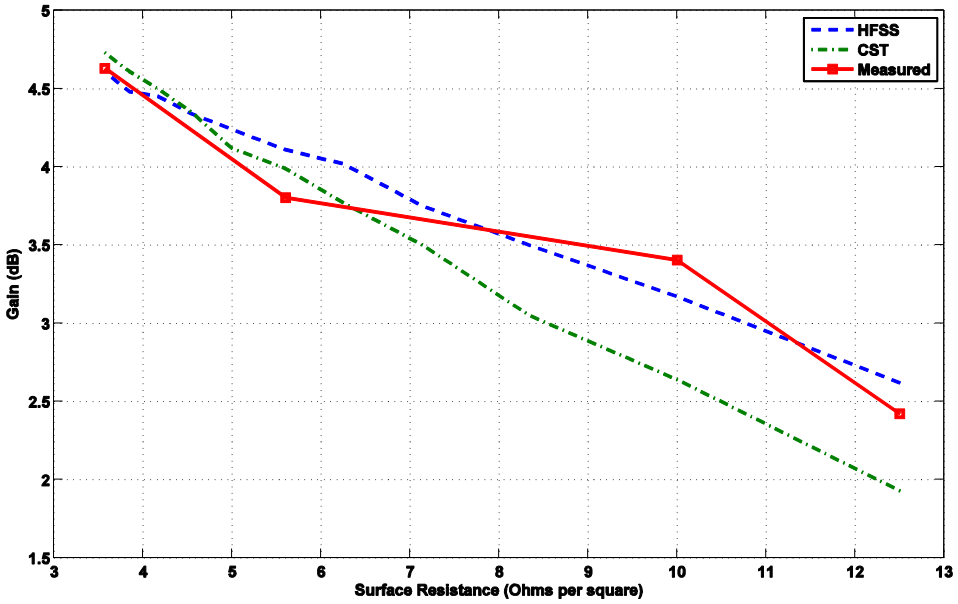

Figure 4.11: Variation of Gain with PPy patch surface resistance

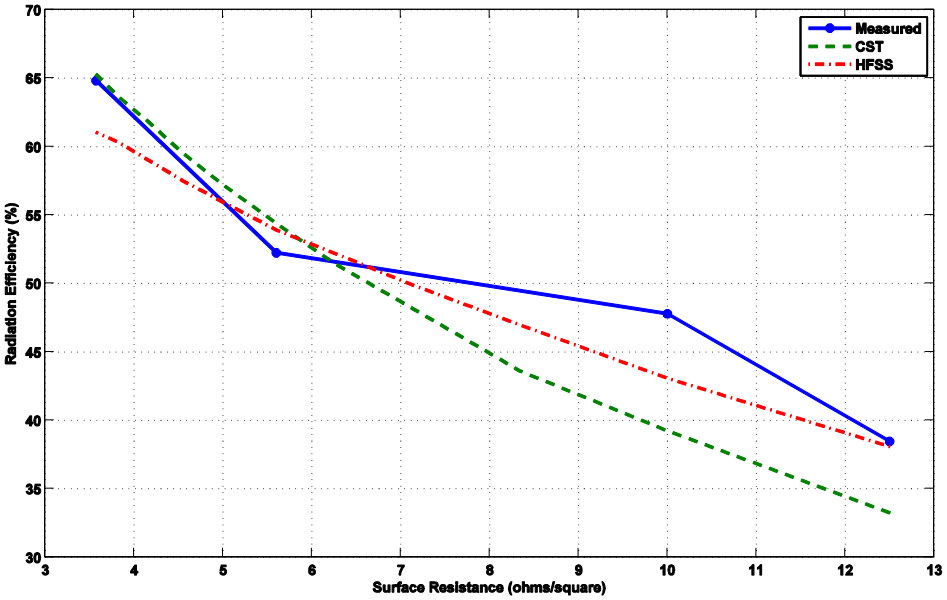

Figure 4.12: Variation of radiation efficiency with PPy patch surface resistance

4.2.3 Summary

In this section, the effect of patch thickness for less conductive material on overall antenna performance has been studied. The conductivity of the PPy material was constant (2000 S/m), while the patch thickness was varied between identically fabricated patch antennas. The thickness of the patches used in this experiment was less than one skin depth (which is calculated to be 168 µm at 4.5 GHz); however the gains of the antenna varied from as low as 2.42 dB (for 40 µm thickness) to 4.63 dB (for 140 µm thickness patch). The variation of antenna gain and radiation efficiency has been graphically presented and it emerges from the experiments reported in this section that: (a) Microwave antennas are possible with very low conductive materials; albeit with modest gain and low radiation efficiency. (b) Furthermore, it is possible to obtain reasonable antenna performance, even if the patch thickness is a fraction of skin depth.

In the next section, the effect of change in conductivity, patch thickness, change in frequency of interest, change in CP material and a different approach for obtaining a CP film (i.e. by ink jet printing) is investigated against antenna performance.

4.3 A Study of Radiation Efficiency in PPy and PEDOT based 6 GHz MPA

In second stage of this study, the conductivity of patch, its thickness, frequency of operation, a different type of CP and even a different method of CP film preparation are explored. This comprehensive study is based on 6 GHz microstrip patch antenna fabricated on Roger's Ultralam® 2000[3] substrate. All antennas used in this study were identically fabricated. Three microstrip patch antennas were fabricated using PPy stand-alone films of different thicknesses; one patch antenna was fabricated with PEDOT film printed on an Arylite™ substrate. An identical copper antenna was also fabricated and tested for reference. The DC conductivity of all the PPy based patches was 2000 S/m, while that of PEDOT based patch was 10,000 S/m. The thicknesses of the PPy film were accurately determined as described previously, by using a Scanning Electron Microscope (SEM). PEDOT film thickness was determined at Intelligent Polymer Research Institute, University of Wollongong[4], using a contact profiler.

The PPy film for the antenna patch was obtained from The Defence Science and Technology Organization (DSTO) in Melbourne, Australia. It was prepared in accordance with the procedure indicated by Truong et al.[1]; i.e. by conducting electrochemical polymerisation in an aqueous solution. Sodium *p*-toluene sulphonate (*p*-TS) was used as dopant. In contrast the PEDOT film was printed on a 200µm thick Arylite™ substrate using Dimatix DMP 2800 inkjet printer. A photograph of the printer is shown in Figure 4.13.

[3] www.rogerscorp.com.
[4] www.ipri.uow.edu.au.

Figure 4.13: Dimatix DMP 2800 inkjet printer

The technical details of the printer are placed at Appendix C. A commercially available preparation of PEDOT called Clevios P™ was used with this printer. This CP solution was obtained from H.C. Starck[5]. The chemical formula is shown in Figure 4.14 and a detailed data sheet of Clevios P™ is also placed in Appendix C.

[5] www.clevios.com.

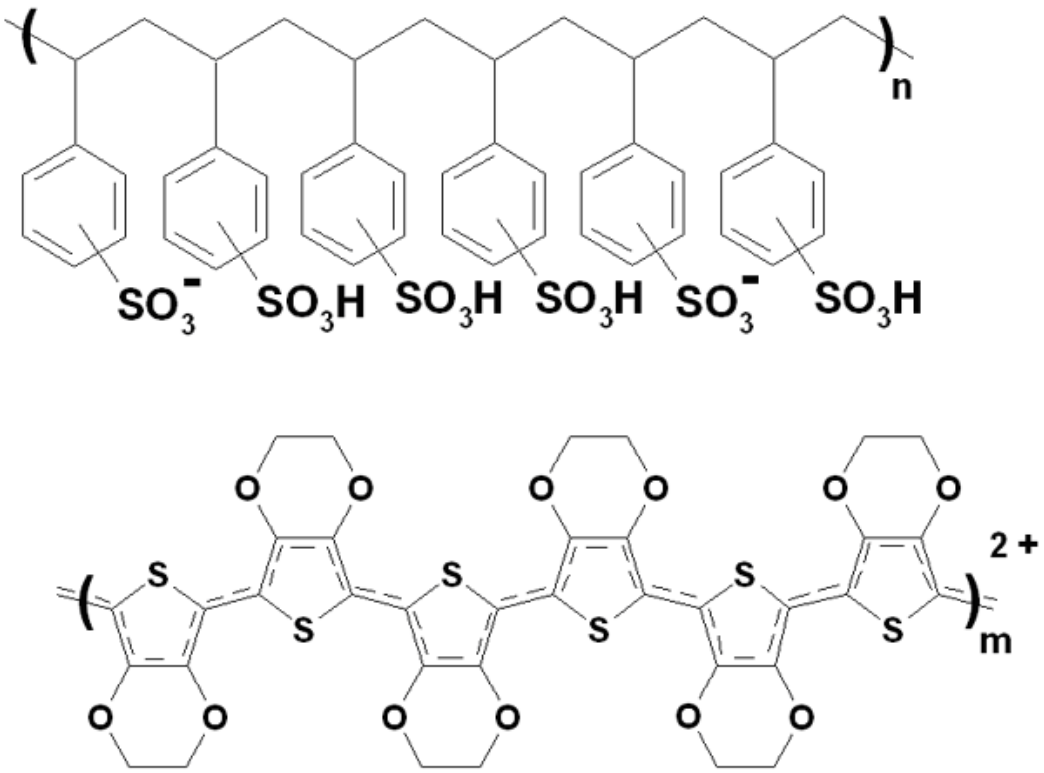

Figure 4.14: Poly(3,4-ethylenedioxythiophene) poly(styrenesulfonate) aqueous dispersion

The thickness of the PEDOT film printed on the Arylite substrate was 7 µm. The Dimatix 2800 inkjet printer is capable of printing very thin films (few nanometre thick) only. However, in order to achieve film thicknesses in micro-metres, several layers were printed on each other, resulting in total thickness of 7 µm. This process has two very important issues to consider (a) the cohesiveness of the films and (b) the drop in overall DC conductivity of stacked films. Printing highly conductive films with thicknesses in the order of micro-metres appears to be a technological challenge at the moment.

4.3.1 Antenna Design

Three PPy, one PEDOT patch and one equivalent Cu-patch antenna was fabricated on Ultralam® 2000 substrate. Examples of fabricated Cu, PPy and PEDOT patch antennas are shown in Figure 4.15.

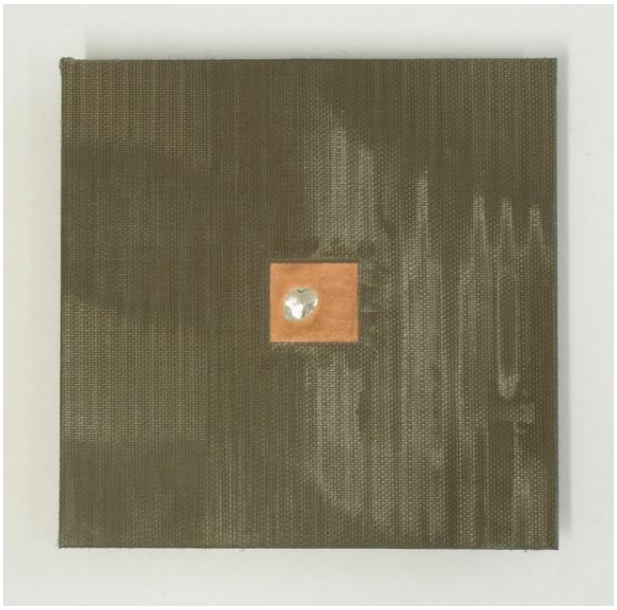

(a) Cu-patch 6 GHz microstrip patch antenna on Ultralam 2000 substrate

(b) PPy-patch 6 GHz microstrip patch antenna on Ultralam 2000 substrate

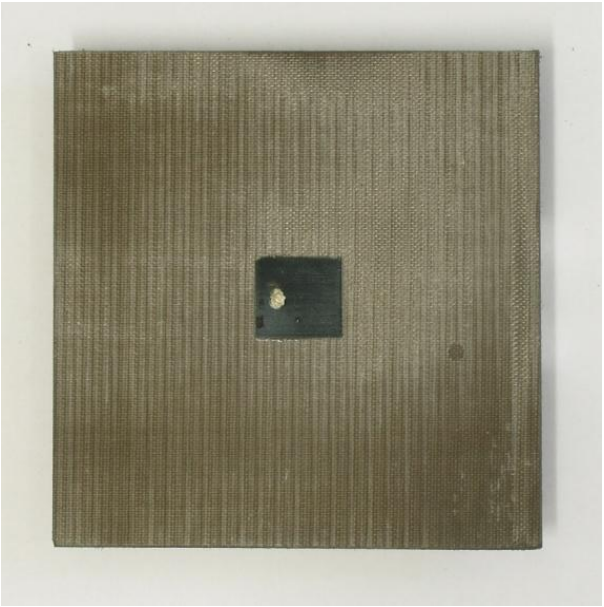

Figure 4.15: (c) PEDOT-patch 6 GHz microstrip patch antenna on Ultralam 2000 substrate

A schematic of the antennas used in this study is shown in Figure 4.16. The films are pasted on the Ultralam 2000™ substrate using epoxy resin. An identical copper patch antenna was fabricated for the validation of simulation and for direct comparison of the relative performance of these patches antennas.

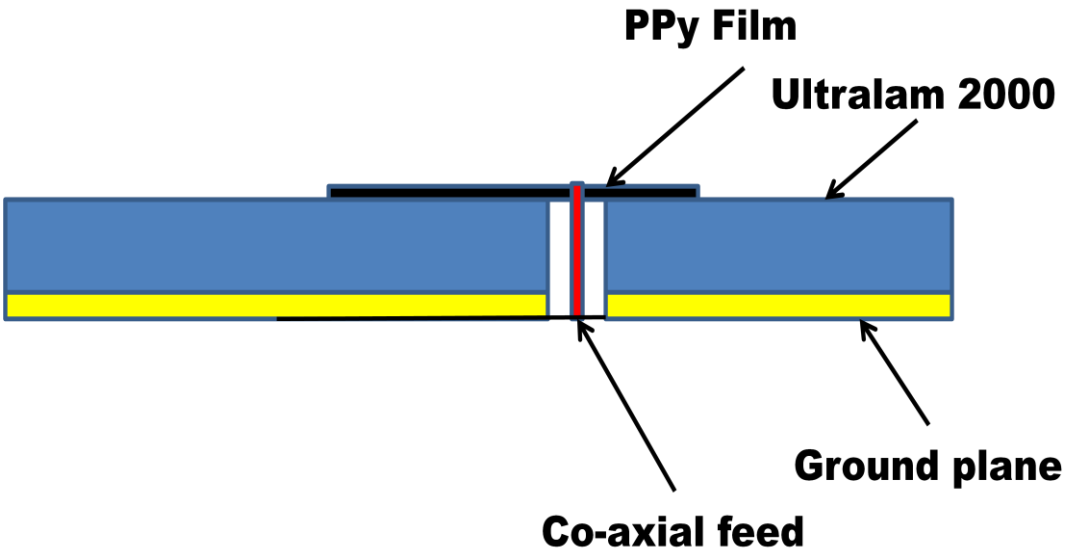

(a)

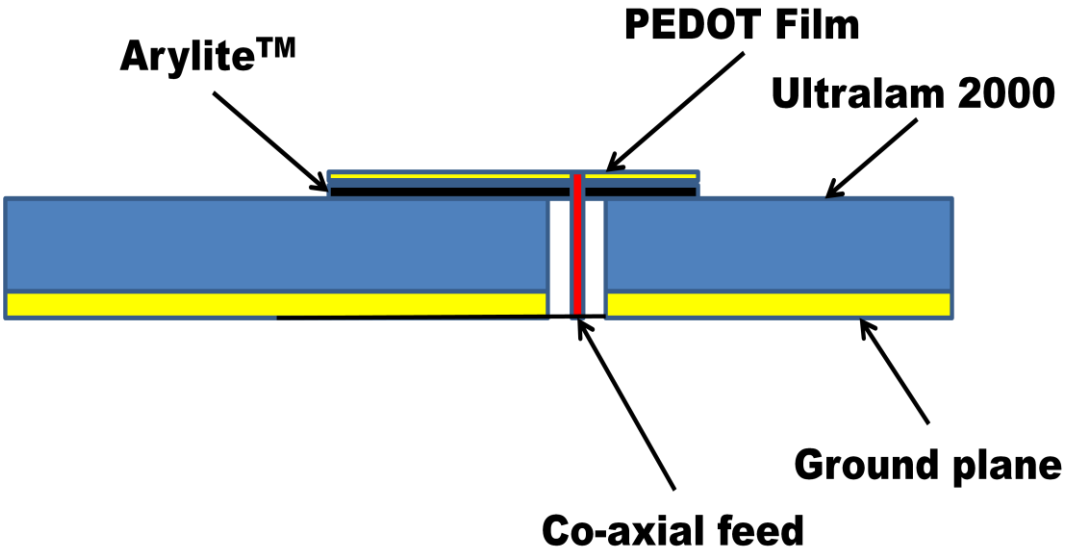

(b)

Figure 4.16: A schematic side view of (a) PPy and (b) PEDOT patch antennas

4.3.1.1 Permittivity of Ultralam 2000 substrate

The permittivity of Ultralam® 2000 substrate at microwave frequencies is indicated to be between 2.4-2.6 in the manufacturer's data sheet (Appendix D). The Ultralam 2000 panel used in this study had a relative permittivity of 2.45. A good match between the simulation and measured parameters was obtained for Ultralam 2000™ relative permittivity of 2.45 (Figure 4.17).

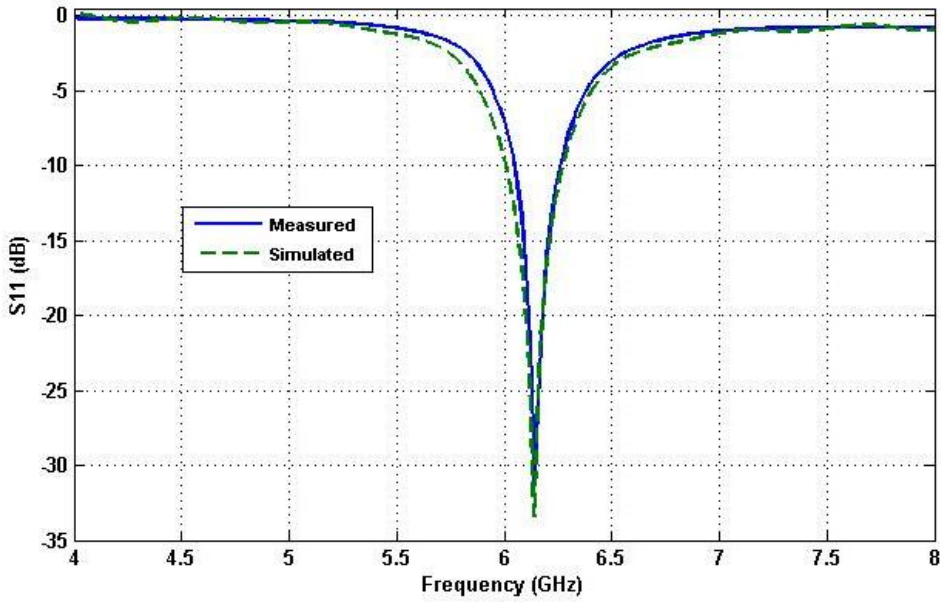

Figure 4.17: Simulated and measured S11 for a Cu-patch antenna on Ultralam 2000™ substrate

4.3.2 Simulations and Design optimizations

The antenna designs were optimized for good impedance match. The design parameters for the microstrip patch antennas are indicated in Table 4.4. The effect of the patch thickness for less conductive materials (such as PPy/PEDOT) is an important consideration in this design. Most antenna designers would consider a couple of skin depths thickness for PPy/PEDOT patch as essential. The skin depths for the patch antennas at 6 GHz are 145 µm for PPy, 65 µm for PEDOT and 0.85 µm for copper. It is evident that the thicknesses of our PPy and PEDOT patches are far less than one skin depth. In contrast, the copper patch thickness is about 20 times its skin depth. The patches were simulated as impedance sheets using HFSS™, to take into account the effect of patch thickness.

Table 4.4 : Optimized design parameters of microstrip patch antennas

Parameter	Cu	PPy			PEDOT
Substrate: Ultralam 2000™					
Thickness	1.8 mm				
Dimension	80x80mm				
Permittivity	2.45				
Patch					
Thickness	**17µm**	**140µm**	**90µm**	**50µm**	**7µm**
DC Conductivity (S/m)	$5.8x10^7$	2000			10000
Length (mm)	14.16	14	14	14	14
Width (mm)	12.9	12.9	12.9	12.9	12.9
Feed point (off centre) (mm)	1.28	3.25	3.25	3.25	3.63

4.3.3 Antenna fabrication

Fabrication of the microstrip antenna using the free-standing PPy patches proved challenging because of the mechanical properties of the material. The PPy film is very delicate and tends to shear along the cut edges. This therefore makes it hard to cut the film to exact patch size or drill holes using computer-assisted tools. The PPy patch was cut to the desired size by hand using a suitable template. Since a systematic fabrication error within tolerances affected the realisation of the optimised parameters, the simulation was later adjusted according to actual dimensions of the fabricated devices. On analysis of the patches cut by hand it emerged that the patch sizes where about 0.1 to 0.2 mm under the optimised design values; the effect of which is evident in the resonant frequency shifting slightly above 6 GHz. The actual antenna parameters achieved are listed in Table 4.5.

Table 4.5 : Realised Antenna parameters

Parameters	PPy			PEDOT
Patch	140µm	90µm	50µm	7µm
Length (mm)	13.9	13.9	13.9	13.85
Feed point (off centre; mm)	3.25	3.2	3.25	3.5

4.3.4 Results

CPs also exhibit dispersion in their electrical conductivity with frequency [2-14]. Therefore, the measured results differed from the simulated results not only due to fabrication errors, but also due to dispersion in electrical conductivity. Figure 4.18 and Figure 4.19 show the measured reflection coefficient for the two CP antennas, together with three sets of simulated results. The optimal design curves correspond to the simulation results achieved before fabrication. The second pair of simulation curves represents the results after correction of the fabrication errors, i.e. mechanical tolerances on the patch length, which corrects the small frequency shift of the resonance. Return loss measurements of other CP antennas are placed in Appendix D.

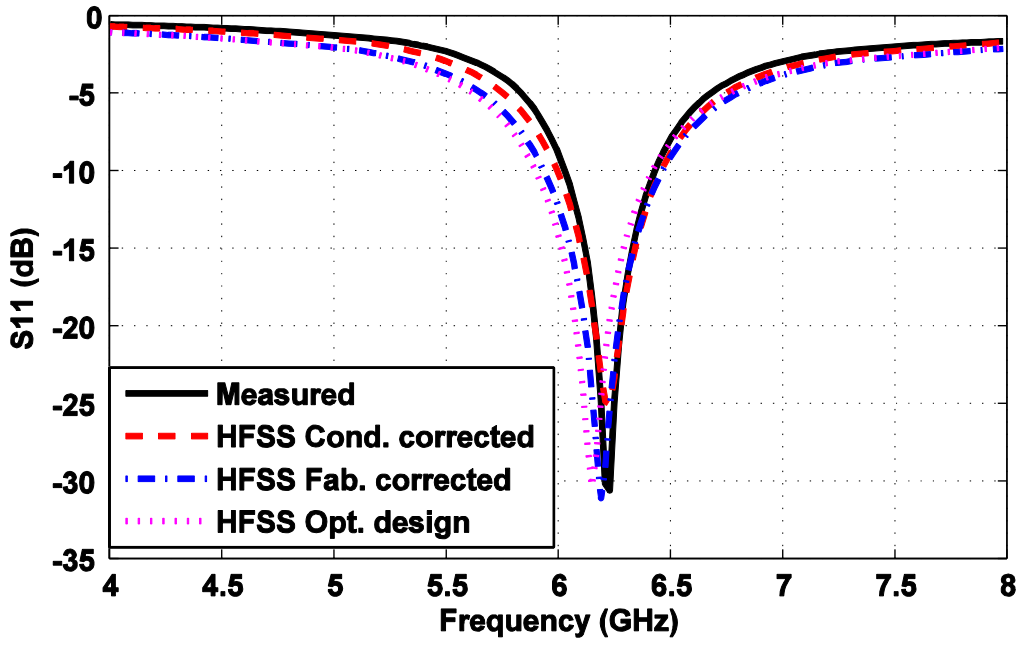

Figure 4.18: Simulated and measured S11 for a 90µm PPy-patch antenna on Ultralam 2000™ substrate

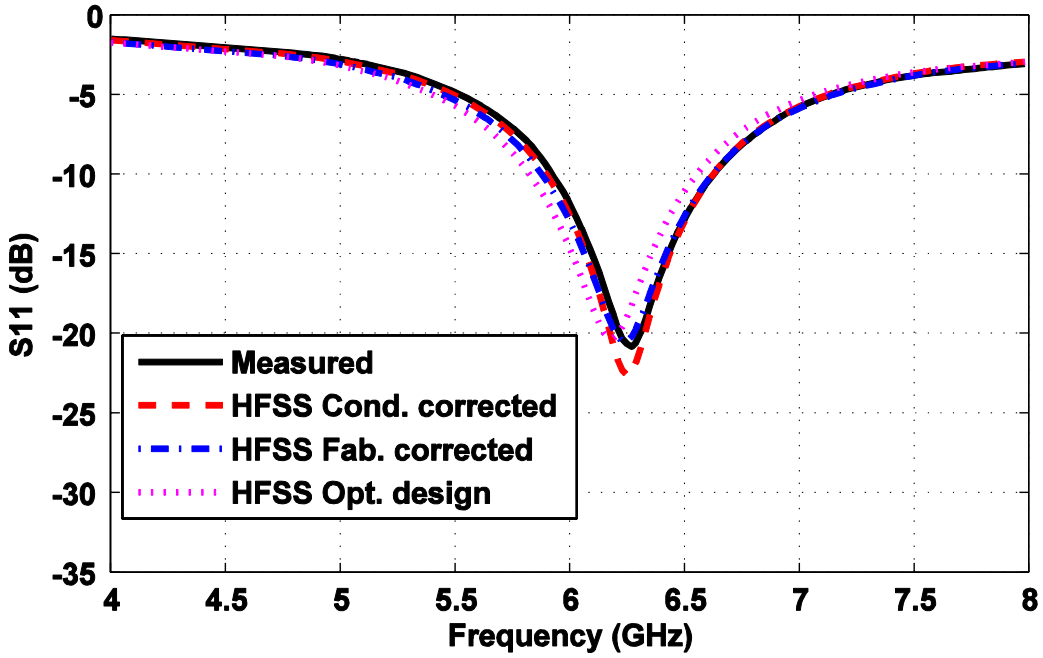

Figure 4.19: Simulated and measured S11 for a 7µm PEDOT-patch antenna on Ultralam 2000™ substrate

Finally, a nearly perfect match to measurements was obtained in the third pair of simulation curves through adjustment of electrical conductivity of the films. The measured DC sheet resistance and adjusted DC surface resistivity at 6 GHz for the PPy and PEDOT films are shown in Table 4.6, and provide evidence of the dispersive increase in conductivity for the CP materials with increasing frequencies.

Table 4.6 : Sheet resistance of CP films

CP Film	Sheet Resistance $(\Omega/\square)$	
	Measured DC	**Adjusted (6 GHz)**
PPy (140µm)	3.6	2.5
PPy (90µm)	5.6	3.0
PPy (50µm)	10.0	6.0
PEDOT (7µm)	14.3	13.0

The co-polarized radiation patterns of the PPy and PEDOT patch antennas and of the corresponding Cu-patch antenna are shown in Figure 4.20 and Figure 4.21 for the E- and H-plane.

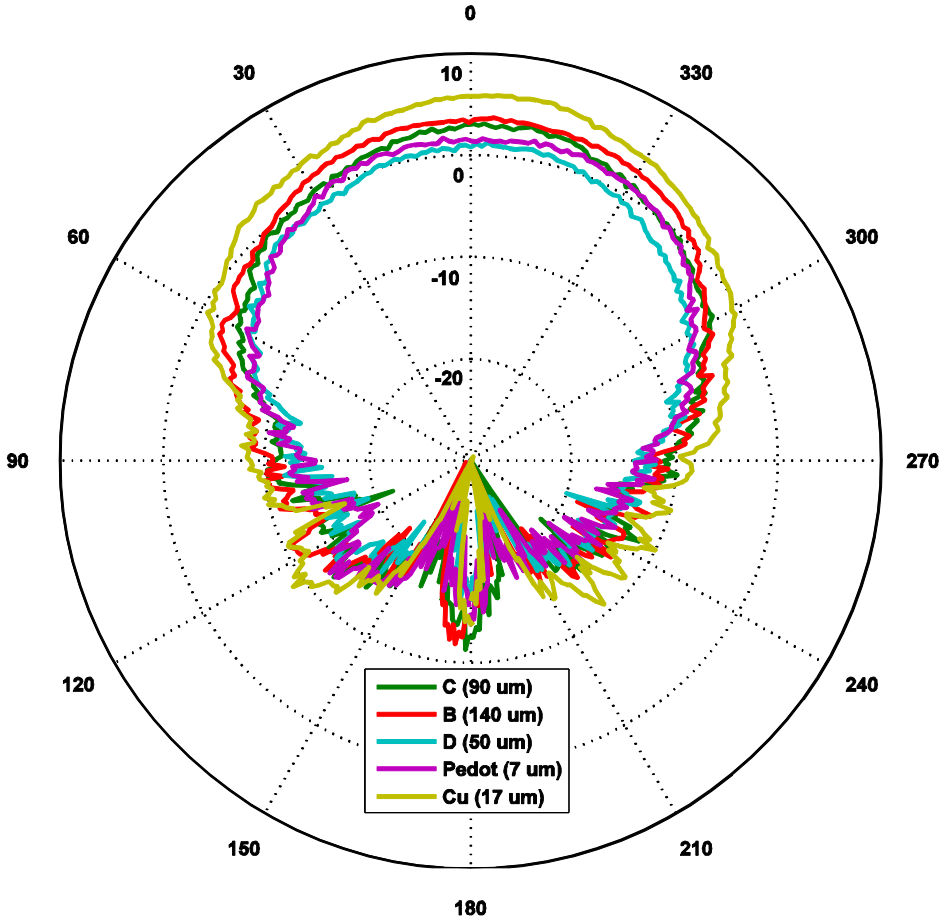

Figure 4.20 : Measured E-plane co-pol antenna gain patterns at 6 GHz

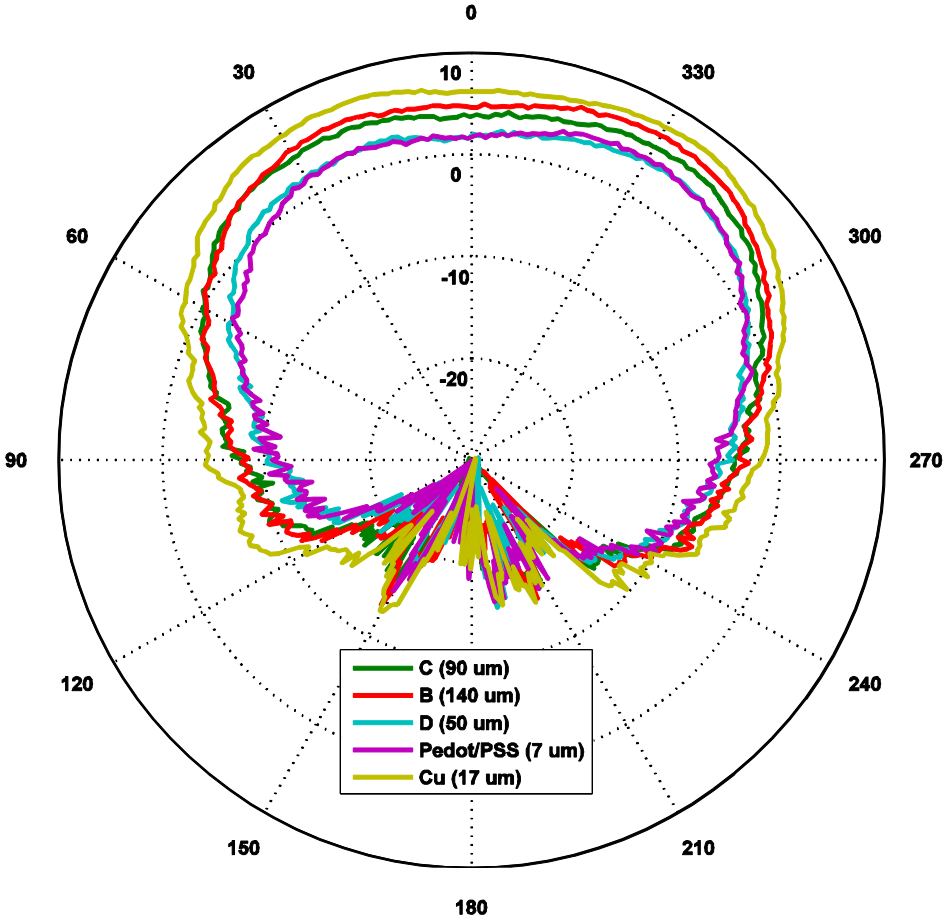

Figure 4.21 : Measured H-plane co-pol antenna gain patterns at 6 GHz

All patterns show a similar broadside shape (i.e. nearly identical directivities), but the different efficiencies explain different gain levels. The IEEE gain and estimated radiation efficiency of the Cu, PPy and PEDOT-microstrip patch antennas are listed in Table 4.7. Additional plots on measured and simulated antenna pattern for various thicknesses of PPy patch and PEDOT patch are placed in Appendix D.

The radiation efficiency of the copper patch antenna was determined from measurement and simulation, while that of PPy and PEDOT-patch antennas was estimated by comparing the measured gain against that of the equivalent Cu-patch antenna. The Cu-patch antenna is resonant at 6.14 GHz

with a -10 dB bandwidth of 236 MHz or 3.8%, while in the case of CP based patch antennas the typical results were: the PPy-patch antenna with 90µm patch thickness had a resonant frequency of 6.24 GHz with a -10 dB bandwidth of about 420 MHz or 6.7% and the PEDOT-patch antenna had a resonant frequency of 6.28 GHz with a -10 dB bandwidth of about 700 MHz or 11%. Details of other PPy patch antennas are placed in Appendix D.

Table 4.7 : Gain and radiation efficiency of microstrip patch antennas

Patch Type	Gain (dB)	Radiation Efficiency (%)
Copper (17 µm)	6.0	96.2
PPy (140µm)	4.8	52.4
PPy (90µm)	3.8	48.2
PPy (50µm)	2.3	34.5
PEDOT (7µm)	2.2	33.6

The observed drop in radiation efficiency and gain between 4.5 GHz (Table 4.3) antenna results and 6 GHz (Table 4.6) antenna may be attributed to substrate thickness of these antennas. The variation in gain and radiation efficiency for a 2000 S/m conducting PPy patch and 10000 S/m PEDOT is shown in Figures 4.22 and 4.23 respectively.

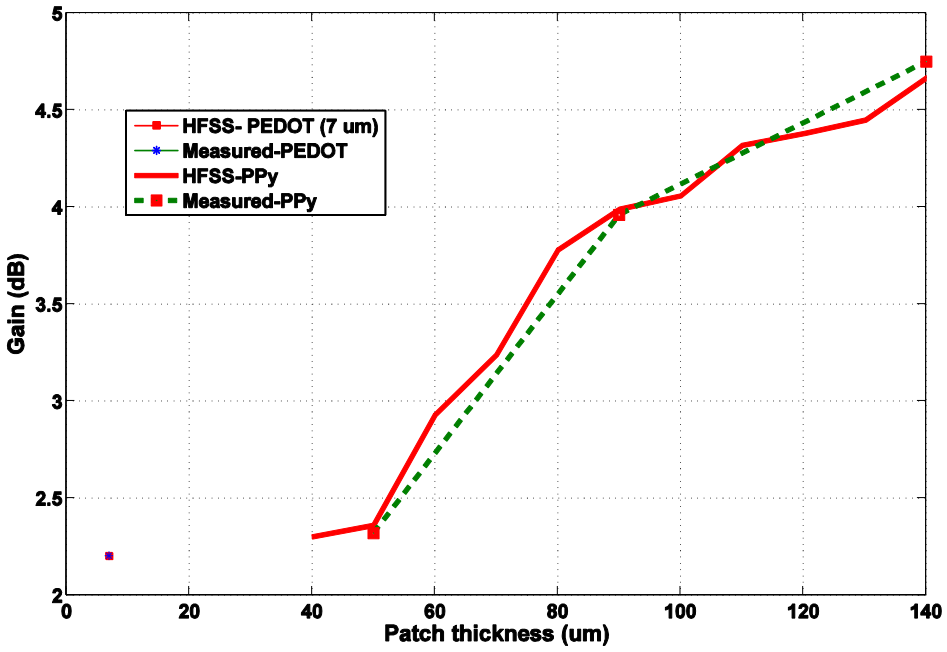

Figure 4.22: Variation of gain with patch thickness

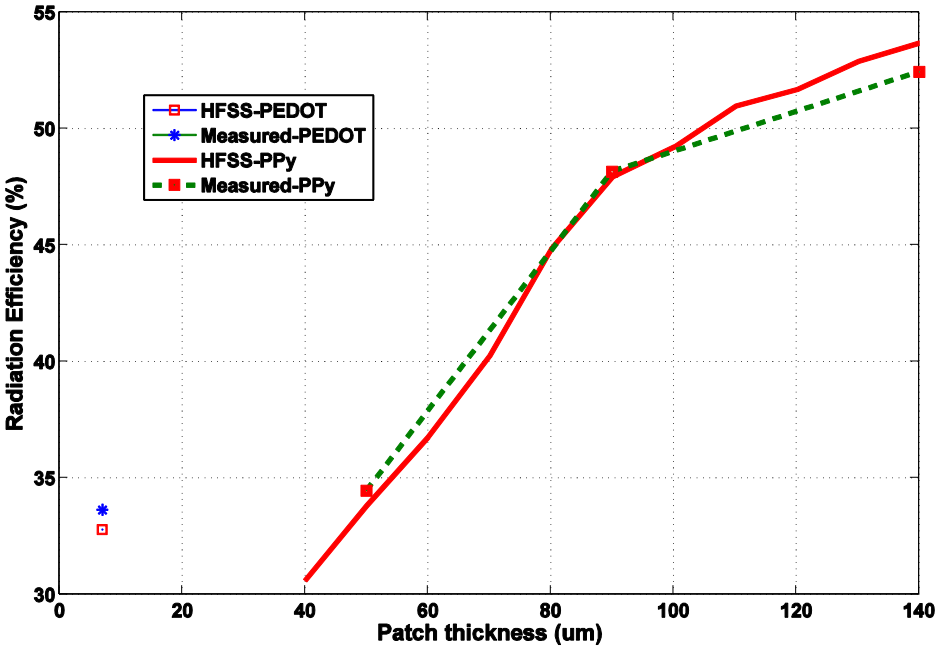

Figure 4.23 : Variation of radiation efficiency with patch thickness

4.3.5 Summary

The design of microwave antennas using CPs is challenging because producing CP films with thicknesses multiple times that of the skin depth is difficult using present manufacturing processes. Furthermore, the conductivity of CP films exhibits a dispersion that needs to be further investigated. The performance of CP-based 6 GHz microstrip patch antennas was presented and compared with an equivalent Cu patch antenna. Despite very low DC conductivities and thicknesses of the CP patches, reasonable antenna performance at microwave frequencies was observed with relatively low radiation efficiencies. The results clearly confirm the potential of polymer materials as antennas. Furthermore, since the electrical conductivity of CPs can be altered dynamically through external stimuli, it makes these antennas potentially very attractive despite their modest radiation efficiency.

4.4 Conclusion

In this chapter we have presented the possibility of using conducting polymer based patches for microwave planar antennas. The results clearly indicate that it is possible to obtain satisfactory antenna performance despite relatively modest conductivity of the patches. Furthermore, work presented in this chapter also highlights that while multiple skin depth thicknesses of the resonant patch is desirable, it is not essential for application where gain and radiation efficiency are not so critical or could be compromised for other advantages. The key impact of this chapter is that it sets the ground for future exciting work on re-configurable antennas using CPs. The problems, constraints and difficulties faced in the simulation and fabrication of CP based antennas, which have been addressed in this chapter, would improve our understanding of CPs and their future exploitation in microwave antennas.

In the next chapter, an overview is presented on the exciting possibilities that CPs hold in the field of antenna applications. The chapter considers, where do we go from here and what we could do with this acquired knowledge on CPs.

References

[1] V. T. Truong and J. G. Ternan, "Complex conductivity of a conducting polymer at microwave frequencies," *Polymer,* vol. 36, pp. 905-909, 1995.

[2] V. N. Prigodin and A. J. Epstein, "Quantum Hopping in metallic Polymers," *Physica B,* vol. 338, pp. 310-317, 2003.

[3] A. J. Epstein, *Physical Properties of Polymers Handbook* vol. VIII. New York: Springer, 2007.

[4] H. C. F. Martens, J. A. Reedijk, H. B. Brom, D. M. de Leeuw, and R. Menon, "Metallic state in disordered quasi-one-dimensional conductors," *Physical Review B,* vol. 63, pp. 073203-1-073203-4, 2001.

[5] A. J. Epstein and V. N. Prigodin, "Low-dimensional Variable Range Hopping in Conducting Polymers," *Synthetic Metals,* vol. 117, pp. 9-13, 2001.

[6] T. A. Ezquerra, F. Kremer, M. Mohammadi, J. Ruhe, G. Wegner, and B. Wessling, "AC Conductivity measurements in Polymeric insulator conductor systems," *Synthetic Metals,* vol. 28, pp. 83-88, 1989.

[7] R. S. Kohlman, J. Joo, Y. Z. Wang, J. P. Pouget, H. Kaneko, T. Ishiguro, and A. J. Epstein, "Drude Metallic response of Polypyrrole," *Physical Review Letters,* vol. 74, pp. 773-776, 30 Jan 1995.

[8] R. S. Kohlman, D. B. Tanner, G. G. Ihas, A. G. MacDiarmid, and A. J. Epstein, "Inhomogenous Insulator-Metal transition in Conducting Polymers," *Synthetic metals,* vol. 84, pp. 709-714, 1997.

[9] B. S. Kumar, H. Hohn, R. Joseph, M. Hajian, L. P. Ligthart, and K. T. Mathew, "Complex permittivity and conductivity of polyaniline at microwave frequencies," *Journal of European Ceramic Society,* vol. 21, pp. 2677-2680, 2001.

[10] C. Y. Lee, H. M. Kim, J. W. Park, Y. S. Gal, J. J. Jin, and J. Joo, "AC Electrical properties of conjugated polymers and theoretical high frequency behaviour of multilayerfilms," *Synthetic Metals,* vol. 117, pp. 109-113, 2001.

[11] H. C. F. Martens and H. B. Brom, "A quantitative evaluation of metallic conduction in conjugated polymers," *Physical Review B,* vol. 70, pp. 241201-1-241201-4, 2004.

[12] L. Olmedo, P. Hourquebie, and F. Jousse, *Microwave Properties of Conductive Polymers* vol. 3: John Wiley & Sons Ltd, 1997.

[13] V. T. Truong, A. R. Codd, and M. Forsyth, "Dielectric properties of conducting polymer composites at microwave frequencies," *Journal of Materials Science,* vol. 29, pp. 4331-4338, 1994.

[14] V. T. Truong, S. Z. Riddell, and R. F. Muscat, "Polypyrrole based microwave absorbers," *Journal of Materials Science,* vol. 33, pp. 4971-4976, 1998.

Chapter 5

Quo-Vadis?

5.1 Conclusion

In this thesis, it has been shown that conducting polymers in the form of conductive films could be used as conducting material for building microwave planar antennas. The thesis presented a brief on different types of CPs and the issues such as stability, ageing, bio-compatibility and bio degradability were also discussed. Work presented in this thesis provides the necessary foundation for any future work on CP-based microwave planar and re-configurable antennas.

The design issues that are important for any multilayer planar antenna have also been presented at Appendix A of this thesis. Multi-layer antenna design is often confronted with the age old problem of estimating the effective permittivity of the multi-layer structure. This is required as a key starting value for commencing the design with some estimation of antenna patch size. This patch size can then be optimised for obtaining desired design specifications by using EM simulation solvers. This process can be very time consuming if the initial design is not based on a close enough estimation of effective permittivity. Further, this problem is also of importance in the design of multi-layer microstrip transmission lines. An effective method was developed using the modified Getsinger's model to overcome this difficulty. The model was shown by way of discrete examples to be more accurate than most available methods for up to three layers. It was also shown that in principle the method could be applied recursively for any number of layers; however it becomes very complex and cumbersome mathematically.

As part of a proof of concept, the research presented in this thesis has highlighted that successful microwave antennas could be built using the CPs. Results of various microstrip patch antennas at 2 GHz, 4.5 GHz and 6 GHz

have been presented. The results have highlighted that despite CPs low DC conductivity and skin depth, the antennas can provide acceptable radiation performance albeit with relatively moderate efficiency. The presently modest performance of these antennas needs to be viewed from the perspective of future trends in CP conductivities, the material's improving stability and the promises that holds for future development in this field. Even in their present level of performance, these antennas provide an attractive alternative for certain bio-medical applications and also in the field of conformal / wearable antennas. CPs definitely are RF material of the future, as they provide excellent light weight alternative to known metal claddings like copper and aluminium. In addition antennas built with this material could be realized as conformal designs.

Furthermore, in this thesis, it was also demonstrated that microstrip patch antennas can be used as an indirect method for determining the permittivity of the substrate and also the AC conductivity of the CP film at the frequency of operation.

The work on these antennas provided a great insight into the problems associated with their simulation and fabrication. It was noticed that it is difficult to simulate accurately the effect of film thickness of CPs with state-of-the art simulation tools, unless the film is considered as an impedance sheet. The accuracy of simulation for such thin-films of imperfect conductors is still an issue that requires considerable iterations before getting a good match between the actual antenna performance and simulation. Fabrication of these antenna prototypes proved difficult, since most of the work was done by hand and therefore desired accuracies were difficult to achieve. Further, the electrical contact between the RF feed connector and the patch was realized using a conductive glue of silver epoxy. This makes the connection delicate for repeated usage and testing. The work presented in this thesis has amply highlighted these problems and also the steps taken to mitigate them within the constraints of what is possible. Proximity feed was not considered as it would have further lowered the efficiency of the planar antenna in the initial studies, but should be considered in the future.

A very fundamental study was also undertaken to study the impact of CP film thickness on overall antenna performance. This study was conducted at 4.5 GHz and it was established that reasonably good antenna performance could be obtained with film thickness being less than a skin depth. The effect of film thickness on antenna performance was analysed and presented. At the moment, the best method for obtaining CP films that are hundreds of microns thick is a fabrication challenge for the material scientists. During this study and that undertaken at 6 GHz as well, it was observed that AC conductivity of the CP films did increase with frequency from its DC value. This supports the research conducted in the material domain about the observed increase in electrical conductivity with frequency in CPs.

Lastly, a comparative study was undertaken on the effect of different, presently available CPs and also on the impact of different fabrication methods on antenna performance. Two different CPs were considered: PPy and PEDOT. PPy was developed as a standalone film, while PEDOT film was printed on Arylite substrate using an ink jet printer. Apart from the differences in their fabrication techniques the films were also distinctly different in their thicknesses too. The performance of the antenna at 6 GHz was satisfactory and clearly indicated that it is possible to have antenna performance at patch thicknesses less than one skin depth. Further it also established that printable conductive polymer antennas are as real a possibility as currently available printable electronic circuits. This development opens the doors for printable all-polymer antennas and also to very flexible and/or conformal antennas.

It is pertinent to mention here that while this study did point to the fact that acceptable antenna performance is feasible for patch thicknesses less than one skin depth, it still needs to be established, as to what minimum film thickness would be needed. This needs to be viewed from the perspective of totally different mechanism of electrical conduction in CPs. It is therefore imperative that dispersion of electrical conductivity is given due consideration; which is not done presently. Currently, the frequency dependence of skin depth for constant conductivity is only considered. In addition, no

consideration was given to the possibility of thin-film having natural defects on the conducting “paths”, between conducting islands.

In conclusion, CPs films even with their low DC conductivities have exhibited unexpectedly good antenna performance at microwave frequencies. These antennas could be an attractive consideration for applications where low cost, printable antennas, conformal, light weight, bio-compatibility and bio degradability is important. All presented results at 2 GHz, 4.5 GHz and 6 GHz confirmed the satisfactory performance.

5.2 Future Musings

CP-based microwave planar antennas open a number of possibilities in the future. Some of these could exploit the fixed high conductivity of the material itself and others would try to exploit the optical and dynamic Insulator-Metal Transition properties. Potentially attractive fields worth investigating in the near future include optically transparent antennas, hybrid antennas, and re-configurable antennas. Furthermore, these applications would equally impact upon phased array antenna designs that would use CP-based antennas. It is possible that CP-based antennas could open the domain of Microwave Identification Tags, similar to RFID tags or importantly could perhaps lead to a fusion of the two techniques. Figure 5.1 below shows the possible directions in which some exciting research possibilities exist.

Any possibility of spectacular success with CPs in microwave antennas depends heavily on conductivity levels that are realistically achievable, stability of the material, fabrication of suitable thicknesses and adaptation of the material to simple printing processes that meet all the electrical requirements. This is very challenging and it is envisaged that works such as this would propagate enough interest in the material domain to foster further research in that direction. On the other hand, accurate modelling of CPs would also pose as a big challenge especially for designing re-configurable antennas.

A number of ideas for the future are listed in Figure 5.1, which are very attractive and have great potential in terms of antenna applications. Interestingly, some of the concepts could well be adapted for certain microwave transmission line structures.

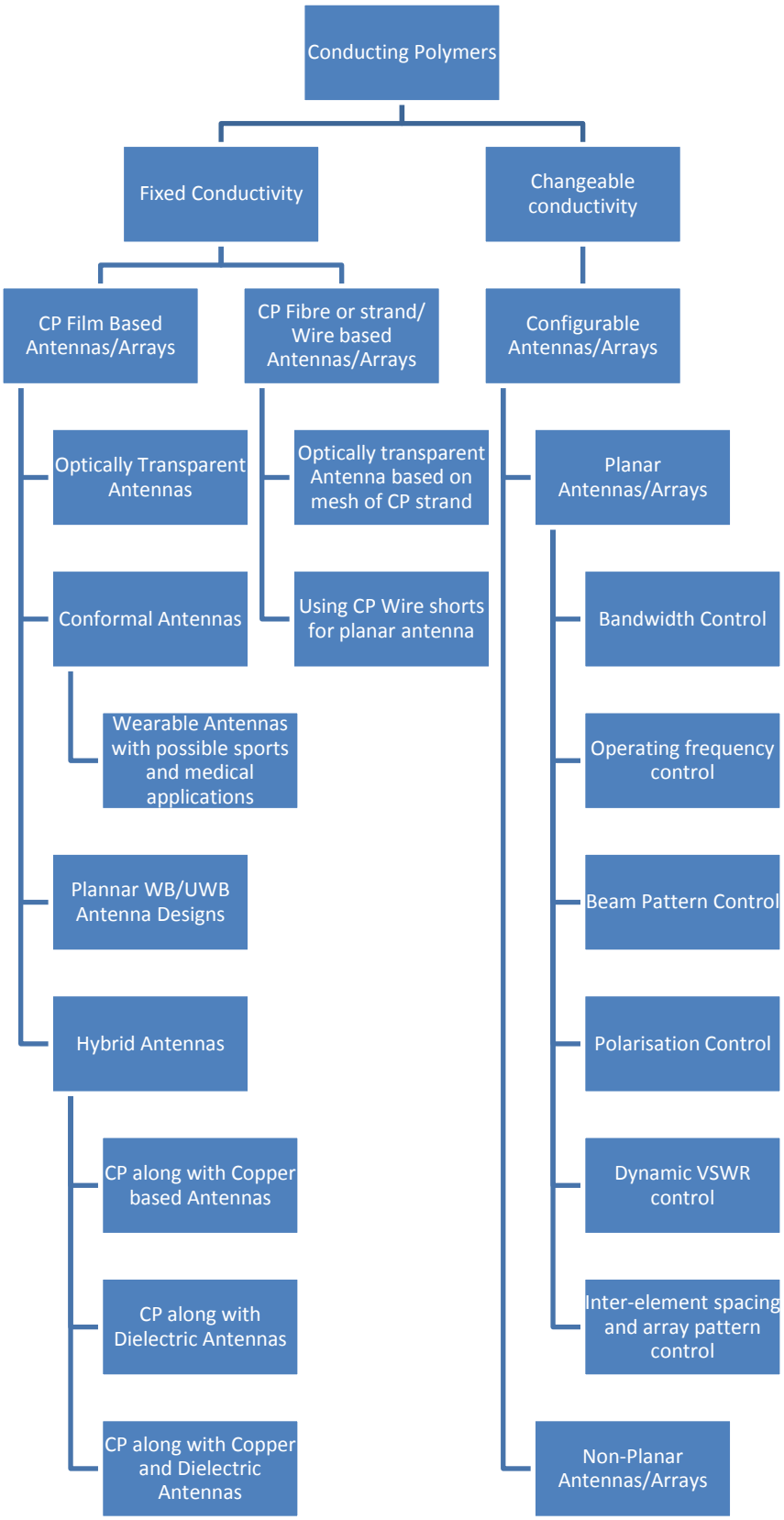

Figure 5.1: Some research possibilities with CP-based antennas.

5.2.1 Optically Transparent Antennas

Optically transparent antennas are very attractive from a commercial applications point of view. They have the potential of changing our lives by the way we communicate and manage our connectivity with information networks. From windscreens of cars to solar panels of satellites, all those large transparent surfaces could become the real estate for future antennas or their arrays.

Making an optically transparent antenna has been a challenge for over two decades now. It is obvious that since light is also an EM wave, both conductivity of the antenna and its optical transparency are diametrically opposite requirements. A highly conductive patch antenna would restrict the amount of light that could pass through it. Hence different approaches need to be explored. One approach could be to have a mesh of closely placed highly conductive carbon nano fibres. The mesh would provide just the right size for about 80-85% Visual Light Transmission (VLT). A sketch below indicates the basic design of the antenna. Interestingly, technology does exist to change/control the conductivity of each carbon nano fibres in the mesh and hence the amount of light passing through the antenna patch.

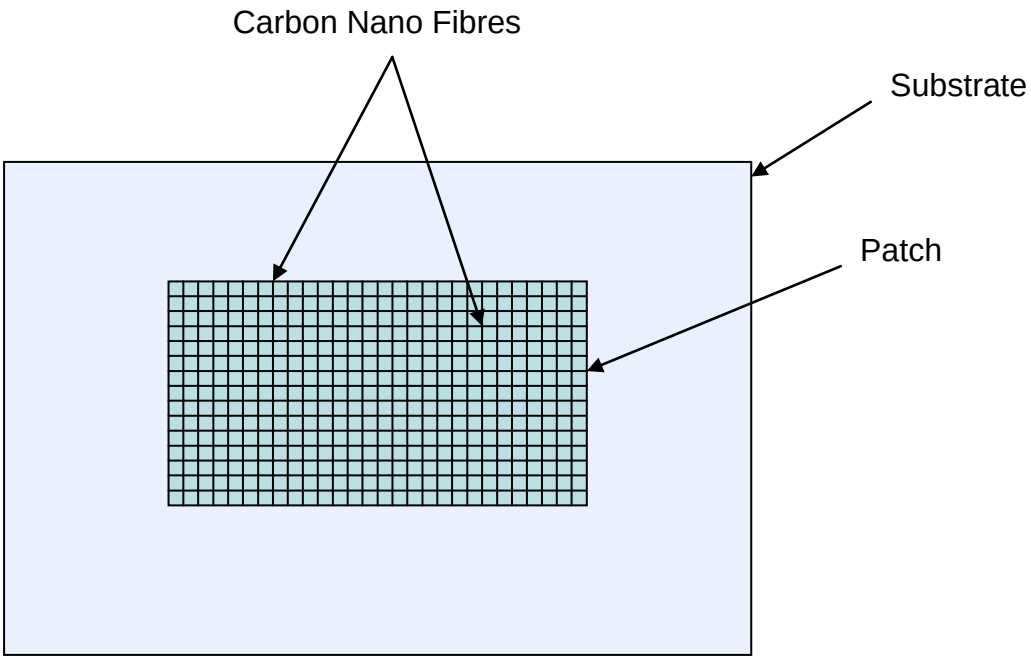

Figure 5.2: A possible design for an optically transparent Antenna with Visual Light Transmission (VLT) that could reach about 80%

5.2.2 Hybrid Antennas

Hybrid antennas could be planar or non-planar antennas that are made of radiating element, which is a combination of CP, polymers, carbon nano-tubes, dielectric resonator antennas (DRA) and/ or copper (metal). These combinations could be between any of these three materials. It would be exciting to design such antennas with an additional degree of freedom of controlling the conductivity/material properties of CP element. In our opinion this sort of antennas could open up possibilities, where a single antenna meets Quality of Service (QoS) requirements for very diverse RF applications.

5.2.3 Other materials with antenna application potential

Other materials such as Graphene (Figure 5.3), which is equally conductive and easy to fabricate/print/spray on substrates of choice, also holds immense possibilities. The films of this material have been tested for conductivity in various thicknesses (few microns to 100s of microns) and generally give about 7000 S/m conductivity (under lab conditions) which is reasonably conductive for applications where antenna efficiency could be compromised a little for other considerations such as ease of fabrication, light weight, low cost, or flexibility for conformal designs.

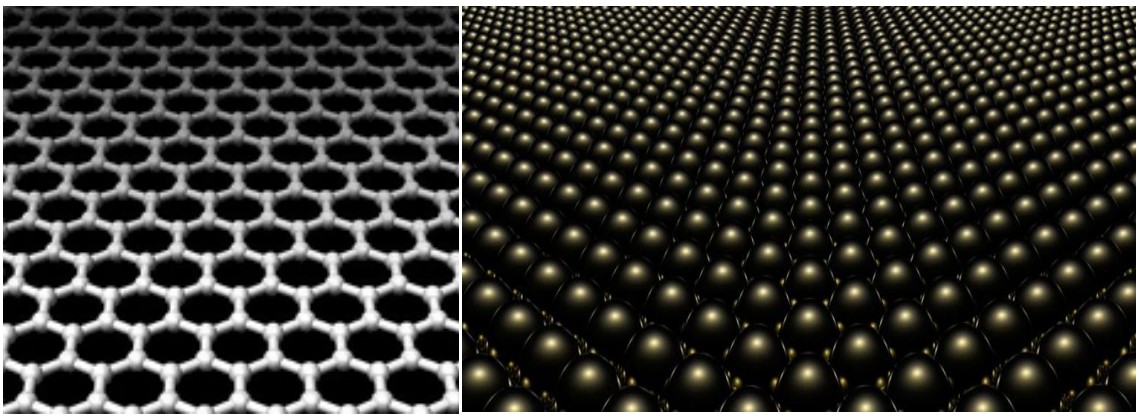

Figure 5.3: Graphene is another material that could have interesting microwave antenna applications (Images: metamordern.com)

In addition there are of course other possibilities of using Graphene in conjunction with other CPs in antenna applications.

5.2.4 Reconfigurable Antennas

Reconfigurable antennas have been realised with standard technologies using diodes, MEMs, etc. These are antennas that can change their operational characteristics based on the EM environment and on suitability for particular applications so as to ensure acceptable level of Quality of Service (QoS). This implies that such antennas or their arrays can support adaptively narrow band applications over a wide frequency band. They could change the shape of the radiation beam to meet particular applications. The antenna could support different polarisations based on either EM environment conditions or as part of particular application requirement. Interleaving of different and very diverse applications may be possible through the same antenna.

In the context of CPs re-configurable antennas could be made possible by changing the conductivity of the polymer in real time in a controlled fashion. This feature of CPs holds immense importance particularly in Defence related applications, where such antennas could be made active only at the time of transmission and could be RF transparent otherwise. This would help reduce the RCS of the transmitting platform. Furthermore such antennas could also provide graceful degradation of service when partially damaged.

There are many exciting challenges that would confront us while trying to fully realise such antennas and their arrays. From the material perspective it would heavily depend on speeds that could be achieved in trying to change bulk (volume metric) conductivity of CPs in real time and its acceptability towards applications that would like to utilise this feature. I understand that certain ion exchange cells have been developed (around year 2007-2008) that could cause change in conductivity of certain CPs at 20 MHz rate. This in my opinion is a good starting point for experimenting while this technology improves further. A number of different planar antenna designs could be tried as proof of concept. A few of such reconfigurable antenna designs are shown in Figure 5.4 to 5.6 which are only indicative of the myriad possibilities that actually exist.

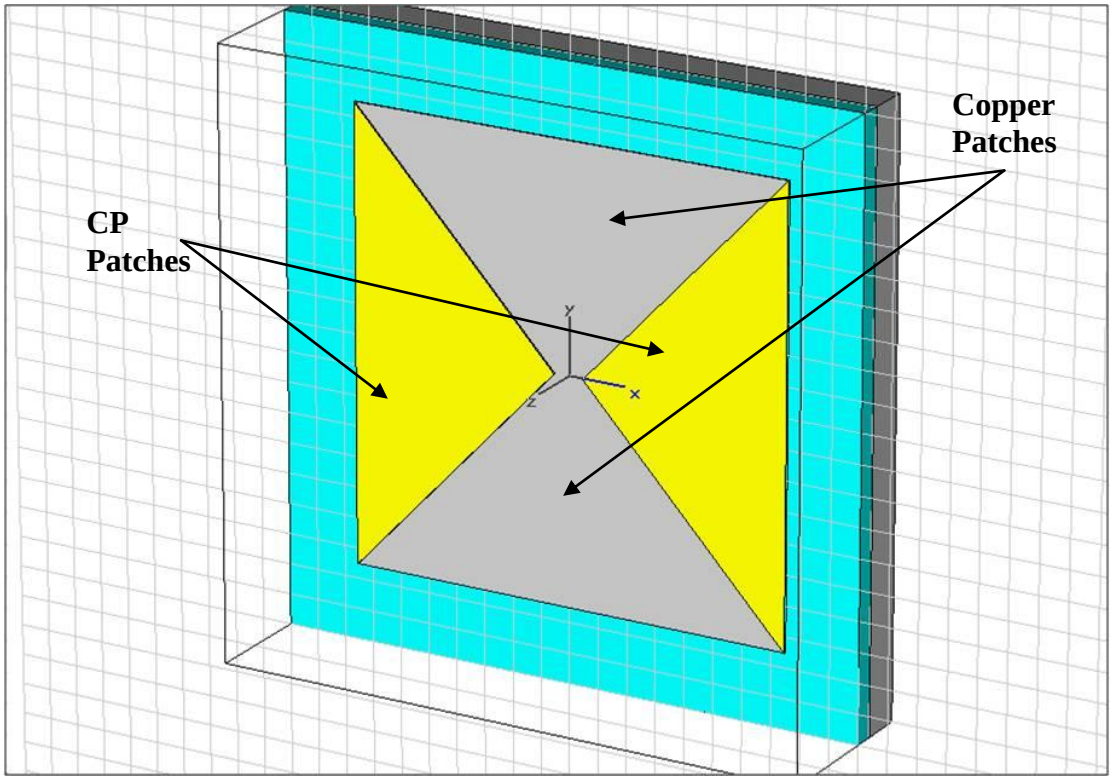

Figure 5.4: A narrow band and wide band switchable planar antenna

Figure 5.4 shows a schematic of a simple narrow band microstrip patch antenna and a wide band Bowtie antenna. This antenna would be narrow band antenna when the CP patches are highly conductive and would be wideband antenna when the CP patches are non-conductive.

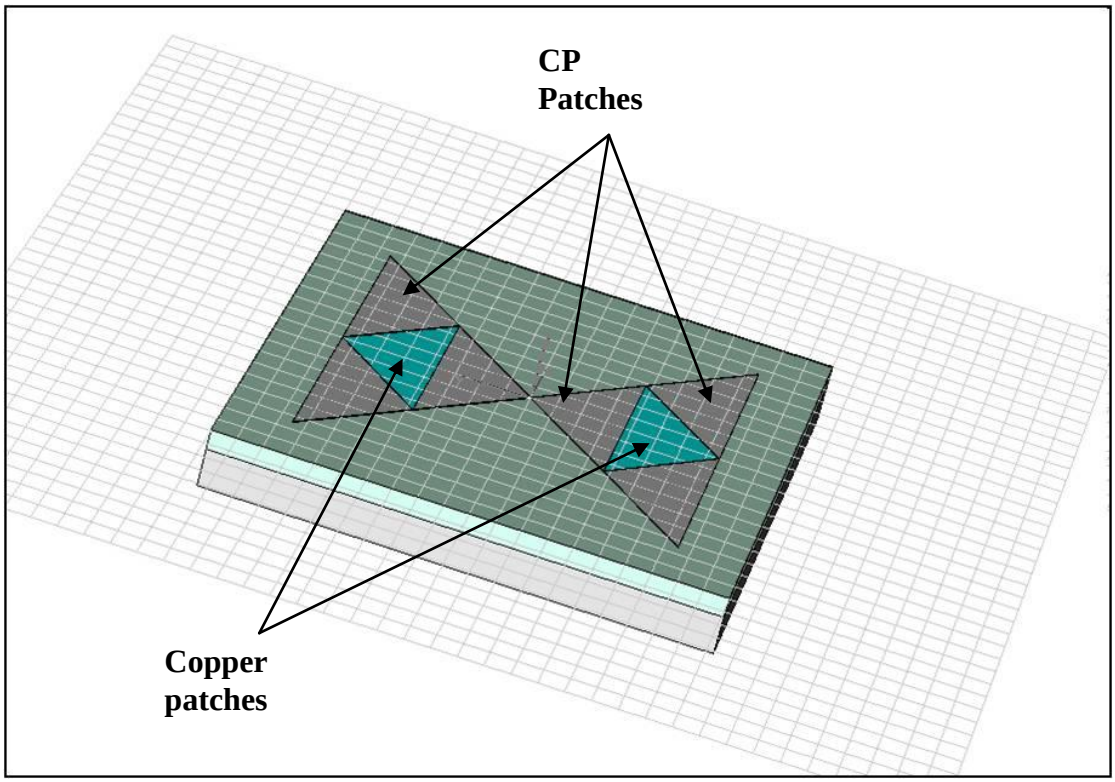

Figure 5.5 : Sierpinski-Bowtie transformation antenna

Figure 5.5 is more of a run of imagination and shows the possible changes that may be made to the patch shape by changing the conductivity of CP segments.

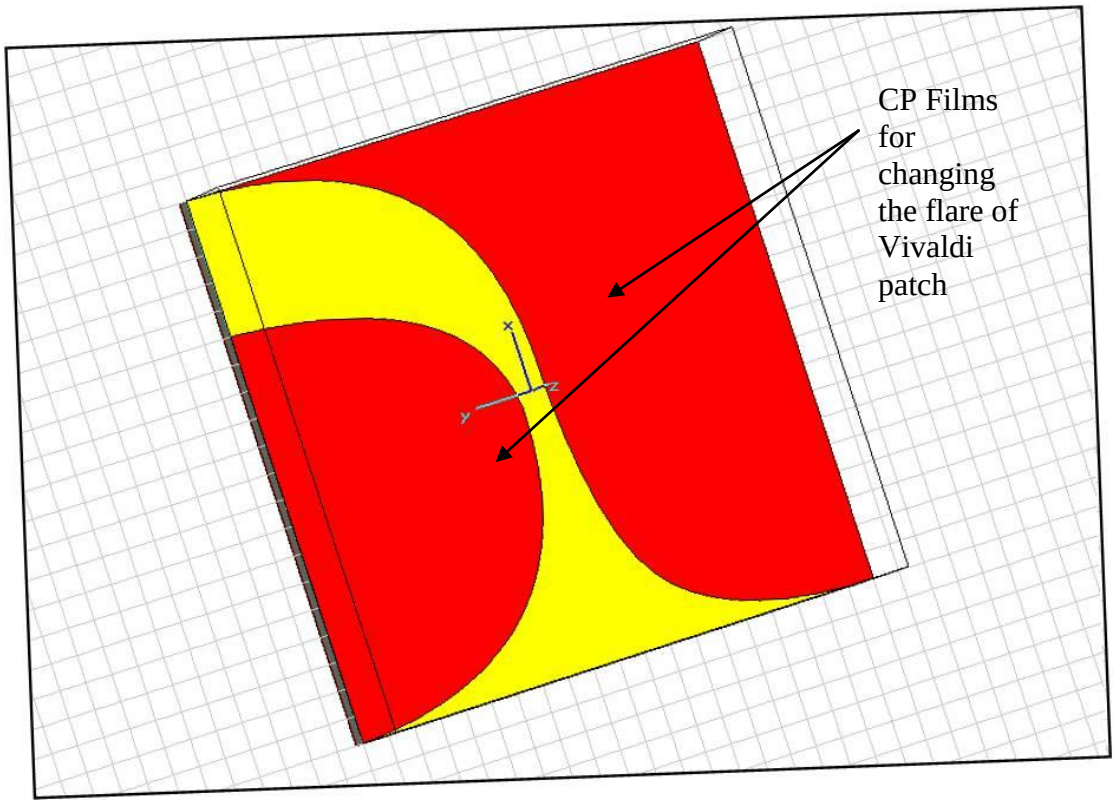

Figure 5.6 : Vivaldi antenna with adjustable flare

Here again in Figure 5.6 an attempt is made to show the possibility of changing the flare or taper of Vivaldi antenna by controlling the bulk conductivity of CP films.

The stability and ageing of CP is another field that would require great experimentation and development of very stable CPs. Literature also indicates exciting prospect of having superconducting CPs. Considering such materials for antenna applications would also promise some very exciting developments in the field of radio telescopes for deep space exploration.

In essence unconventional materials such as CPs, carbon nano-tubes, and Graphene hold promise towards development of microwave antennas that are low cost, light weight, re-configurable and conformal. Antennas and arrays developed with these exotic materials would impact upon plethora of fields such as automobile industry, construction industry, sports, medical applications, indoor appliances, toys, Microwave RF ID tracking, deep space exploration and space applications. This thesis is just the beginning, a small

step towards achieving greater understanding of these materials and their application as microwave antennas.

Appendix-A

Determination of Effective Permittivity of Multi-layer Microstrip lines using a Modified Getsinger's Model

A.1 Introduction

Microstrip transmission lines are known to be dispersive. A number of attempts were made by earlier researchers to provide a closed form equation that could accurately describe the dispersion in microstrip transmission lines. The works of Itoh et al. [1, 2], Jansen et al. [3], Jackson et al. [4], Pues et al. [5], Kuester et al. [6] and Getsinger [7] are some of the earlier attempts to describe dispersion due to permittivity in microstrip transmission lines.

The motivation for the present analysis is to obtain an accurate closed form expression for the dispersive effective permittivity of multilayered structures, such as a suitable RF substrate with PPy film or PET coated PEDOT film in a planar antenna. This knowledge of the effective permittivity is essential when utilising rectangular patch antenna design equations, as a starting point for full field electromagnetic simulations.

The microstrip line dispersion model proposed by Getsinger [7] is based on the assumption that the quasi TEM mode on microstrip lines is primarily a single Longitudinal Section Electric (LSE) mode. The dispersion in such a model can therefore be easily analysed. Getsinger's model was further improved by works presented by Edwards et al. [8], and Kirschning et al. [9]. Kirschning has accurately reported the dispersion in the effective dielectric

constant of a microstrip transmission line with a range of validity stretching up to millimetre wave frequencies.

It is pertinent to mention here that most of the reported work in this field is focused on characterizing dispersion in single layered dielectric microstrip lines. However, multilayered microstrip line structures have been studied extensively for the computation of quasi-static effective dielectric constant. In this regards, different techniques have been applied to determine the quasi static effective dielectric constant in multilayered microstrip lines, e.g. the variational approach based works by Yamashita et al. [10-12]; Variational and Transmission line (TL) approach by Chang et al. [13], Crampagne et al. [14] and Khalid et al. [15]; and conformal mapping methods by Yoon et al. [16], and Svacina et al. [17].

The dispersion of the effective dielectric constant in multilayered microstrip lines has been reported by Verma et al. [18, 19]. Verma's approach is an amalgamation of the variational and TL approach for determination of quasi-static dielectric constant of multilayered dielectric microstrip and the conformal mapping method for the determination of permittivity constant for an equivalent single layered structure which are, finally combined to the Getsinger's LSE model to determine the dispersion due to the effective dielectric constant. Verma et al. [18, 19] calls the technique for determining the equivalent single layered constant of permittivity for a multilayered microstripline structure as "Single Layer Reduction" (SLR) technique and the final application of this into Getsinger's model as the "Unified Dispersion Model" (UDM).

In this chapter, the possibility of applying multilayered dielectric microstrip line structures directly to the Getsinger model is explored and the performance of this model is evaluated against UDM and a reference solution obtained using 2D finite-element eigenmode analysis from the port solution in Ansoft's HFSS^{TM}. The UDM applies SLR to quasi-static dielectric constants determined by using Variational and TL (Verma's approach), conformal

approaches (Svacina's and Yoon's method) and simple static series capacitance methods.

A.2 Single Layer Reduction and Unified Dispersion Model

The SLR and UDM proposed by Verma et al. [18, 19] is at its core based on the logic that:

(a) The quasi-static effective dielectric constant ϵ_{e0} can easily be determined for multi-layer dielectric microstrip lines through application of the Variational and TL approach of Chang et al. [13].

(b) From Wheeler [20, 21], the relationship between ϵ_{e0} and ϵ_s (where 'ϵ_s' is the relative dielectric constant of a single layered dielectric in a Microstrip transmission line) is given by:

$$\epsilon_{e0} = 1 + q(\epsilon_s - 1) \tag{A.1}$$

where q is the effective filling fraction of the dielectric material. Wheeler [21] opines that the effective filling fraction depends mainly on the shape and less on the dielectric material. Verma et al. [19] considers equation (A.1) for deriving an equivalent relative dielectric constant ϵ_{seq} for a single layered microstrip transmission line, which would exhibit similar dispersion characteristics. This approach has been termed as SLR. The empirical expression for q obtained by Schneider [22] is considered to be close enough for practical purposes and is given as:

$$q = \frac{1}{2}\left(1 + \frac{1}{\sqrt{1 + \frac{10b}{W}}}\right) \tag{A.2}$$

where b is the thickness of the dielectric substrate and W is the width of the microstrip line. Re-arranging equation (A.1) the expression for equivalent relative dielectric constant ϵ_{seq} is:

$$\epsilon_{seq} = 1 + \frac{1}{q}(\epsilon_{e0} - 1) \tag{A.3}$$

(c) Finally using the values obtained for ϵ_{e0} and ϵ_{seq} and applying these in Getsinger's LSE model, provides dispersion characteristics for multilayered dielectric microstrip transmission line. This has been termed by Verma et al. [18, 19] as the UDM. The salient features of Getsinger's LSE model have been presented in the next section.

A.3 Salient Features of Getsinger's Model

Getsinger's proposed LSE model provides analytical simplicity in determining the dispersion of effective dielectric constant for a microstrip line. Getsinger considers microstrip propagation as a single LSE mode. He justifies the validity of his model on the basis that if an analyzable model exhibits similar measurable characteristics to the actual structure, then the model is valid and acceptable. His model is based on the fact that electric field lines emanating from the lower surface of the microstrip pass only through the dielectric. The electric field lines emanating from the top portion of the microstrip occupy a much larger space mostly in air. This space is approximated by a large air filled section in the model. Further, near the strip edges, the magnetic field is predominantly normal to the air-dielectric boundary (or interface), while the electric field is tangential to, this boundary. This is the characteristic of the LSE mode [23]. The details of a simple single layered microstrip transmission line are depicted in Figure A.1 and while Figure A.2 details the Getsinger's LSE model.

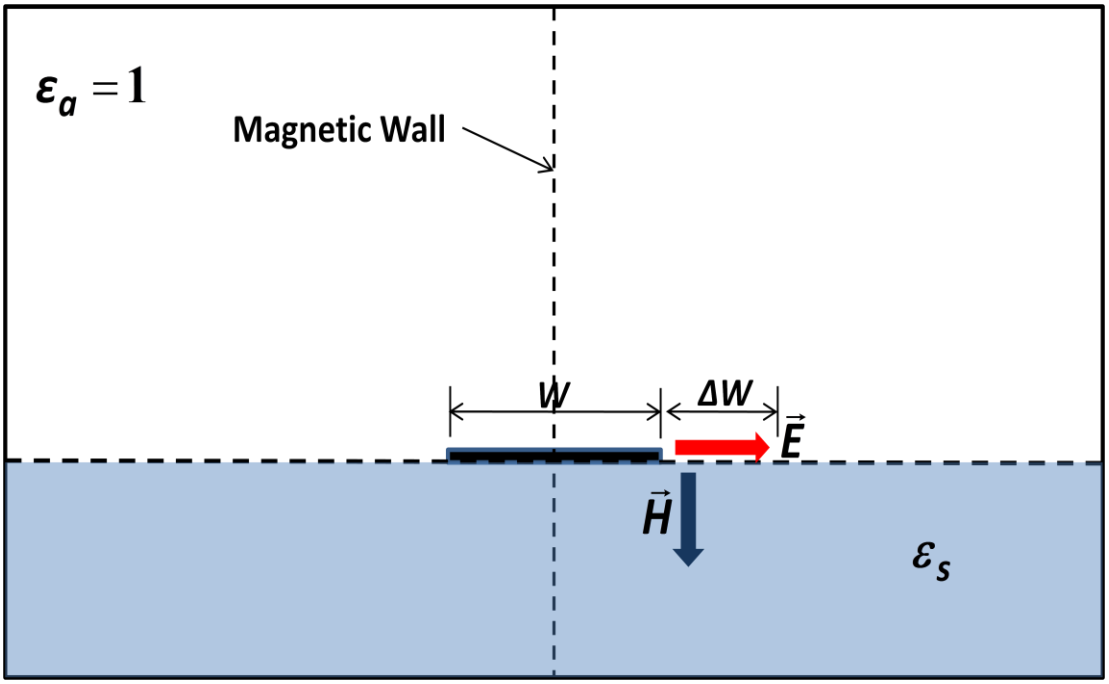

Figure A.1 : Single-layer microstrip transmission line

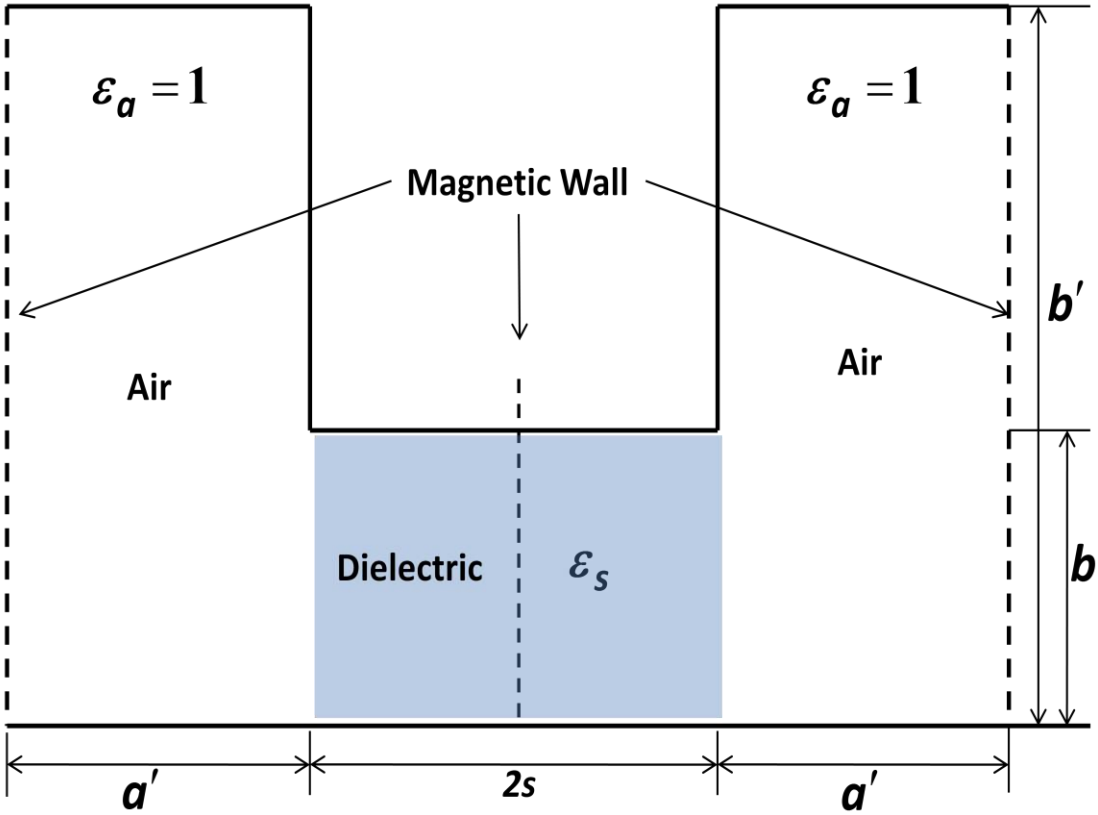

Figure A.2 : LSE model for single layer dielectric microstrip line

The magnetic walls are present on the two sides and at the centre of the model as shown in Figure A.2. Getsinger's model in essence joins two parallel plate transmission lines, one with dielectric and the other with air. For the purpose of computational ease, no junction capacitance at the union of the two transmission lines is assumed. The solution for the dispersion of effective permittivity ϵ_e is simple and is obtained through the application of Transverse Resonance (TR) technique [23, 24]. The closed form expression for effective permittivity as a function of frequency is given as:

$$\epsilon_e = \epsilon_s - \frac{\epsilon_s - \epsilon_{e0}}{1 + P(f)} \tag{A.4}$$

where $P(f)$ has been accurately determined by Kirschning et al. [9].

Ideally one would expect the Getsinger LSE model to be as shown in Figure A.3. However, interestingly, Getsinger in his model (shown at Figure A.2) considers the length of air-dielectric interface to be same as the thickness of the dielectric substrate. It is pertinent to mention here that since junction capacitance between the two parallel plate waveguides has been neglected in this model, the overall effect of the "length of air-dielectric interface" per se is not taken into account. This point is important, if not central to developing a multilayered Getsinger LSE model.

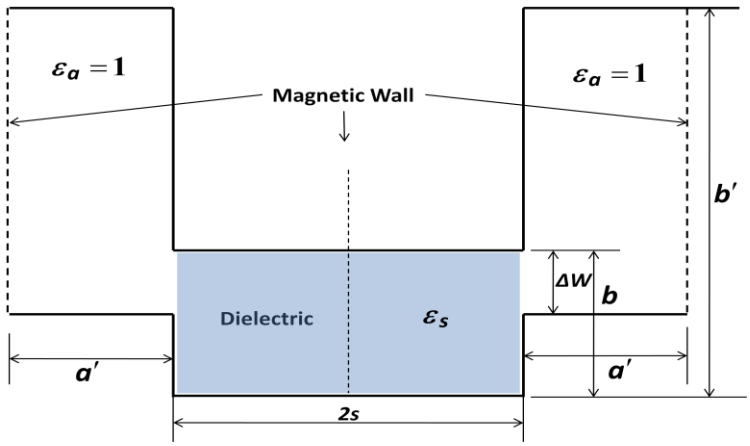

Figure A.3 : LSE model for single layer dielectric microstrip line modified to take into account the air-dielectric interface length

A.4 Double layered Getsinger's LSE Model for Dispersion of permittivity in Microstrip lines

In principle a multilayered version of Getsinger's LSE model may be developed by recursive application of the transverse resonance method. However, a general closed form expression for dispersion due to effective permittivity is too complex and cumbersome. In this work, we therefore restrict to the analysis and development of closed form expression for two and three layered microstrip line structures only. An alternate approach to overcome cumbersome algebra is proposed at the end of the two and three layered microstrip line structures analysis. A double (or two layered) microstrip line structure is shown in Figure A.4.

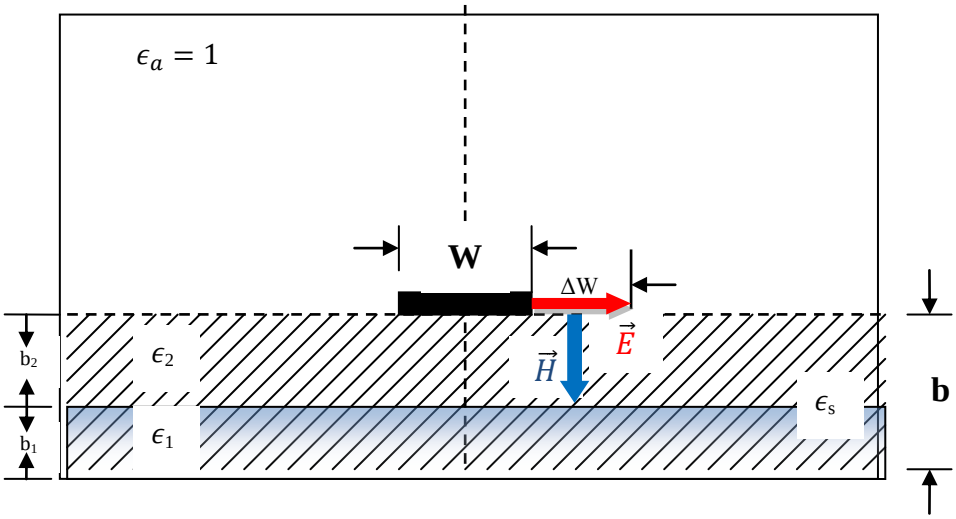

Figure A.4 : Two-layer microstrip transmission line

The corresponding LSE model for the two-layered dielectric microstrip transmission line is shown in Figure A.5[1]:

[1] In Figure A.5 we have considered the air-dielectric interface to be equal to the thickness of the top layer b_2, similarly to the approach adopted by Getsinger in his LSE model. This approach has no bearing on the final outcome of the model towards computation of dispersion of permittivity.

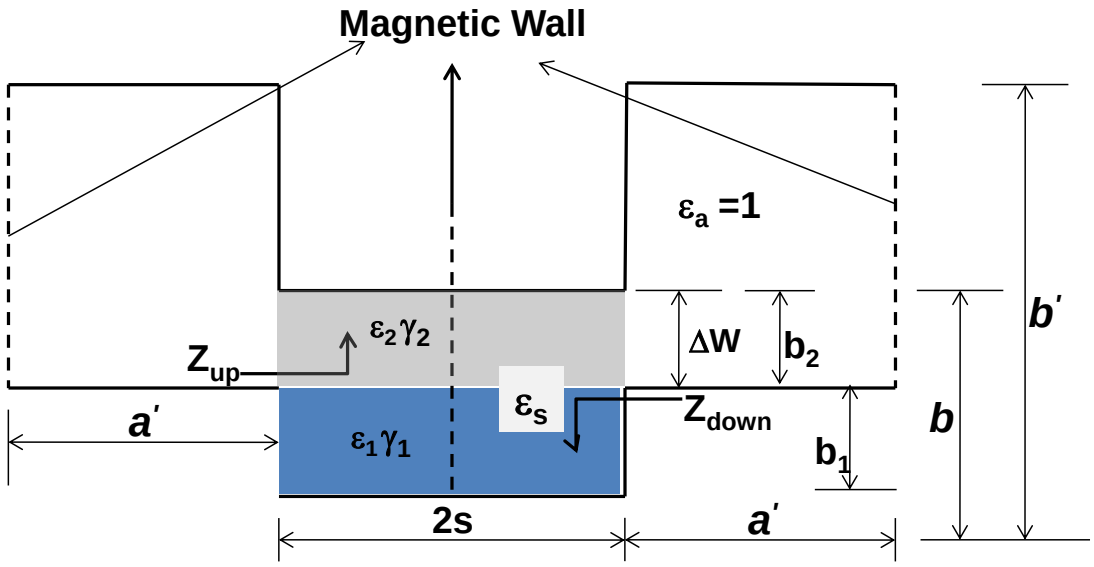

Figure A.5 : LSE model for a two-layer dielectric microstrip line

From the microstrip line structure (Figure A.4) it is possible to compute the inductance and capacitance of the microstrip line per unit length at zero frequency (static) as

$$\frac{L'}{\mu_0} = \frac{Z_0}{\eta_0}\sqrt{\epsilon_{e0}} \tag{A.5}$$

and

$$\frac{\boldsymbol{C'}}{\boldsymbol{\epsilon_0}} = \frac{\boldsymbol{\eta_0}}{\boldsymbol{Z_0}}\sqrt{\boldsymbol{\epsilon_{e0}}} \tag{A.6}$$

where z_0 is the characteristic impedance and where free space impedance is

$$\eta_0 = \sqrt{\frac{\mu_0}{\epsilon_0}} = 377\Omega \tag{A.7}$$

Similarly, static computations based on LSE model (Figure A.2 and Figure A.5) yield:

$$\frac{L'}{\mu_0} = \frac{1}{2\left[\frac{a'}{b'} + \frac{s}{b}\right]} \tag{A.8}$$

as the inductance per unit length.

Next the equivalent dielectric constant for the dielectric layers sandwiched between the two parallel plates is assumed to be given by ϵ_s. It is important to

understand here that ϵ_s is different from the effective dielectric permittivity for the microstrip line at zero frequency, indicated as ϵ_{e0}. The effective dielectric constant for the microstrip line at zero frequency ϵ_{e0} (static) includes the effect of air above the microstrip line and the dielectric layers below the strip conductor. In contrast the equivalent dielectric constant ϵ_s takes into consideration only the combined effect of the permittivity of the dielectric layers that are sandwiched between the parallel conducting plates.

Similarly, the static capacitance from the LSE model is indicated as

$$\frac{C'}{\varepsilon_0} = 2\left(\frac{a'}{b'} + \epsilon_s \frac{s}{b}\right) \tag{A.9}$$

Further, since the effect of junction capacitances are being neglected, it is possible to consider the two parallel plate transmission line sections as separate parallel plate waveguides for ease of analysis. Consider the section of parallel plate transmission line with two dielectric layers shown below in Figure A.6. Let γ_1 be the propagation constant through layer 1 in the 'y' direction. Similarly, let γ_2 be the propagation constant through layer 2 in the 'y' direction. Next, the propagation constant in the 'z' or 'x' direction will be same (due to the layered structure and orientation of the layers) and will be defined by the combined effect of both the layers and is given as γ_s.

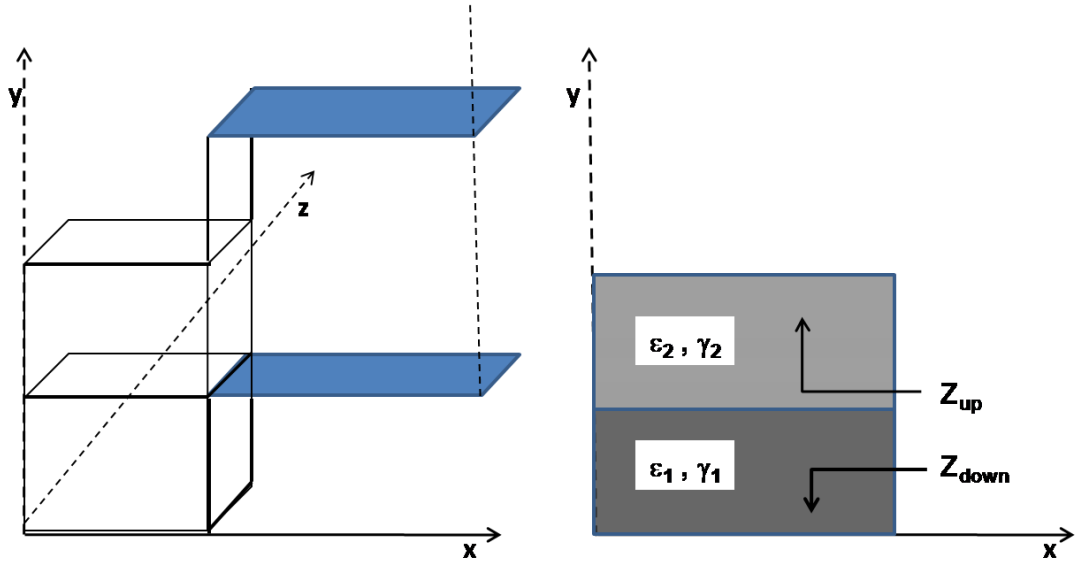

Figure A.6 : (a) Orientation of the LSE model, (b) Cross sectional YZ plane view of the LSE model with propagation constants along the 'y' direction.

The basic philosophy behind the modified Getsinger model for double layer dielectric is depicted in Figure A.7. As indicated in Figure A.7, the actual LSE model of double-layer microstrip line is replaced by an equivalent single-layer LSE model. This task requires determination of the relationship between the permittivity of the single-layer substrate 'ϵ_s' and the permittivity of double-layer substrates 'ϵ_1' and 'ϵ_2'.

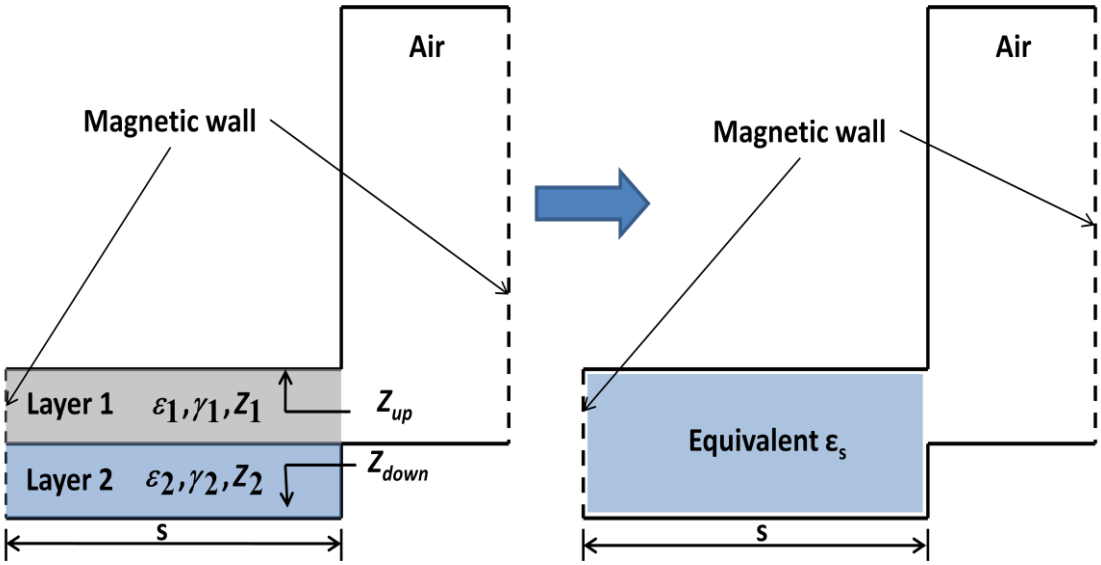

Figure A.7 : Equivalence of LSE model

From the TR technique [23-25] the input impedance, as seen looking upwards, towards the top plate (which is PEC, and therefore acts as a short) from the junction of the two dielectric interfaces (Figure A.6), is given by

$$Z_{up} = Z_{02} \tanh \gamma_2 b_2 \tag{A.10}$$

Similarly, since the bottom plate is also PEC and acts as a short. Hence, input impedance Z_{down} is given by

$$Z_{down} = Z_{01} \tanh \gamma_1 b_1 \tag{A.11}$$

where Z_{01} and Z_{02} are the characteristic impedance of the two layers respectively. Hence from the transverse resonance (TR) condition we have that

$$Z_{up} + Z_{down} = 0 \tag{A.12}$$

From (A.10), (A.11) and (A.12) it follows that

$$Z_{02} \tanh \gamma_2 b_2 + Z_{01} \tanh \gamma_1 b_1 = 0 \tag{A.13}$$

Since the propagation in the multilayered microstrip line is TM, the transcendental equation above at (A.13) could be simplified further by applying following:

(a) Characteristic impedance $Z_{0i} = \frac{\gamma_i(\,propagation\ constant\ of\ layer)}{\omega\epsilon_i\,(permittivity\ of\ layer)}$ ([25, 26])

(b) $\tanh x \approx \frac{1}{\frac{1}{x}+\frac{x}{3}}$ for $x \leq 1$. It is pertinent to highlight here that Getsinger uses the tanh(x) approximation[2] within an error of about 1.5%, by considering that x is within $-1 \leq x \leq 1$.

After some algebraic manipulations, this gives

$$\frac{3\gamma_1^2 b_1}{\epsilon_1(3+\gamma_1^2 b_1^2)} + \frac{3\gamma_2^2 b_2}{\epsilon_2(3+\gamma_2^2 b_2^2)} = 0 \tag{A.14}$$

$$\epsilon_2\gamma_1^2 b_1(3+\gamma_2^2 b_2^2) + \epsilon_1\gamma_2^2 b_2(3+\gamma_1^2 b_1^2) = 0 \tag{A.15}$$

Furthermore, the propagation constants of the two layers are related by

$$\gamma_1^2 + \gamma_s^2 + \epsilon_1 k_0^2 = 0 \tag{A.16}$$

$$\gamma_2^2 + \gamma_s^2 + \epsilon_2 k_0^2 = 0 \tag{A.17}$$

The longitudinal (i.e. in the 'z' direction, Figure A.6(a)) propagation constant γ_s can be expressed in terms of effective dielectric constant ϵ_s as

$$\gamma_s^2 = -k_0^2\epsilon_s \tag{A.18}$$

From (A.16), (A.17) and (A.18) it follows

$$\gamma_1^2 = k_0^2(\epsilon_s - \epsilon_1) \tag{A.19}$$

[2] It is important to note that this approximation is valid only for tanhx and cannot be applied to cothx as reciprocal of tanhx

Similarly,

$$\gamma_2^2 = k_0^2(\epsilon_s - \epsilon_2) \tag{A.20}$$

Next applying equations (A.19) and (A.20) to (A.15) we obtain the following equations

$$\Big[3\big((\epsilon_1 b_2 + \epsilon_2 b_1)\epsilon_s - \epsilon_1\epsilon_2 b\big) + b_1 b_2 k_0^2(\epsilon_2 b_2 + \epsilon_1 b_1)[\epsilon_s^2 - (\epsilon_1 + \epsilon_2)\epsilon_s + \epsilon_1\epsilon_2]\Big] = 0 \tag{A.21}$$

Let us now define

$\alpha_1 = b_1 b_2 k_0^2(\epsilon_1 b_1 + \epsilon_2 b_2)$

$\alpha_2 = \epsilon_1 b_2 + \epsilon_2 b_1$

Therefore we have from (A.21):

$$\alpha_1\epsilon_s^2 + [3\alpha_2 - \alpha_1(\epsilon_1 + \epsilon_2)]\epsilon_s + (\alpha_1 - 3b)\epsilon_1\epsilon_2 = 0 \tag{A.22}$$

Hence,

$$\epsilon_s = \frac{[3\alpha_2 - \alpha_1(\epsilon_1 + \epsilon_2)] \pm \{[3\alpha_2 - \alpha_1(\epsilon_1 + \epsilon_2)]^2 - 4\alpha_1\epsilon_1\epsilon_2(\alpha_1 - 3b)\}^{\frac{1}{2}}}{2\alpha_1} \tag{A.23}$$

For situations where $b_2 = 0$ (or $b_1 = 0$), would imply that $\gamma_2 = \gamma_1$. To check the consistency of the model it is prudent to apply these conditions to (A.14), resulting in

$$\frac{3\gamma_1^2 b_1}{\epsilon_1(3 + (\gamma_1 b_1)^2)} = 0 \text{ for } b_2 = 0 \tag{A.24}$$

This implies that

$\gamma_1^2 = 0$ and from (A.19) it follows that

$$k_0^2(\epsilon_s - \epsilon_1) = 0 \tag{A.25}$$

Hence,

$$\epsilon_s = \epsilon_1 \tag{A.26}$$

It can similarly be shown that for the case where $b_1 = 0$, $\epsilon_s = \epsilon_2$.

For finding the effective permittivity ϵ_e of the two-layered microstrip line structure, ϵ_s obtained from (A.23) can be substituted into Getsinger's equation at (A.4).

A.4.1 Simulations and Results

A two-layered microstrip line was simulated using Ansoft HFSS. The simulations were run by considering the port boundaries of the microstrip line as radiation, or Perfect Magnetic Conductor (PMC), or Perfect Electric Conductor (PEC), or Perfectly Matched Layer (PML). The consistency of results across various port boundary conditions (as indicated above) validates the results obtained on the effective permittivity dispersion in the model.

A 1 GHz microstrip line was designed using standard design equations given by Hammerstad et al. [27]. The details of the design are placed in Table A.1. Using SLR in conjunction with various methods for determining the quasi-static effective dielectric constant (such as Variational and TL, conformal mapping and series capacitance method), UDM was applied to obtain the dispersion of effective permittivity. In addition dispersion was also determined using the proposed multilayered Getsinger's LSE model.

Table A.1 : Design data of 1 GHz microstrip line

Parameter	Value
Bottom Layer: Layer 1	
Permittivity constant layer 1 ϵ_1	4.4
Thickness b_1	0.8mm
Top Layer: Layer 2	
Permittivity constant layer 2 ϵ_2	2.33
Thickness b_2	0.15mm
Microstrip line width W	1.41mm

The results of the investigation are shown in Figure A.8 and indicate that the multilayered Getsinger's LSE model provides the closest dispersion of permittivity to the full wave simulation results. Svacina's CMA model is also close to the reference for frequencies below 10 GHz. (Figure A.8 and Figure A.9).

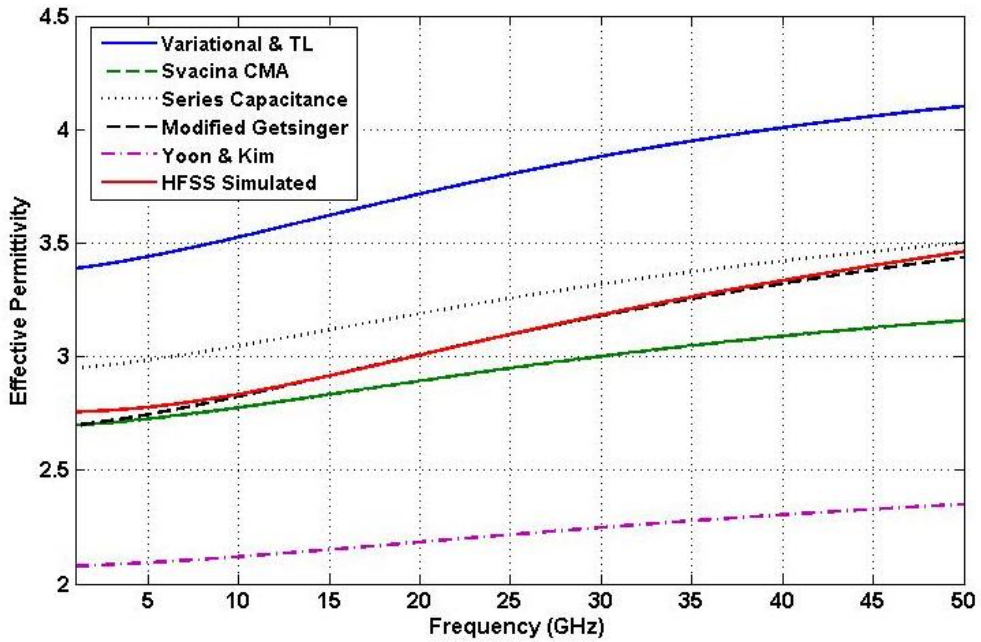

Figure A.8 : Dispersion of Effective Permittivity in Microstrip line with double layered dielectric (with ϵ_1 =4.4 and ϵ_2 = 2.33)

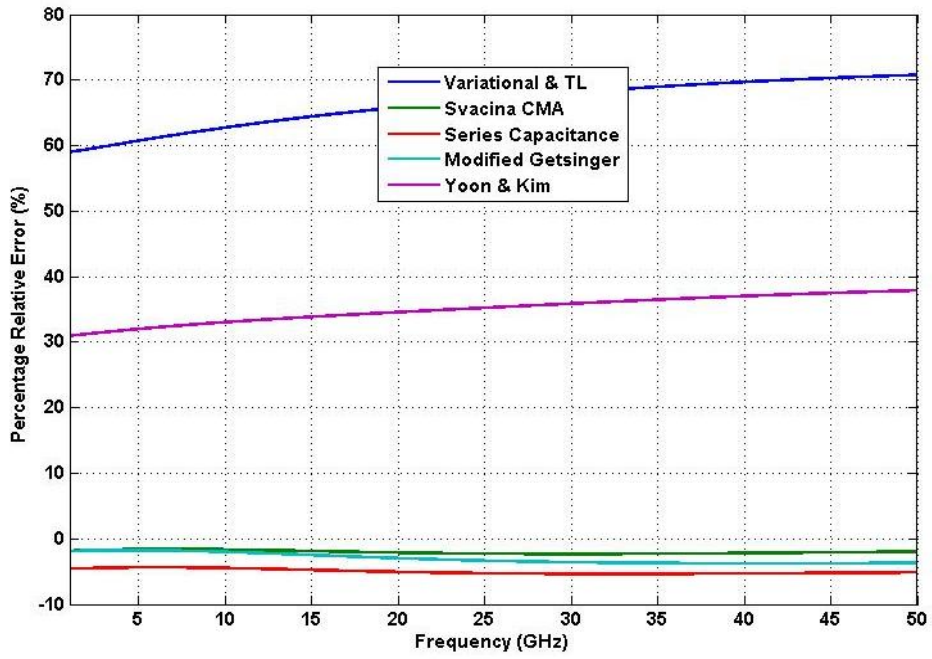

Figure A.9 : Dispersion of relative error percentage (with ϵ_1 = 2.33 and ϵ_2 = 4.4)

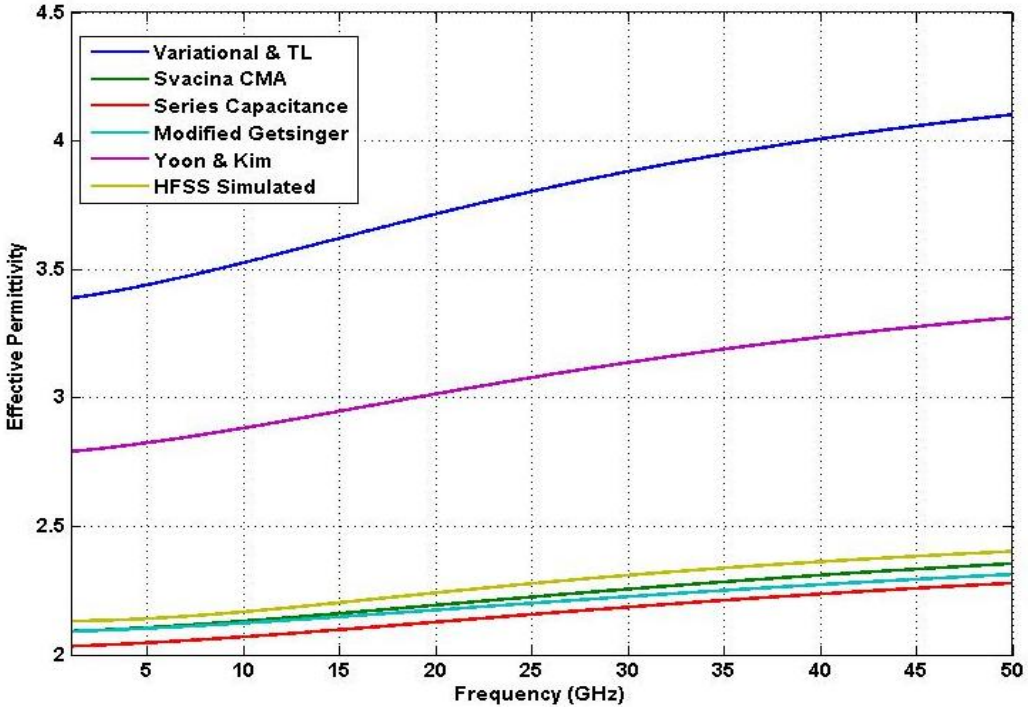

Figure A.10 : Dispersion of Effective Permittivity in Microstrip line with double layered dielectric (with ϵ_1 = 2.33 and ϵ_2 = 4.4)

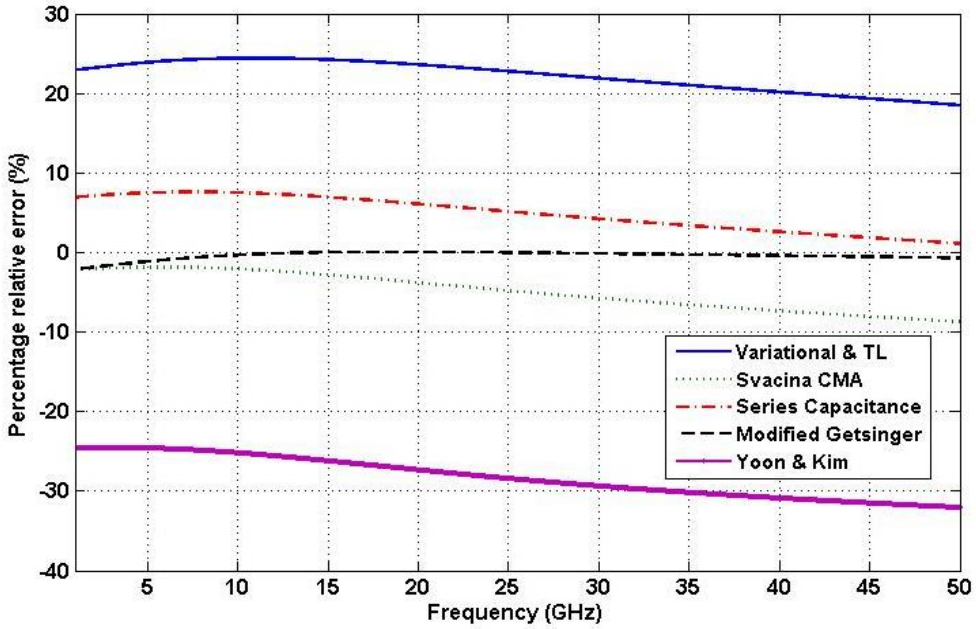

Figure A.11 : Dispersion of relative error percentage (with ϵ_1 = 4.4 and ϵ_2 = 2.33)

Similarly, the two layered microstrip line was also investigated with top and bottom layers swapped (i.e. ϵ_1= 2.33 and ϵ_2= 4.4; keeping the layer

thicknesses the same, i.e. b_1= 0.8 mm and b_2= 0.15 mm). Results are plotted in Figure A.10 and Figure A.11.

It is clearly evident from Figure A.9 and A.11 that the percentage relative error for Getsinger's multilayered model is lower than for the other models that are based on UDM in the present example. It is also interesting to observe that the multilayer Getsinger's model has errors less than 1.5% up to 50 GHz, while Svacina's CMA offers results within 9% error, for frequencies up to 50 GHz. The relative performance of other models is generally far from satisfactory. Another example with different substrate thickness and relative permittivity is shown in Figure A.12 and Figure A.13 to highlight the better accuracy of the proposed model.

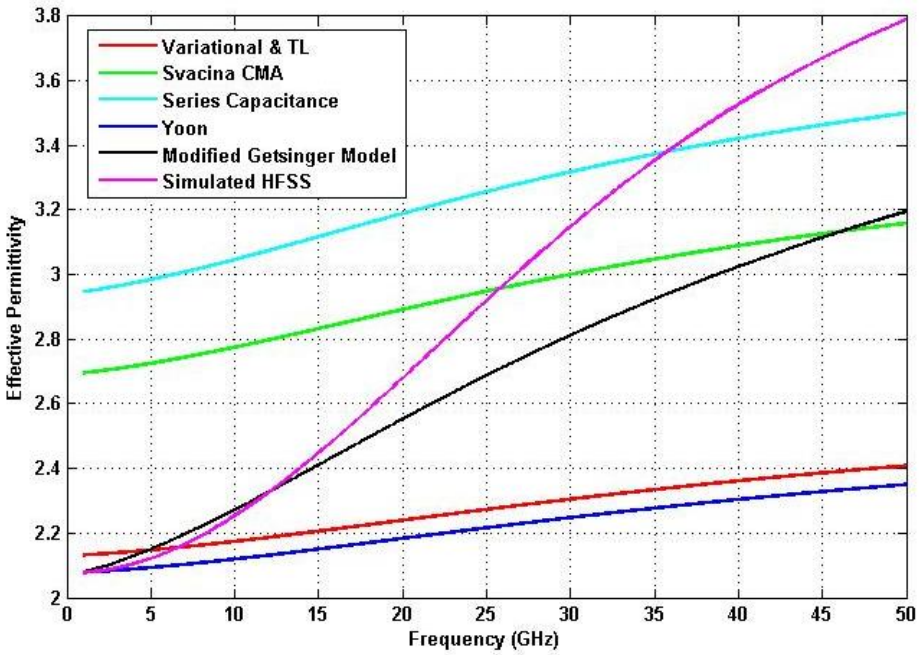

Figure A.9 : Dispersion of Effective Permittivity in Microstrip line with double layered dielectric (with ϵ_1 = 4.5, b_1 = 1.6 mm and ϵ_2 = 2.5, b_2 = 0.8 mm)

However, these examples cannot be considered as a general proof on the effectiveness of this model. The limitation for presenting such a proof is the inability in accounting for all possible combinations of substrate permittivity and thicknesses. Furthermore, since the suggested model substitutes the multi-layer substrate with a single layer (homogenous) substrate having suitable equivalent permittivity 'ε_s' and the fact that the dispersion of effective permittivity is based on accepted Getsinger's LSE model, it could be

conjectured that the proposed model would have the same limitations as indicated in [28] namely $1 \leq \varepsilon_s \leq 20$ and $0.1 \leq {}^{W}/_{b} \leq 100$. It is however difficult to translate the limitations of equivalent permittivity 'ε_s' and thickness 'b' in terms of permittivity constant and thicknesses of individual substrate layers.

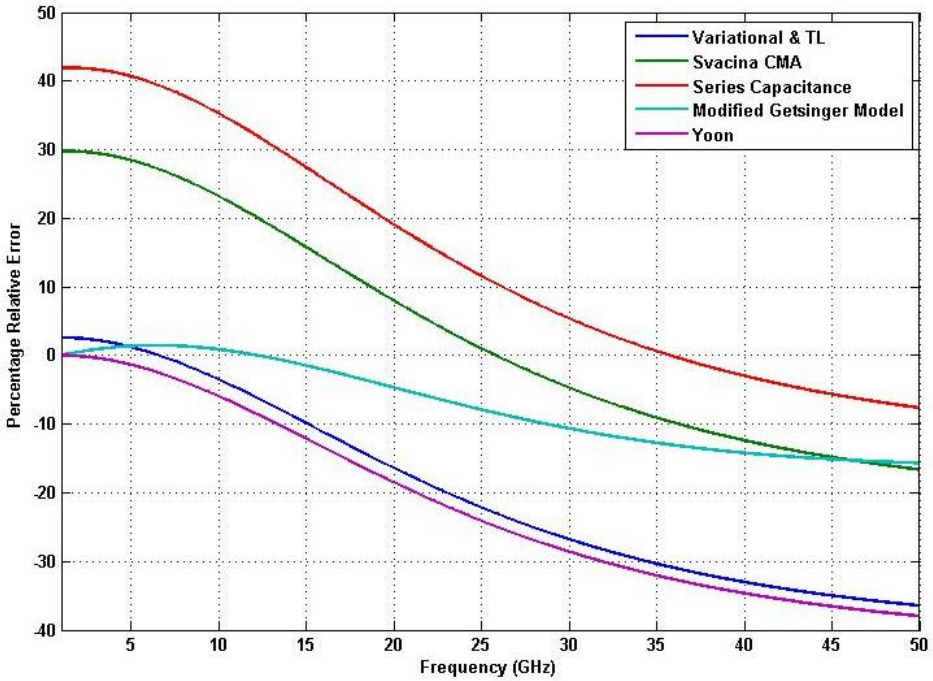

Figure A.10 : Dispersion of relative error percentage (with ϵ_1 = 4.5, b_1 = 1.6 mm and ϵ_2 = 2.5, b_2 = 0.8 mm)

A.4.2 Alternative Approach

The present day computational power of computers allows us to solve numerically transcendental equations of the type indicated at equation (A.13). Some examples of such softwares that allow computation of transcendental equations are Maplesoft™[3], Mathematica™[4] etc. The advantage of this approach is that no approximation of the hyperbolic tangent functions is required, which results in more accurate solutions without range limitations.

In equation (A.13), the propagation constants are substituted from equations (A.19) and (A.20). Further, in accordance with [25, 26] the

[3] http://www.maplesoft.com
[4] http://www.wolfram.com

characteristic impedance of the layers are also substituted in the equation as indicated below:-

$$\frac{\gamma_2}{\omega\epsilon_2}\tanh\gamma_2 b_2 + \frac{\gamma_1}{\omega\epsilon_1}\tanh\gamma_1 b_1 = 0 \qquad \text{(A.27)}$$

and from equations (A.19) and (A.20) following transcendental equation is obtained

$$\epsilon_1\sqrt{\epsilon_s - \epsilon_2}\tanh\left(b_2 k_0\sqrt{\epsilon_s - \epsilon_2}\right) + \epsilon_2\sqrt{\epsilon_s - \epsilon_1}\tanh\left(b_1 k_0\sqrt{\epsilon_s - \epsilon_1}\right) = 0 \qquad \text{(A.28)}$$

Solving for ϵ_s and eliminating non-physical solutions, the found values of ϵ_s are applied to Getsinger's LSE model. This then provides dispersion of the effective permittivity of a double-layer microstrip line structure. It is observed that both approaches provide similar results within acceptable accuracy.

A.5 Triple layered Getsinger's LSE Model for Dispersion of permittivity in Microstrip lines

In this section we intend to extend the model to cover the dispersion of permittivity in a three-layer microstrip line structure is shown in Figure A.14. The corresponding schematic of the Getsinger's LSE model for this three-layer microstrip line is depicted in Figure A.15.

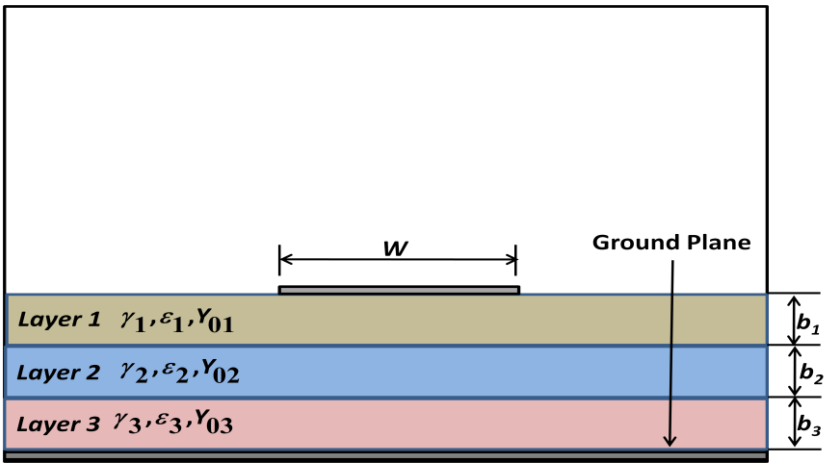

Figure A.11 : Triple layer dielectric microstrip line

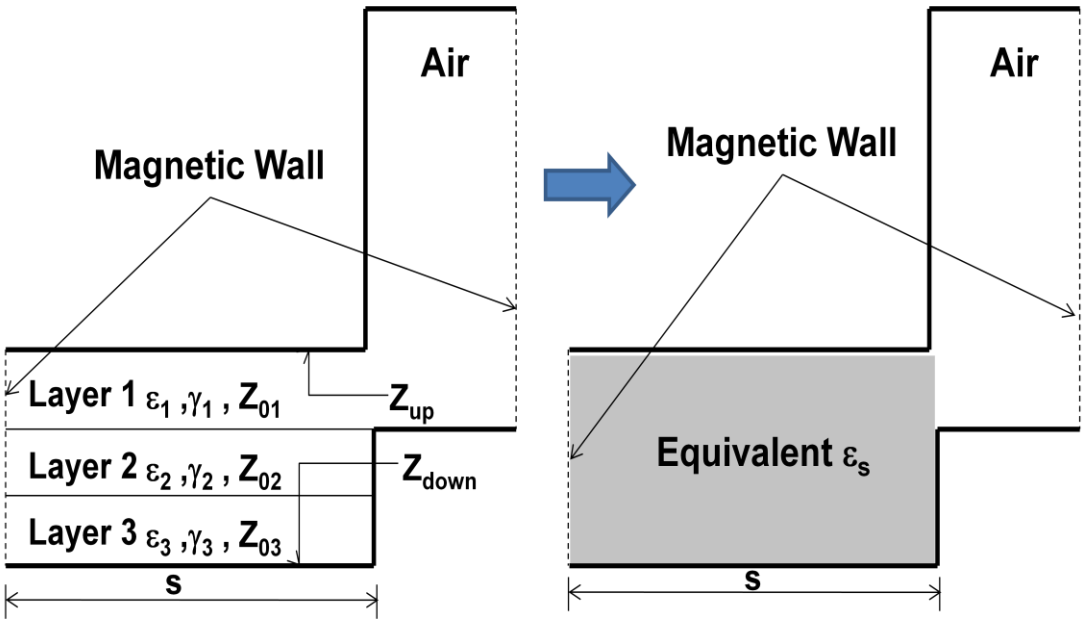

Figure A.12 : Three-layer Getsinger's LSE model

Similarly, as in the previous analysis, the TR method is applied to obtain the transcendental equation. Hence,

$$Z_{up} + Z_{down} = 0 \tag{A.29}$$

$$Z_{up} = Z_{01} \tanh \gamma_1 b_1 \tag{A.30}$$

$$Z_{down} = Z_{02} \left[\frac{Z_L + Z_{02} \tanh \gamma_2 b_2}{Z_{02} + Z_L \tanh \gamma_2 b_2} \right] \tag{A.31}$$

where

$$Z_L = Z_{03} \tanh \gamma_3 b_3 \tag{A.32}$$

Therefore from (A.26), (A.27), (A.28) and (A.29) it follows that

$$Z_{02} \left[\frac{Z_{03} \tanh \gamma_3 b_3 + Z_{02} \tanh \gamma_2 b_2}{Z_{02} + Z_{03} \tanh \gamma_3 b_3 \tanh \gamma_2 b_2} \right] + Z_{01} \tanh \gamma_1 b_1 = 0 \tag{A.33}$$

This implies that

$$Z_{01}Z_{02} \tanh \gamma_1 b_1 + Z_{01}Z_{03} \tanh \gamma_3 b_3 \tanh \gamma_2 b_2 \tanh \gamma_1 b_1 + Z_{02}Z_{03} \tanh \gamma_3 b_3 + Z_{02}^2 \tanh \gamma_2 b_2 = 0 \tag{A.34}$$

Applying the conditions given at section A.3 about characteristic impedance and approximation for hyperbolic tangent to (A.32) gives

$$\frac{\gamma_1\gamma_2}{\epsilon_1\epsilon_2}\left[\frac{3\gamma_1 b_1}{3+\gamma_1^2 b_1^2}\right]+\frac{\gamma_1\gamma_3}{\epsilon_1\epsilon_3}\left[\frac{3\gamma_3 b_3}{3+\gamma_3^2 b_3^2}\right]\left[\frac{3\gamma_2 b_2}{3+\gamma_2^2 b_2^2}\right]\left[\frac{3\gamma_1 b_1}{3+\gamma_1^2 b_1^2}\right] + \frac{\gamma_2\gamma_3}{\epsilon_2\epsilon_3}\left[\frac{3\gamma_3 b_3}{3+\gamma_3^2 b_3^2}\right]+\frac{\gamma_2^2}{\epsilon_2^2}\left[\frac{3\gamma_2 b_2}{3+\gamma_2^2 b_2^2}\right]=0 \quad \text{(A.35)}$$

This simplification gives:

$$\gamma_1^2\gamma_2\epsilon_3 b_1(3+\gamma_2^2 b_2^2)(3+\gamma_3^2 b_3^2)+9\gamma_3^2\gamma_2\gamma_1^2\epsilon_2 b_3 b_2 b_1 + \gamma_3^2\gamma_2\epsilon_1 b_3(3+\gamma_2^2 b_2^2)(3+\gamma_1^2 b_1^2) + \frac{\gamma_2^3\epsilon_1\epsilon_3 b_2}{\epsilon_2}(3+\gamma_1^2 b_1^2)(3+\gamma_3^2 b_3^2)=0 \quad \text{(A.36)}$$

As before, since the propagation constants are related by:

$$\gamma_s^2=-k_0^2\epsilon_s \quad \text{(A.37)}$$

$$\gamma_1^2=k_0^2(\epsilon_s-\epsilon_1) \quad \text{(A.38)}$$

$$\gamma_2^2=k_0^2(\epsilon_s-\epsilon_2) \quad \text{(A.39)}$$

$$\gamma_3^2=k_0^2(\epsilon_s-\epsilon_3) \quad \text{(A.40)}$$

Substitution of above equations into (A.34), results in:

$$(\rho_1+\tau_1)\epsilon_s^3+(\alpha_1+\beta_1+\rho_2+\tau_2)\epsilon_s{}^2+(\alpha_2+\beta_2+\rho_3+\tau_3)\epsilon_s + (\alpha_3+\beta_3+\rho_4+\tau_4)=0 \quad \text{(A.41)}$$

Where:

$$\rho_1=k_0^4 b_1^2 b_2^2 b_3\epsilon_1\epsilon_2$$

$$\rho_2=\left(3k_0^2 b_2^2+3k_0^2 b_1^2-k_0^4 b_1^2 b_2^2 b_3\epsilon_1\epsilon_2(\epsilon_1+\epsilon_2+\epsilon_3)\right)$$

$$\rho_3=(9+k_0^4 b_1^2 b_2^2\epsilon_1\epsilon_2)b_3\epsilon_1\epsilon_2-b_3\epsilon_1\epsilon_2\epsilon_3\left(3k_0^2 b_2^2+3k_0^2 b_1^2-k_0^4 b_1^2 b_2^2(\epsilon_1+\epsilon_2)\right)$$

$$\rho_4=-b_3\epsilon_1\epsilon_2\epsilon_3(9+k_0^4 b_1^2 b_2^2\epsilon_1\epsilon_2)$$

$$\tau_1=k_0^4 b_1^2 b_3^2 b_2\epsilon_1\epsilon_3$$

$$\tau_2=\left(3k_0^2 b_1^2+3k_0^2 b_3^2-k_0^4 b_1^2 b_3^2 b_2\epsilon_1\epsilon_3(\epsilon_1+\epsilon_2+\epsilon_3)\right)$$

$$\tau_3=(9+k_0^4 b_1^2 b_3^2\epsilon_1\epsilon_3)b_2\epsilon_1\epsilon_3-b_2\epsilon_1\epsilon_2\epsilon_3\left(3k_0^2 b_1^2+3k_0^2 b_3^2-k_0^4 b_1^2 b_3^2(\epsilon_1+\epsilon_3)\right)$$

$$\tau_4=-b_2\epsilon_1\epsilon_2\epsilon_3(9+k_0^4 b_1^2 b_3^2\epsilon_1\epsilon_3)$$

$$\alpha_1 = k_0^2 b_2^2 b_1 \epsilon_2 \epsilon_3$$
$$\alpha_2 = 3 b_1 \epsilon_2 \epsilon_3 - k_0^2 b_2^2 b_1 \epsilon_2 \epsilon_3 (\epsilon_1 + \epsilon_2)$$
$$\alpha_3 = k_0^2 b_2^2 b_1 \epsilon_1 \epsilon_2^2 \epsilon_3 - 3 b_1 \epsilon_1 \epsilon_2 \epsilon_3$$
$$\beta_1 = 9 k_0^2 \epsilon_2^2 b_1 b_2 b_3$$
$$\beta_2 = -9 k_0^2 \epsilon_2^2 b_1 b_2 b_3 (\epsilon_1 + \epsilon_3)$$
$$\beta_3 = 9 k_0^2 \epsilon_2^2 \epsilon_1 \epsilon_3 b_1 b_2 b_3$$

For situations where $b_3 = 0$ would imply that $\gamma_3 = \gamma_2$ and applying these conditions into (A.33) reduces it to:

$$\frac{\gamma_1 \gamma_2}{\epsilon_1 \epsilon_2} \left[\frac{3 \gamma_1 b_1}{3 + \gamma_1^2 b_1^2} \right] + \frac{\gamma_2^2}{{\epsilon_2}^2} \left[\frac{3 \gamma_2 b_2}{3 + \gamma_2^2 b_2^2} \right] = 0 \quad \text{(A.42)}$$

This could be further reduced to

$$\epsilon_2 \gamma_1^2 b_1 (3 + \gamma_2^2 b_2^2) + \epsilon_1 \gamma_2^2 b_2 (3 + \gamma_1^2 b_1^2) = 0 \quad \text{(A.43)}$$

This equation (A.43) is similar to (A.15) for the two-layer case and therefore the solution of (A.43) could be obtained by following the method described for two-layered microstrip line structure.

For finding the effective permittivity ϵ_e of the three-layered microstrip line structure, ϵ_s obtained from (A.41) can be substituted into Getsinger's equation at (A.4).

A.5.1 Simulations and Results

Several examples of three-layer microstrip lines were simulated using the eigenmode solver of Ansoft HFSS™. The simulations were run by considering the port boundaries of the microstrip line as radiation, or Perfect Magnetic Conductor (PMC), or Perfect Electric Conductor (PEC), or Perfectly Matched Layer (PML). The consistency of results across various port boundary conditions (as indicated above) validates the results obtained on the effective permittivity dispersion in the model.

A 1 GHz microstrip line was designed using standard design equations given by Hammerstad et al. [27]. Different commercially available RF substrates were considered for this study. These substrates are:

- Case-I: (a) RO 4350 (ε_r= 3.66), (b) RT/Duroid 5870 (ε_r= 2.33), and (c) RO 4003 (ε_r= 3.55),
- Case-II: (a) RO 3006 (ε_r= 6.15), (b) RT/Duroid 6002 (ε_r= 2.94), and (c) RO 3010 (ε_r= 10.2).

The general idea was to use realistic values for substrates permittivity and thickness. The details of the design are as shown in Figure A.16 (a) and Figure A.17 (a) for both cases of substrate combinations. SLR in conjunction with Variational and TL method is used for comparison of dispersion of effective permittivity with the proposed multilayered Getsinger's LSE model.

Figure A.16(a) shows the cross sectional layout of a microstripline of width 1.41 mm over three layers of substrates with different thicknesses and permittivity.

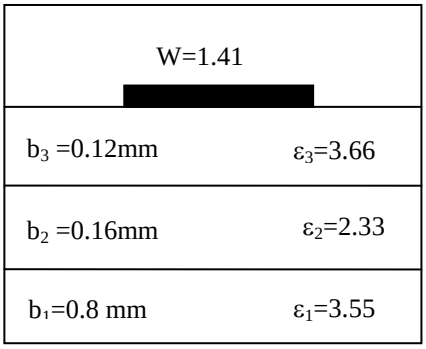

(a) General layout of three layered microstrip line

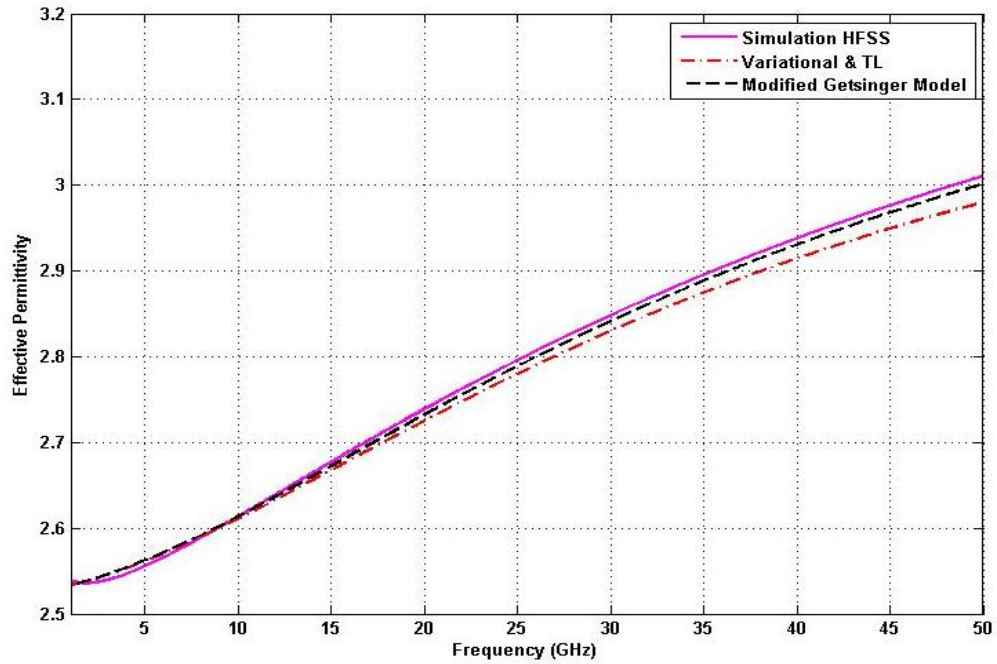

(b) Dispersion of Effective Permittivity

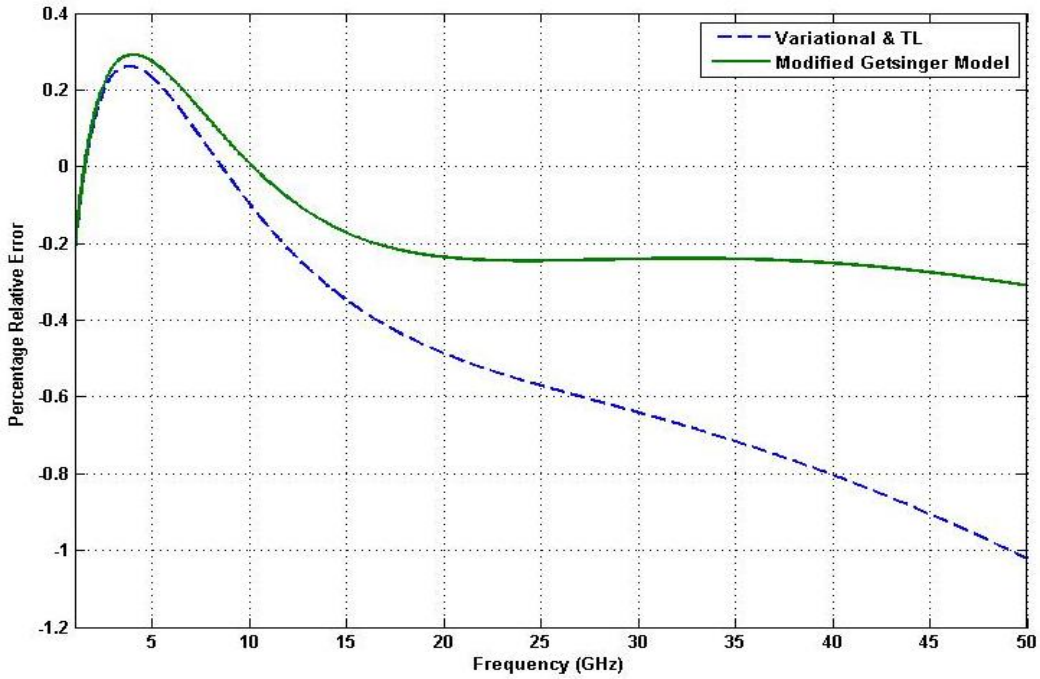

(c) Percentage Relative Error

Figure A.13 : (a) Layout of three layered microstrip line for case-I (b) dispersion of effective permittivity and (c) percentage relative error

Figure 16(b) presents the dispersion of effective permittivity of the three layer microstrip line structure over 1 to 50 GHz. While Figure 16(c) shows the percentage error in the effective permittivity observed between different

models that are considered against the actual effective permittivity obtained by using an eigen mode solver. Figure A.17(a), like Figure A.16(a) shows the cross sectional layout of a microstripline of width 1.41 mm over three layers of substrates with different thicknesses and permittivity.

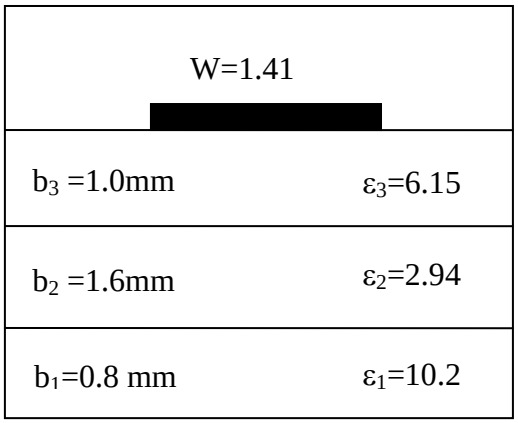

(a) General layout of three layered microstrip line

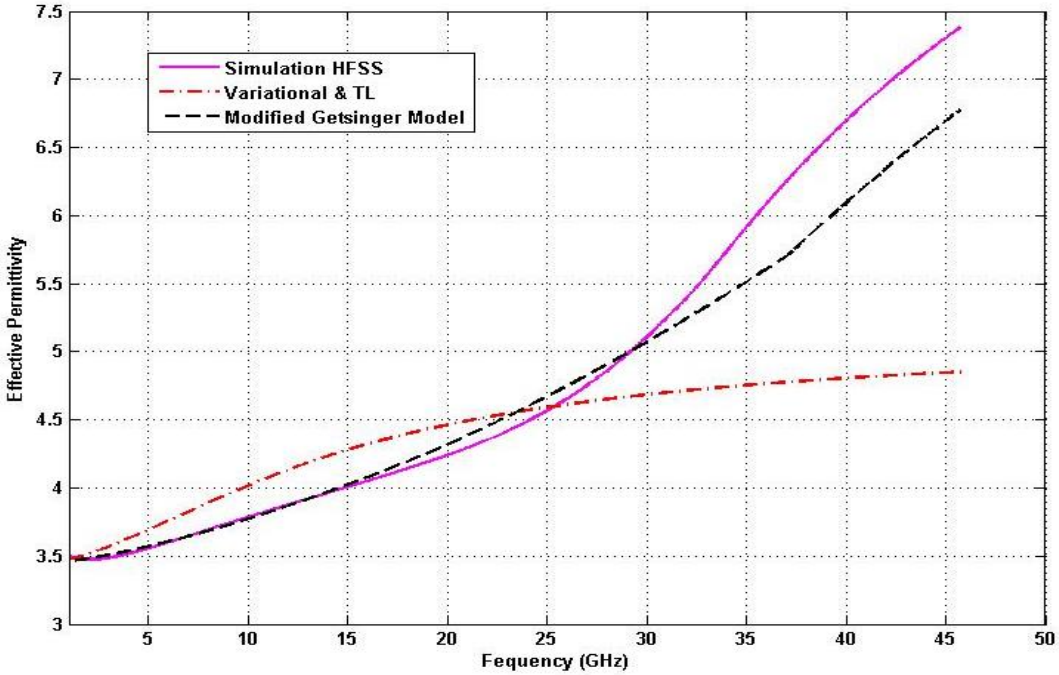

(b) Dispersion of Effective Permittivity

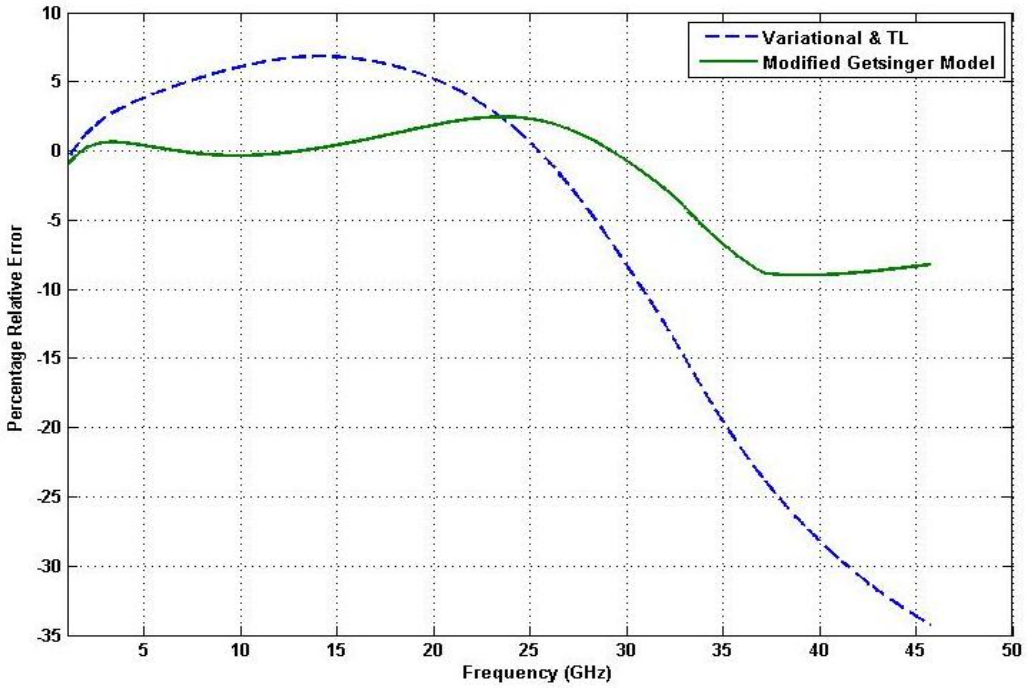

(c) Percentage Relative Error

Figure A.14 : (a) Layout of three layered microstrip line for case-II (b) dispersion of effective permittivity and (c) percentage relative error

Figure 17(b) presents the dispersion of effective permittivity of the three layer microstrip line structure over 1 to 50 GHz. While Figure 17(c) shows the percentage error in the effective permittivity observed between different models that are considered against the actual effective permittivity obtained by using an eigen mode solver.

A few additional examples with different thicknesses of substrates and realistic values relative permittivity are shown below to highlight the relatively better accuracy of modified Getsinger's model over other known models.

(a) Case III: A three layer microstripline with thickness 1.41 mm and substrate thicknesses and permittivity as shown in Figure A 18. The relative permittivity of top and bottom layers is almost identical, while the middle layer is comparatively thicker.

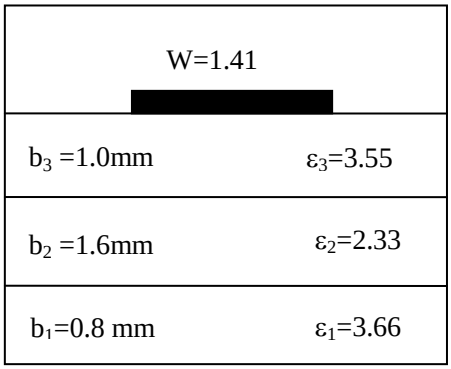

(a) General layout of three layered microstrip line

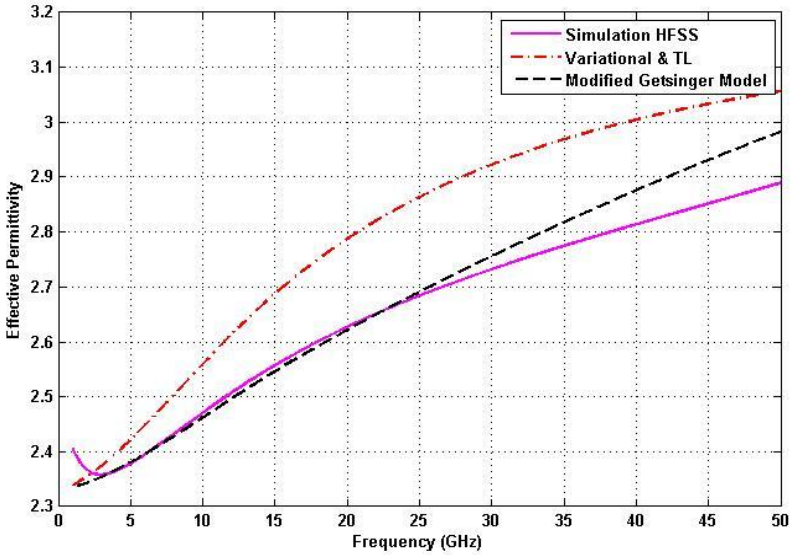

(b) Dispersion of Effective Permittivity

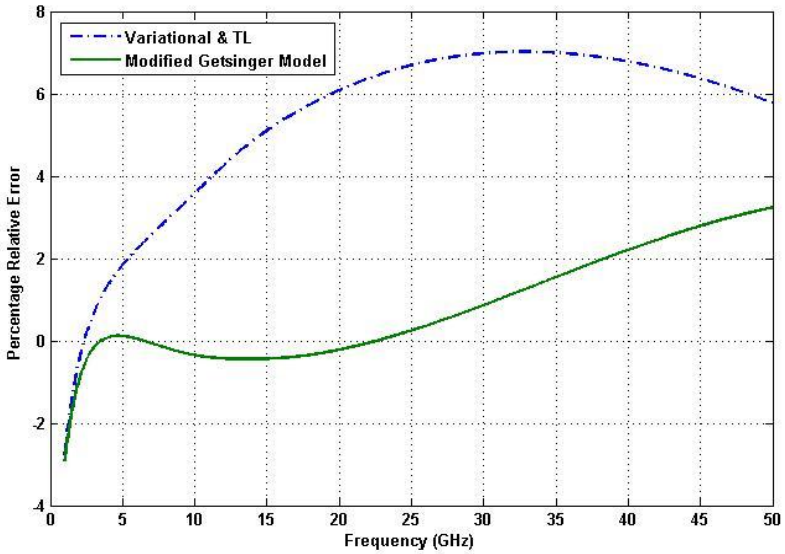

(c) Percentage Relative Error

Figure A.18 : (a) Layout of three layered microstrip line for case-III (b) dispersion of effective permittivity and (c) percentage relative error

(b) Case IV: A three layer microstripline with thickness 1.41 mm and substrate thicknesses and permittivity as shown in Figure A 19. The relative permittivity of top layer is higher than rest of the layers. Thickness of the layers is identical to Case III.

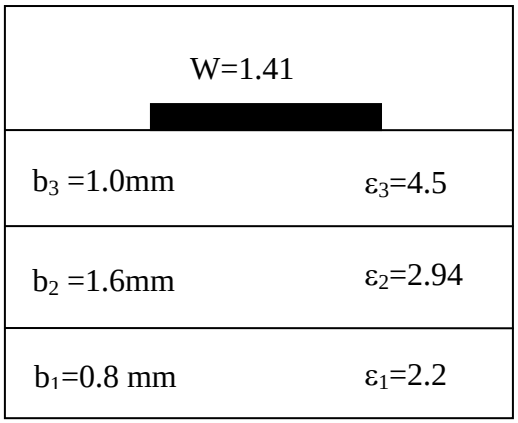

(a) General layout of three layered microstrip line

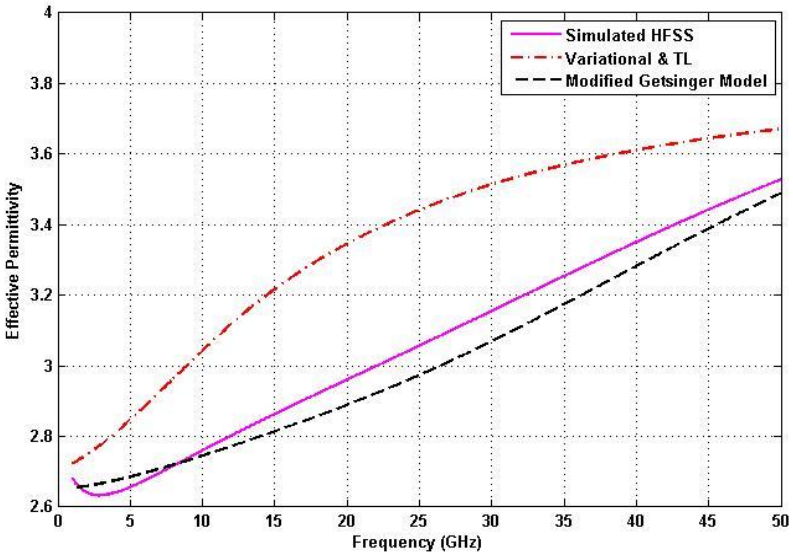

(b) Dispersion of Effective Permittivity

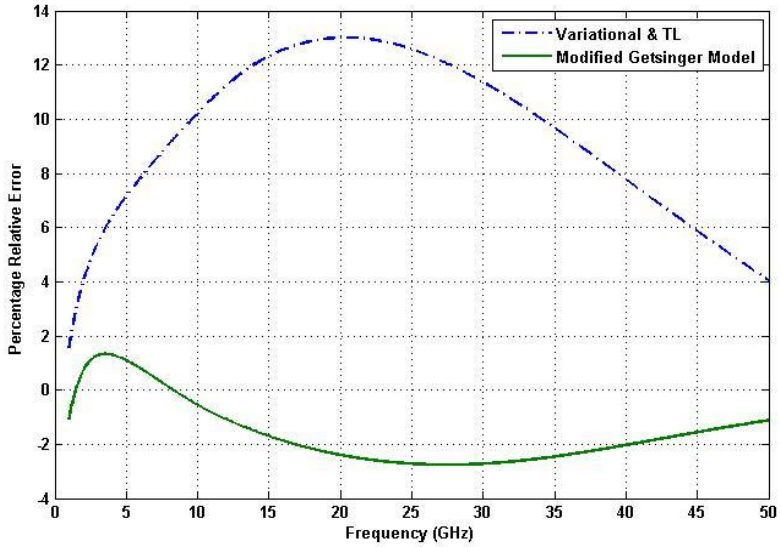

(c) Percentage Relative Error

Figure A.19 : (a) Layout of three layered microstrip line for case-IV (b) dispersion of effective permittivity and (c) percentage relative error

(c) Case V: A three layer microstripline with thickness 1.41 mm and substrate thicknesses and permittivity as shown in Figure A 20. In this case both the relative permittivity and the thickness of the substrate layer is increasing from top to bottom.

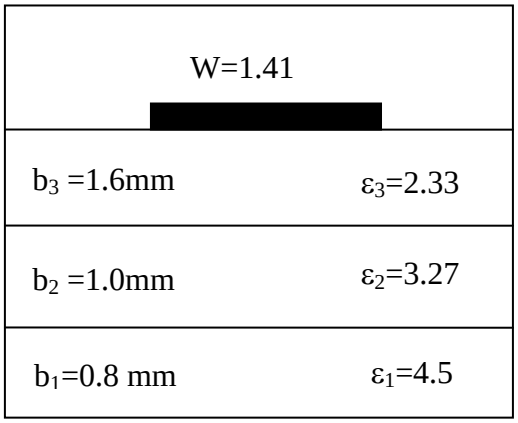

(a) General layout of three layered microstrip line

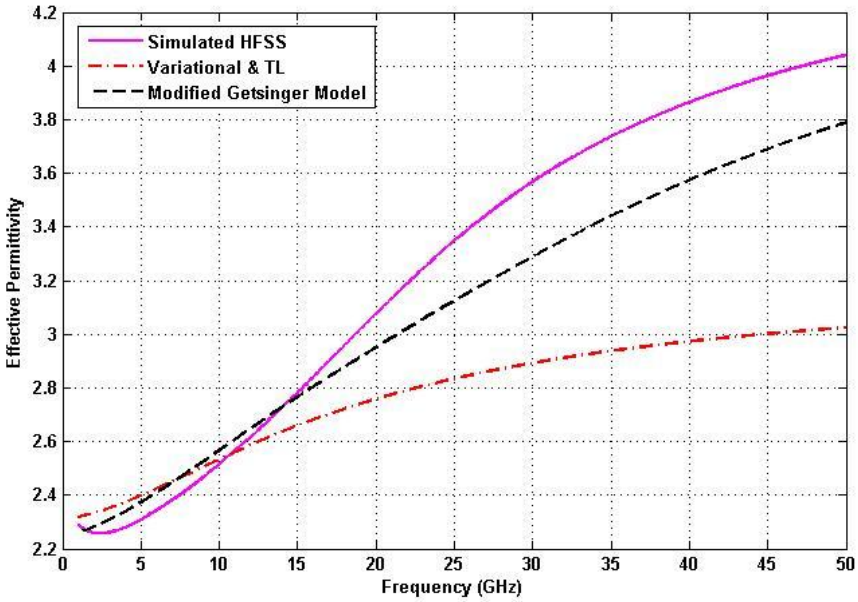

(b) Dispersion of Effective Permittivity

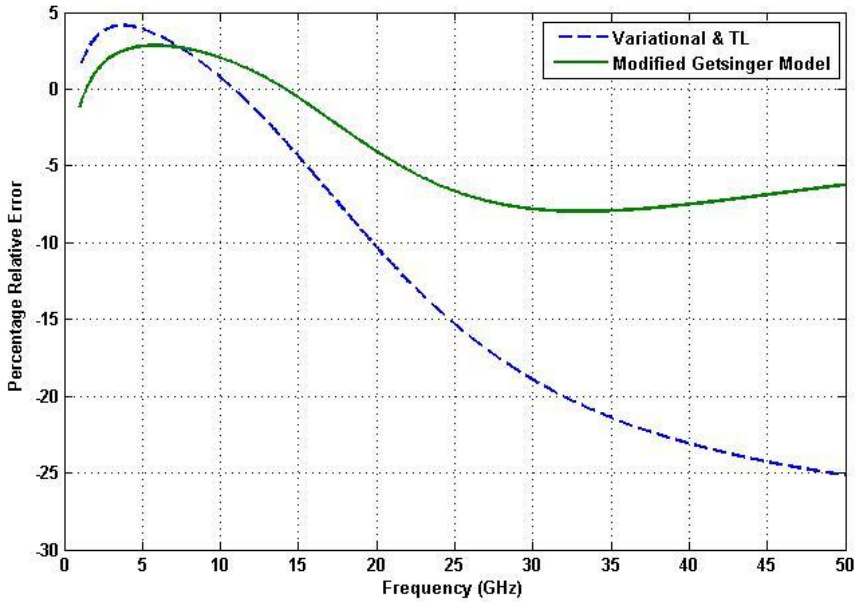

(c) Percentage Relative Error

Figure A.20 : (a) Layout of three layered microstrip line for case-V (b) dispersion of effective permittivity and (c) percentage relative error

A.5.2 Alternative Approach

As stated before, transcendental equations of the type (A.34) can be solved directly. The advantage of this approach is that we do not need to

approximate hyperbolic tangent functions and is therefore relatively more accurate.

In equation (A.34), the propagation constants are substituted from equations (A.38), (A.39) and (A.40). Further, in accordance with [25, 26] the characteristic impedance of the layers are also substituted in the equation as indicated below

$$\frac{\gamma_1\gamma_2}{\epsilon_1\epsilon_2}\tanh\gamma_1 b_1 + \frac{\gamma_1\gamma_3}{\epsilon_1\epsilon_3}\tanh\gamma_1 b_1 \tanh\gamma_2 b_2 \tanh\gamma_3 b_3 + \frac{\gamma_2\gamma_3}{\epsilon_2\epsilon_3}\tanh\gamma_3 b_3 + \frac{\gamma_2^2}{\epsilon_2^2}\tanh\gamma_2 b_2 = 0 \quad \text{(A.44)}$$

which translates into the following transcendental equation

$$\begin{aligned}&\epsilon_3\epsilon_2\sqrt{(\epsilon_s-\epsilon_1)(\epsilon_s-\epsilon_2)}\tanh\left(k_0 b_1\sqrt{(\epsilon_s-\epsilon_1)}\right)\\&+\epsilon_2^2\sqrt{(\epsilon_s-\epsilon_1)(\epsilon_s-\epsilon_3)}\tanh\left(k_0 b_1\sqrt{(\epsilon_s-\epsilon_1)}\right)\tanh\left(k_0 b_2\sqrt{(\epsilon_s-\epsilon_2)}\right)\tanh\left(k_0 b_3\sqrt{(\epsilon_s-\epsilon_3)}\right)\\&+\epsilon_1\epsilon_2\sqrt{(\epsilon_s-\epsilon_2)(\epsilon_s-\epsilon_3)}\tanh\left(k_0 b_3\sqrt{(\epsilon_s-\epsilon_3)}\right)+\epsilon_1\epsilon_3\,(\epsilon_s-\epsilon_2)\tanh\left(k_0 b_2\sqrt{(\epsilon_s-\epsilon_2)}\right)=0\end{aligned} \quad \text{(A.45)}$$

Solving for ϵ_s and applying the physically feasible value of ϵ_s to Getsinger's LSE model provides the dispersion of effective permittivity for a three layered microstrip line structure.

A.6 'n' layered Getsinger's LSE Model for Dispersion of permittivity in Microstriplines

The 'n' layered Getsinger LSE model could be developed based on the previously described method. This implies recursively applying the transmission line equations for obtaining the transcendental equation. The strategy for extending the LSE model to a 'n' layered dielectric microstrip line is outlined in the following

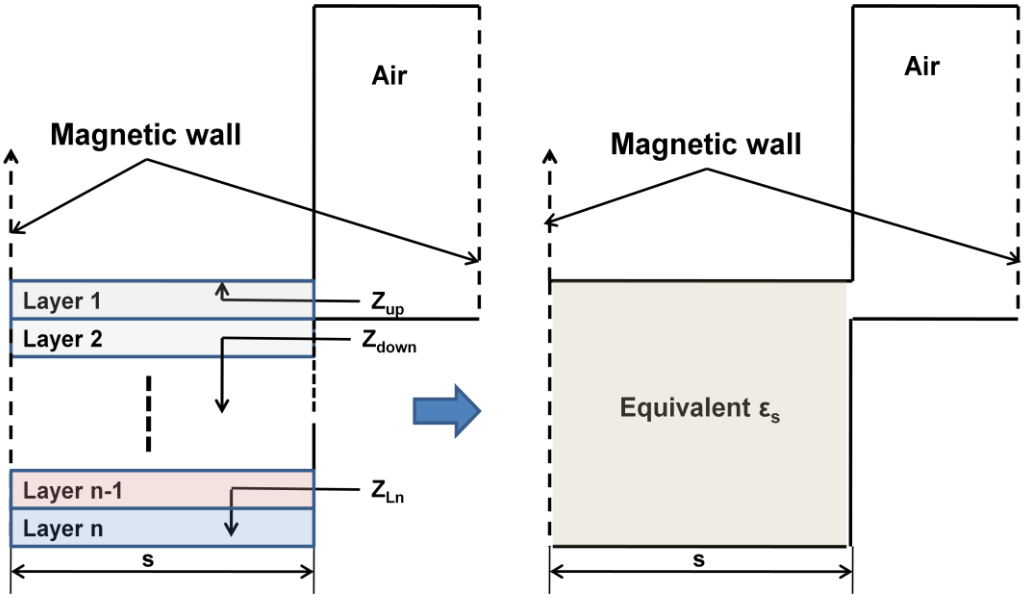

Figure A.21 : 'n'-layer Getsinger's LSE model

Similarly, as in the previous analysis, the TR method is applied to obtain the transcendental equation. Hence, since

$$Z_{up} = Z_{01} \tanh \gamma_1 b_1 \tag{A.46}$$

$$Z_{down} = Z_{02} \left[\frac{Z_L + Z_{02} \tanh \gamma_2 b_2}{Z_{02} + Z_L \tanh \gamma_2 b_2} \right] \tag{A.47}$$

$$Z_{Ln} = Z_{0n} \tanh \gamma_n b_n \tag{A.48}$$

$$Z_{Ln-1} = Z_{0n-1} \left[\frac{Z_{Ln} + Z_{0n-1} \tanh \gamma_{n-1} b_{n-1}}{Z_{0n-1} + Z_{Ln} \tanh \gamma_{n-1} b_{n-1}} \right] \tag{A.49}$$

$$Z_{Ln-1} = Z_{0n-1} \left[\frac{Z_{0n} \tanh \gamma_n b_n + Z_{0n-1} \tanh \gamma_{n-1} b_{n-1}}{Z_{0n-1} + Z_{0n} \tanh \gamma_n b_n \tanh \gamma_{n-1} b_{n-1}} \right] \tag{A.50}$$

These equations need to be applied recursively and finally the transcendental equation is obtained from

$$Z_{up} + Z_{down} = 0 \tag{A.51}$$

To solve the transcendental equation the conditions mentioned in section A.3 are applied. The equations on the relationship between propagation constant and dielectric constant are applied prior to solving the 'n' dimensional polynomial of ϵ_s ; which are

$$\gamma_s^2 = -k_0^2 \epsilon_s \tag{A.52}$$

$$\gamma_i^2 = k_0^2(\epsilon_s - \epsilon_i) \text{where } i = [1, n] \tag{A.53}$$

Only valid and physically possible solutions of ϵ_s are considered for finding the effective permittivity ϵ_e of the 'n' layered microstrip line structure. It is also important to notice, that this generalisation is valid only for the case$|\gamma_i b_i| \ll 1$; for $i = 1,2,3 \ldots \ldots n$. The ϵ_s obtained from the transcendental equation (A.51) can be substituted into Getsinger's equation at (A.4). It may be conjectured here that the transcendental equation would be a 'n' degree polynomial of ϵ_s, with coefficients as function of frequency, layer thickness and permittivity.

A.7 Conclusions

In this Appendix, the Getsinger model has been modified for multilayered microstrip line structures. The results presented for two and three-layered microstrip lines indicate better performance in comparison to other models or approaches (such as UDM). In the case of two-layered microstrip line, it was empirically found that the results were generally within 4% to 15% (depending on the permittivity of the substrates, their thicknesses and their arrangement) error for the modified Getsinger model, against other approaches where the errors were in excess of 9% in the lower side and above 30% on the higher side. Similar results were obtained for three-layered microstrip line and it was shown that the modified Getsinger model gave results within a typical error margin of 5 to 10%, against other approaches where the errors were within 15% to 35%. The modified Getsinger's model therefore provides a good starting approach for solving multilayered microstrip line problems. This would help in expediting electro-magnetic solution for such problems.

This approach would be very useful while designing multilayered reconfigurable planar antenna using CPs. CPs in these reconfigurable antennas would transition from highly conductive state (metallic) to an insulator or dielectric state. The permittivity of the CP would change from a negative value to a positive value. As a consequence of which the overall effective permittivity of the antenna structure would change and affect the antenna's performance.

References

[1] T. Itoh and R. Mittra, "Spectral Domain approach for calculating the dispersion characteristics of microstrip lines," *IEEE Transactions on Microwave Theory and Techniques,* vol. 21, pp. 496-499, 1973.

[2] T. Itoh and R. Mittra, "A Technique for computing dispersion characteristics of Shielded Microstripline," *IEEE Transactions on Microwave Theory and Techniques,* pp. 896-898, 1974.

[3] R. H. Jansen, "A novel CAD tool and concept compatible with the requirement of multilayer GaAs MMIC technology," *IEEE MTT-S Microwave Symposium Digest,* pp. 711-714, 1985.

[4] D. Jackson and N. Alexopoulos, "Analysis of planar strip geometries in a substrate-superstrate configuration," *IEEE Transactions on Antennas and Propagation,* vol. 34, pp. 1430-1438, Dec. 1986.

[5] H. Pues and A. R. Van de Capelle, "Approximate Formulas For Frequency Dependence of Microstrip Parameters," *Electronics letters,* vol. 16, pp. 870-871, 1980.

[6] E. Kuester and D. Chang, "An Appraisal of Methods for Computation of the dispersion characteristics of open Microstrip," *IEEE Transactions on Microwave Theory and Techniques,* vol. 27, pp. 691-694, 1979.

[7] W. J. Getsinger, "Micristrip Dispersion Model," *IEEE Transactions on Microwave Theory and Techniques,* vol. 21, pp. 34-39, 1973.

[8] T. Edwards and R. Owens, "2-18 GHz Dispersion Measurements on 10-100 Ohm Microstriplines on Saphire," *IEEE Transactions on Microwave Theory and Techniques,* vol. 24, pp. 506-513, Aug. 1976.

[9] M. Kirschning and R. H. Jansen, "Accurate model for effective dielectric constant of microstrip with validity up to millimeter wave frequencies," *Electronics Letters,* vol. 18, pp. 272-273, 1982.

[10] E. Yamashita and R. Mittra, "Variational Method for the Analysis of Microstrip Lines," *IEEE Transactions on Microwave Theory and Techniques,* vol. 16, pp. 251-256, April 1968.

[11] E. Yamashita, "Variational Method for the Analysis of Microstripline-like Transmission Lines," *IEEE Transactions on Microwave Theory and Techniques,* vol. 16, pp. 529-535, Aug. 1968.

[12] E. Yamashita and K. Atsuki, "Stripline with Rectangular Outer Conductor and Three Dielectric Layers," *IEEE Transactions on Microwave Theory and Techniques,* vol. 18, pp. 238-244, May 1970.

[13] Y. Chang and I. C. Chang, "Simple Method For the Variational Analysis of A Generalised N-Dielectric Layer Transmission Line," *Electronics letters,* vol. 6, 1970.

[14] R. Crampagne, *et al.*, "A Simple Method for Determining the Green's Function for a Large Class of MIC Lines Having Multilayered Dielectric Structures," *IEEE Transactions on Microwave Theory and Techniques,* vol. 26, pp. 82-87, Feb. 1978.

[15] K. B. Khalid and A. H. Shaari, "Analysis of Multilayered Microstrip and Its Application for Designing Microstrip Moisture Sensor," *ICSE 2000 Proceedings,* pp. 207-216, Nov. 2000.

[16] Y. J. Yoon and B. Kim, "A New Formula for effective Dielectric Constant in Multi-Dielectric Layer Microstrip Structure," *IEEE Conference on Electrical Performance of Electronic Packaging,* pp. 163-167, 23-25 Oct. 2000.

[17] J. Svacina, "Analysis of Multilayer Microstriplines by a Conformal Mapping Method," *IEEE Transactions on Microwave Theory and Techniques,* vol. 40, pp. 769-772, Apr. 1992.

[18] A. K. Verma and G. H. Sadr, "Unified Dispersion Model for Multilayer Microstrip Line," *IEEE Transactions on Microwave Theory and Techniques,* vol. 40, pp. 1587-1591, 1992.

[19] A. K. Verma and R. Kumar, "A New Dispersion Model for Microstrip Line," *IEEE Transactions on Microwave Theory and Techniques,* vol. 46, pp. 1183-1187, Aug. 1998.

[20] H. A. Wheeler, "Transmission-Line Properties of Parallel Strips Separated by Dielectric Sheet," *IEEE Transactions on Microwave Theory and Techniques,* vol. 13, pp. 172-185, Mar 1964.

[21] H. A. Wheeler, "Transmission Line Properties of a Strip on a Dielectric Sheet on a Plane," *IEEE Transactions on Microwave Theory and Techniques,* vol. 25, pp. 631-647, Aug. 1977.

[22] M. Schneider, "Microstrip lines for microwave integrated circuits," *Bell Systems Technical Journal,* vol. 48, May 1969.

[23] R. E. Collin, *Field Theory of Guided Waves*, 2nd ed. New York: IEEE Antennas and Propagation Society, 1991.

[24] N. Marcuvitz, *Waveguide Handbook*. London: P. Peregrinus on behalf of the Institution of Electrical Engineers, 1986.

[25] X. Shanjia and M. Zhewang, "Network Analysis of Eigenvalue Problem for Multilayer Dielectric Wave guide Consisting of Arbitrary Number of layers," *International Journal of Infrared and Millimeter Waves*, vol. 9, Apr. 1988.

[26] H. Hasegawa, *et al.*, "Properties of microstrip line on Si-SiO_2 system," *IEEE Transactions on Microwave Theory and Techniques*, vol. MTT-19, pp. 869-881, Nov. 1971.

[27] E. O. Hammerstad and T. H. Norges, *Microstrip Handbook*. Trondheim: Norwegian Institute of Technology, 1985.

[28] M. Kirschning and R. H. Jansen, "Accurate Model for Effective Dielectric Constant of Microstrip with Validity up to Millimeter-wave Frequencies," *Electronics letters*, vol. 18, pp. 272-273, 18 March 1982.

Appendix-B

Results of 4.5 GHz PPy Patch Antenna

B.1 S11 Measurements

In this appendix result of 4.5 GHz PPy patch antennas of different patch thicknesses is presented. The results presented below highlight the importance of patch thickness towards good antenna performance. In addition they also show that reasonable antenna performance is possible at patch thicknesses less than a skin depth.

PPy-Patch antenna

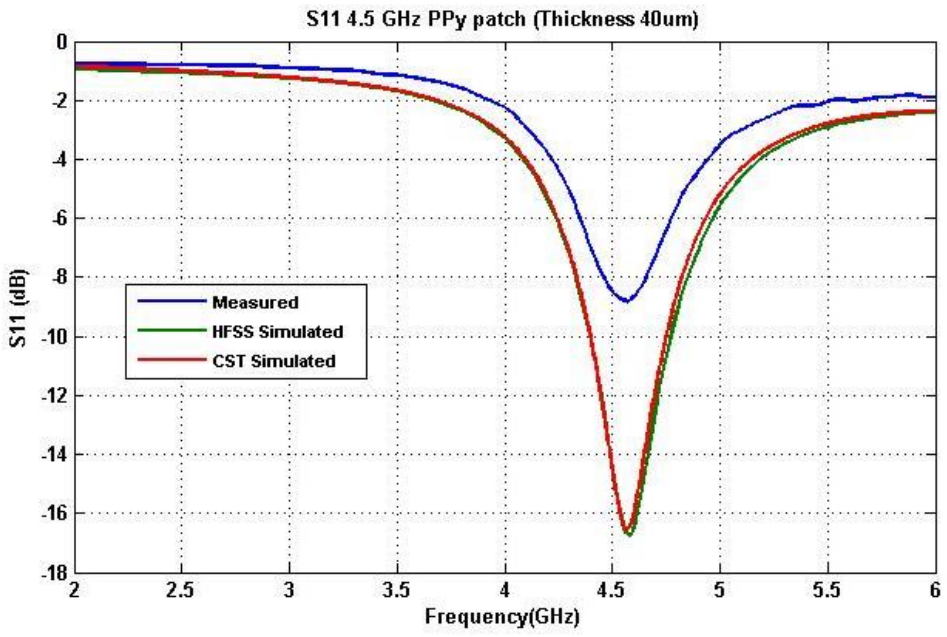

Figure B.1: S11 measurement for 40 µm thick PPy patch antenna at 4.5 GHz

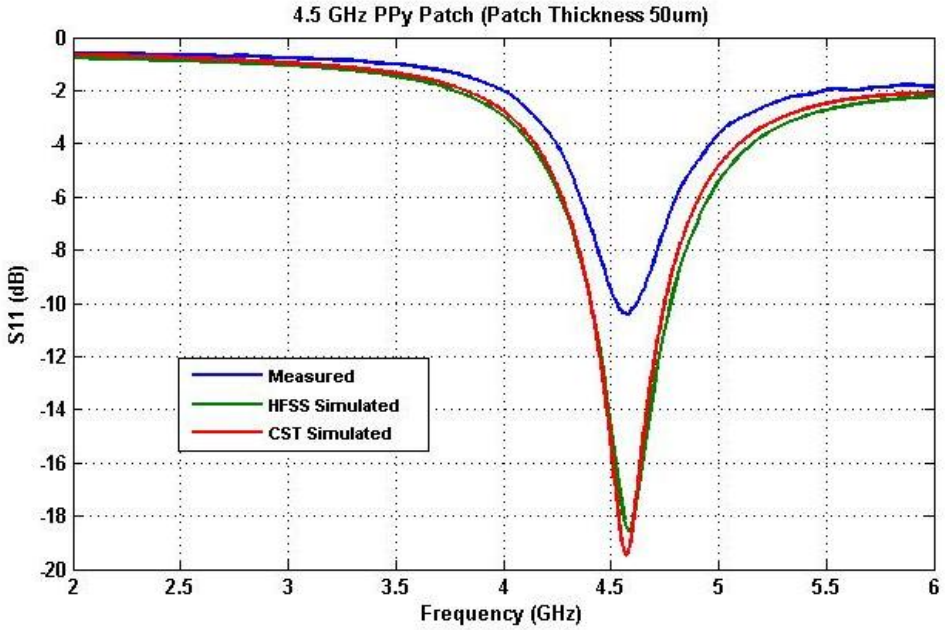

Figure B.2: S11 measurement for 50 µm thick PPy patch antenna at 4.5 GHz

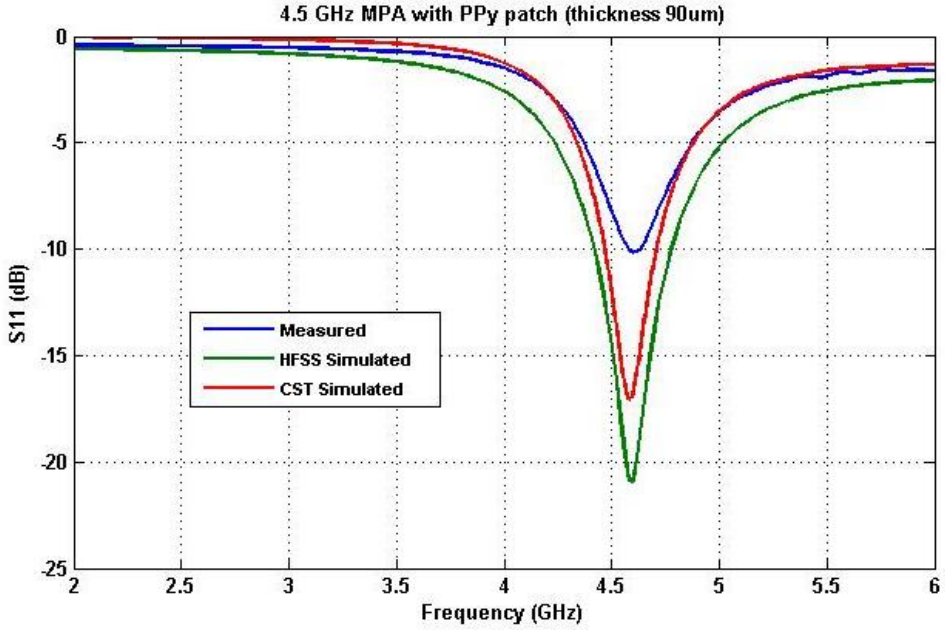

Figure B.3: S11 measurement for 90 µm thick PPy patch antenna at 4.5 GHz

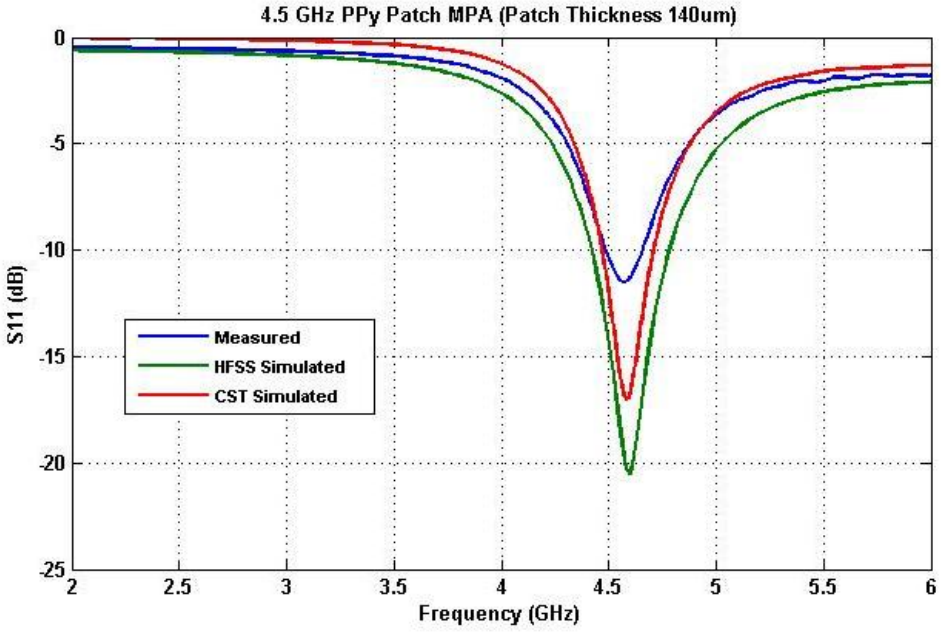

Figure B.4: S11 measurement for 140 µm thick PPy patch antenna at 4.5 GHz

B.2 Radiation Pattern Measurements

Cu-Patch antenna

In Figure B.5 the E-plane Co-polarisation radiation measurements of copper patch antenna are presented along with its simulated measurements.

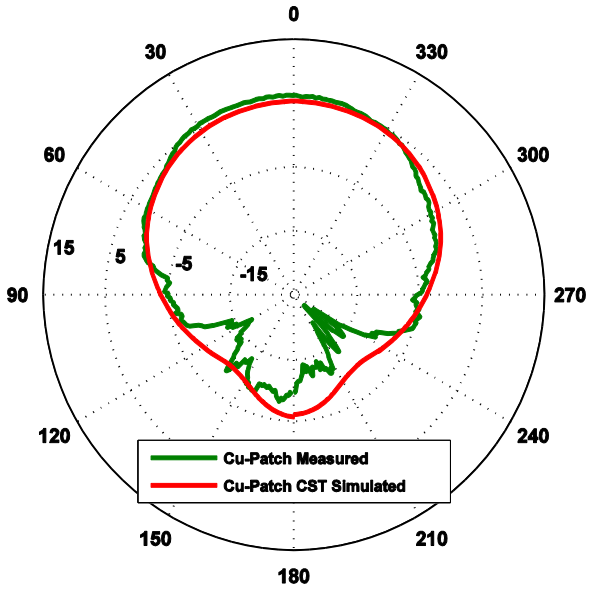

Figure B.5: 4.5 GHz Copper patch E-Copol measurements and simulation results

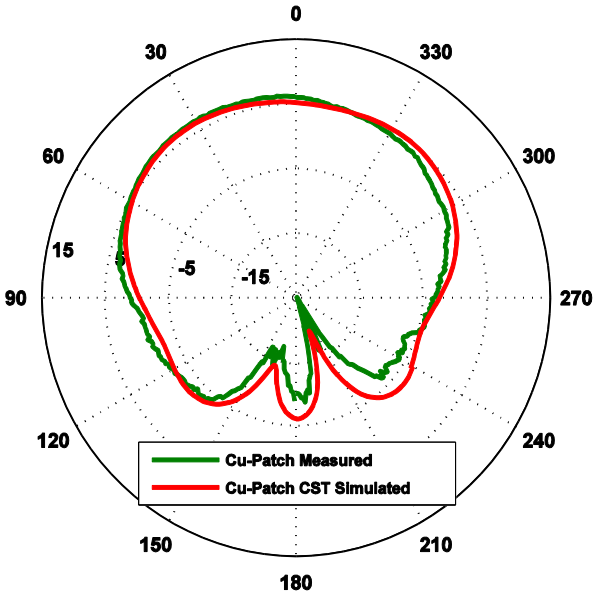

Figure B.6: 4.5 GHz Copper patch H-Copol Measurements and simulation results

Similarly Figure B.6 presents the H-plane Co-polarisation measurements and simulation results of the copper patch antenna.

PPy-Patch Antennas

Figure B.7 indicates the E-plane Co-polarisation radiation measurements and simulation results of PPy patch antenna with patch thickness of 40 µm. Similarly Figure B.8 presents the H-plane Co-polarisation measurements and simulation results of the PPy patch antenna (40 µm). Similar radiation plots are shown in subsequent Figures for different thicknesses of the PPy patches.

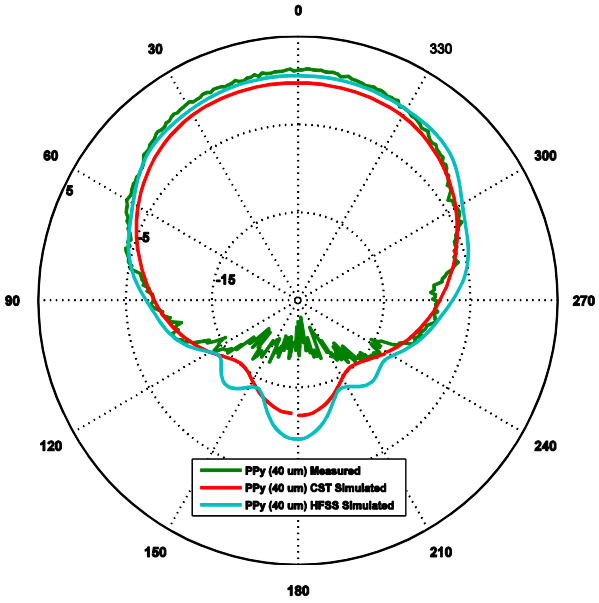

Figure B.7: 4.5 GHz PPy (40 µm) patch E-Copol measurements and simulation results

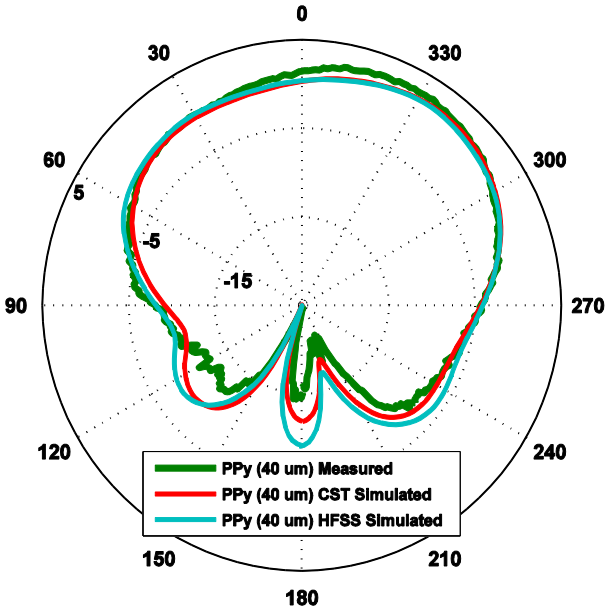

Figure B.8: 4.5 GHz PPy (40 µm) patch H-Copol measurements and simulation results

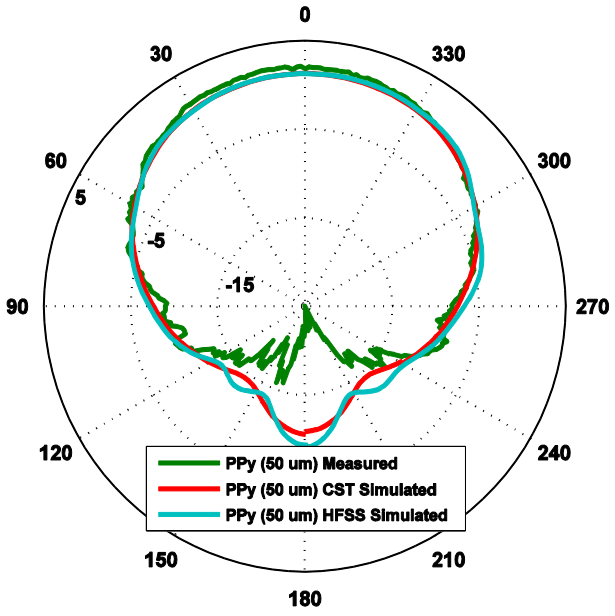

Figure B.9: 4.5 GHz PPy (50 µm) patch E-Copol measurements and simulation results

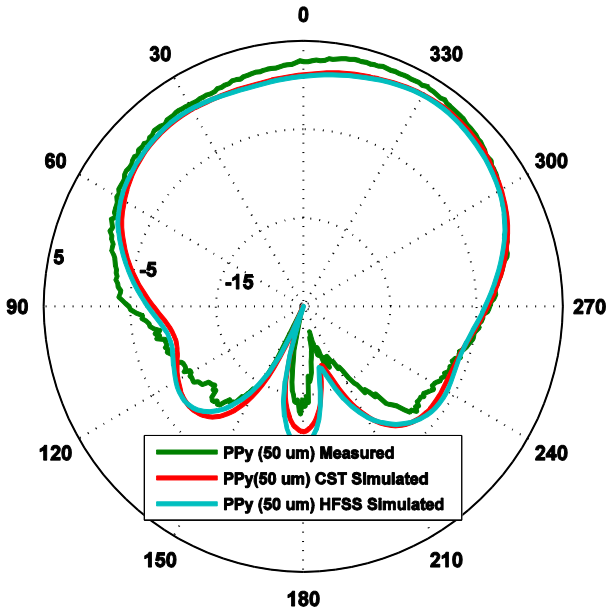

Figure B.10: 4.5 GHz PPy (50 µm) patch H-Copol measurements and simulation results

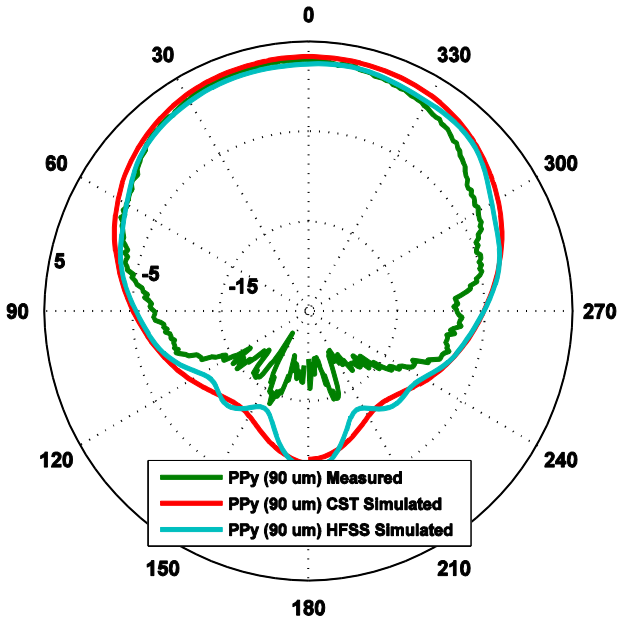

Figure B.11: 4.5 GHz PPy (90 µm) patch E-Copol measurements and simulation results

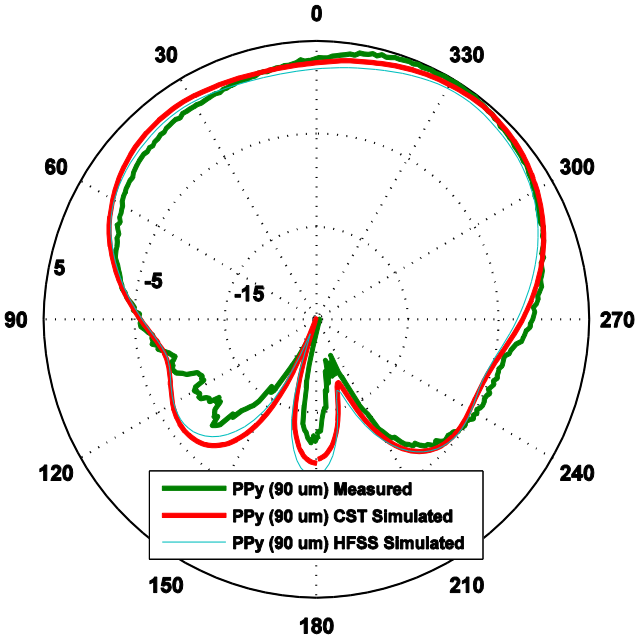

Figure B.12: 4.5 GHz PPy (90 µm) patch H-Copol measurements and simulation results

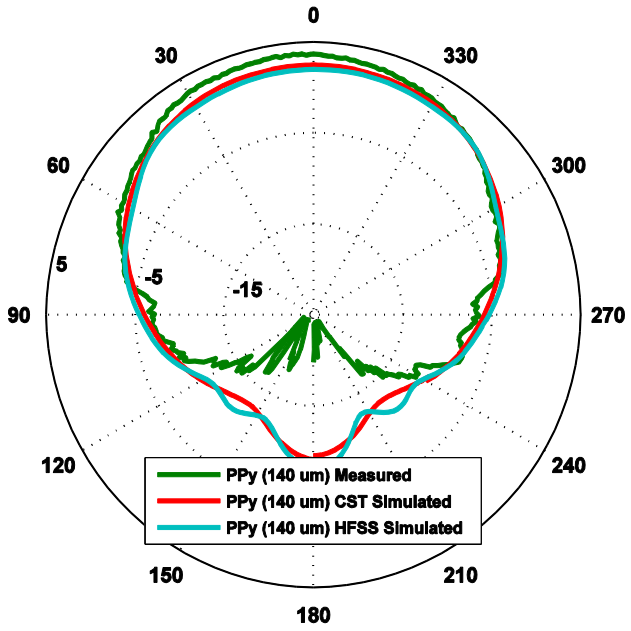

Figure B.13: 4.5 GHz PPy (140 µm) patch E-Copol measurements and simulation results

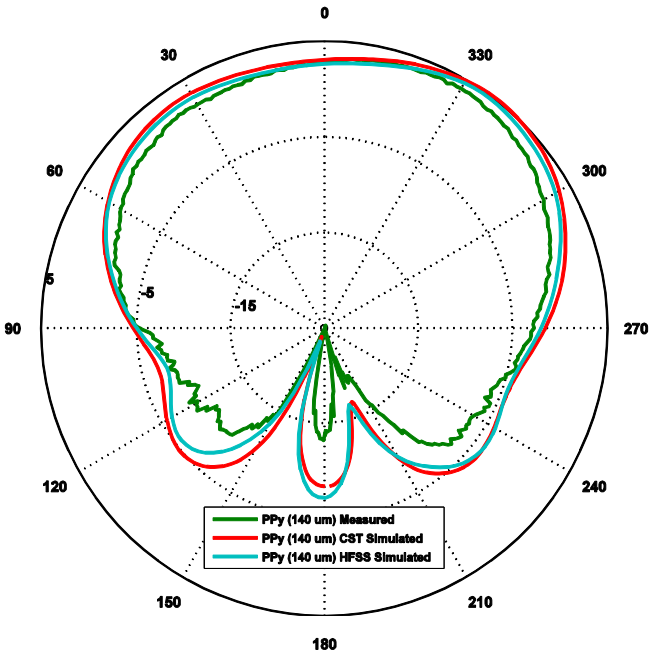

Figure B.14: 4.5 GHz PPy (140 µm) patch H-Copol measurements and simulation results

Appendix-C

Data Sheets

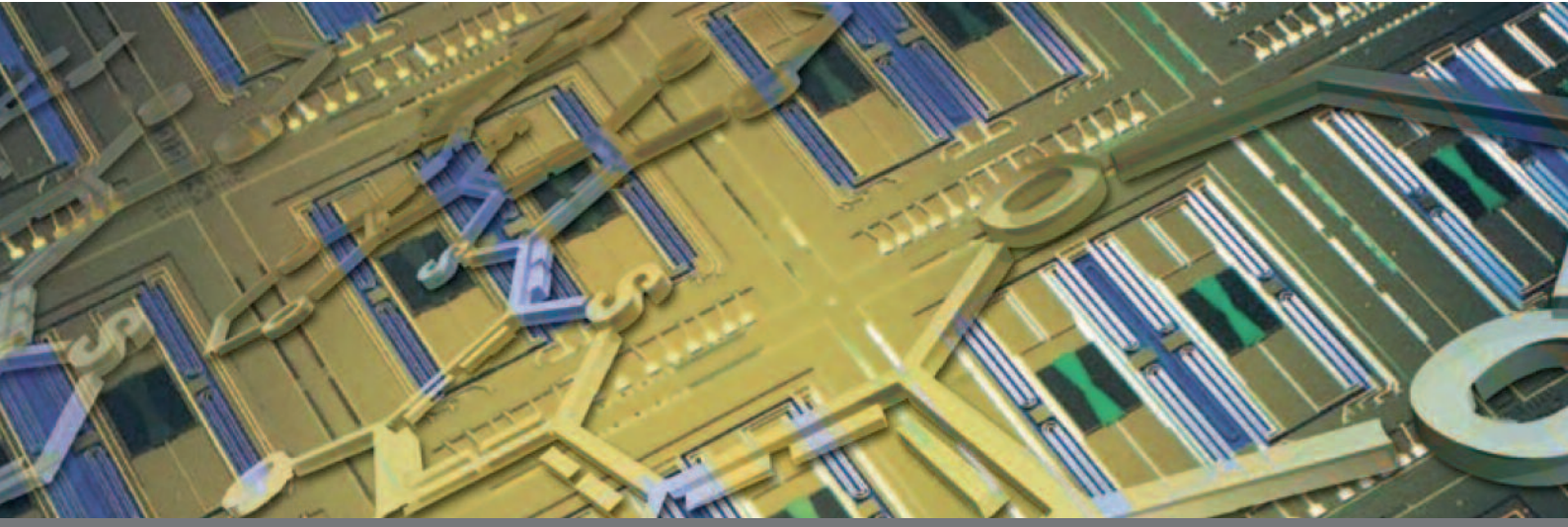

Materials | Development | Solutions

CLEVIOS™ P Jet HC and P Jet N

Inkredible!

CLEVIOS™ **P Jet HC** and ***CLEVIOS***™ **P Jet N** are based on PEDOT / PSS – chemistry for electronic applications. The unique properties of this polymer, providing both conductivity and transparency, allow a range of novel and technically advanced applications.

CLEVIOS™ **P Jet HC** has been specially formulated for use in inkjet applications where higher conductivity is required. ***CLEVIOS***™ **P Jet N** is a pH neutralized version for pH sensitive printheads and substrates.

CLEVIOS™ **P Jet HC** and ***CLEVIOS***™ **P Jet N** can be used directly or be further formulated in combination with solvents or binders, then applied by inkjet to various surfaces, such as Polycarbonate, PS or PET.

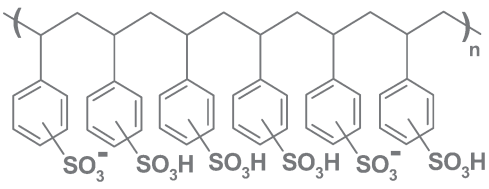

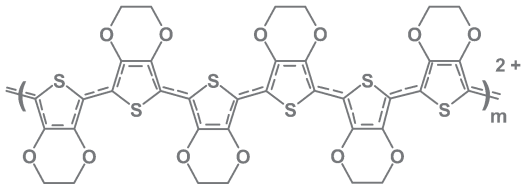

Application:

For use as conductive lines and contact electrodes on flexible plastic electronics.

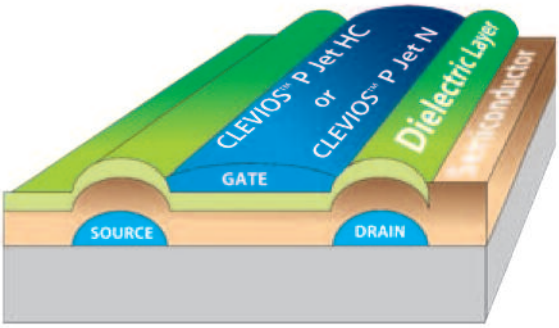

Physical Characteristics:

		CLEVIOS™ P Jet HC		*CLEVIOS*™ P Jet N	
	Unit	Min	Max	Min	Max
Viscosity	mPas (700 sec^{-1})*	15	25	8	18
Conductivity	S/cm	50	90	30	90
Solids Content	%	1.8	2.2	0.6	1.0
pH Value	—	2	3	5	8

****CLEVIOS***™ **P Jet HC** and ***CLEVIOS***™ **P Jet N** can be diluted with a mixture of 80:20 water and ethanol (w/w) to reduce viscosity.

Quality:

Heraeus provides batch specific technical analysis to maintain conductivity and transparency caracteristics.

Heraeus' other development products for TFTs:

For Printable Electronics

Dendritic oligothiophenes, Hex-4T-Hex (see Kirchmeyer et al Adv. Functional Mat. 2003, 13,591)

For Evaporation Processes

Oligothiophenes such as Hex-6T-Hex and Dec-6T-Dec (see Kirchmeyer et al., Advanced Materials 2003, 15,917)

Heraeus

Europe

Heraeus Clevios GmbH
CHEMPARK Leverkusen, Building B 202
51368 Leverkusen,
Germany
John Bayley
T +49 (214) 30-26718
F +49 (214) 30-56284
john.bayley@heraeus.com

North America

Heraeus Materials Technology LLC
24 Union Hill Road
W. Conshohocken PA 19428
USA
Dr. Ron Lubianez
T +1 (617) 828 4478
F +1 (610) 825 70 61
ron.lubianez@heraeus.com

Asia

Heraeus K.K.
5-1 Nibancho, Chiyoda-ku
102-0084 Tokyo
Japan
Tetsuya Suzuki
T +81 (3) 521539-22
F +81 (3) 521539-21
tetsuya.suzuki@heraeus.com

Heraeus Materials Korea Ltd
#813, Kolon Digital Tower Villant II
222-8, Guro 3 dong, Guro-gu
Seoul, 152-727
Korea
Gihong Park
T +82 (2) 865-0950
F +82 (2) 865-0951
gihong.park@heraeus.com

(Responsible for Hong Kong, Taiwan and S.E. Asia)

Heraeus Materials Technology Shanghai Ltd.
No. 1 Guangzhong Road, Minhang District
201108 Shanghai
China
Harry Zhu
T +86 (21) 3357-5688
F +86 (21) 3357-5699
harry.zhu@heraeus.com

Heraeus Ltd.
30 On Chuen Street, On Lok Tsuen
Hong Kong
China (Hongkong)
Emily Shu
T +(852) 2675-1200
F +(852) 2682-3220
emily.shu@heraeus.com

Heraeus Clevios GmbH

CHEMPARK Leverkusen
Building B 202
51368 Leverkusen
Germany

T +49 (214) 30-1

clevios@heraeus.com

www.clevios.com
www.heraeus.com

Appendix-D

Results of 6 GHz PPy and PEDOT Patch Antennas

D.1 S11 Measurements

In this appendix result of 6 GHz PPy and PEDOT patch antennas of different patch thicknesses is presented. The results presented below highlight the importance of patch thickness towards good antenna performance. Furthermore, reasonable antenna performance is reported using PEDOT inkjet printed antennas, which could be printed along with low cost inkjet printed electronics circuits.

PPy-Patch antenna

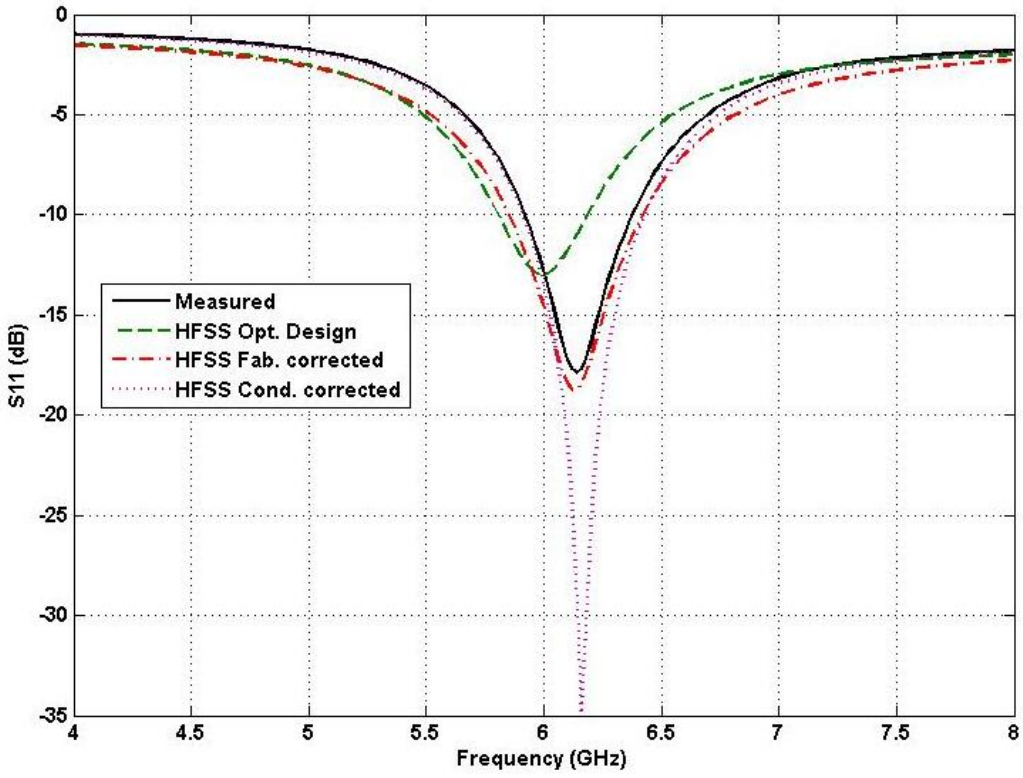

Figure D.1 : S11 measurement and simulation for 50 µm thick PPy patch antenna at 6 GHz

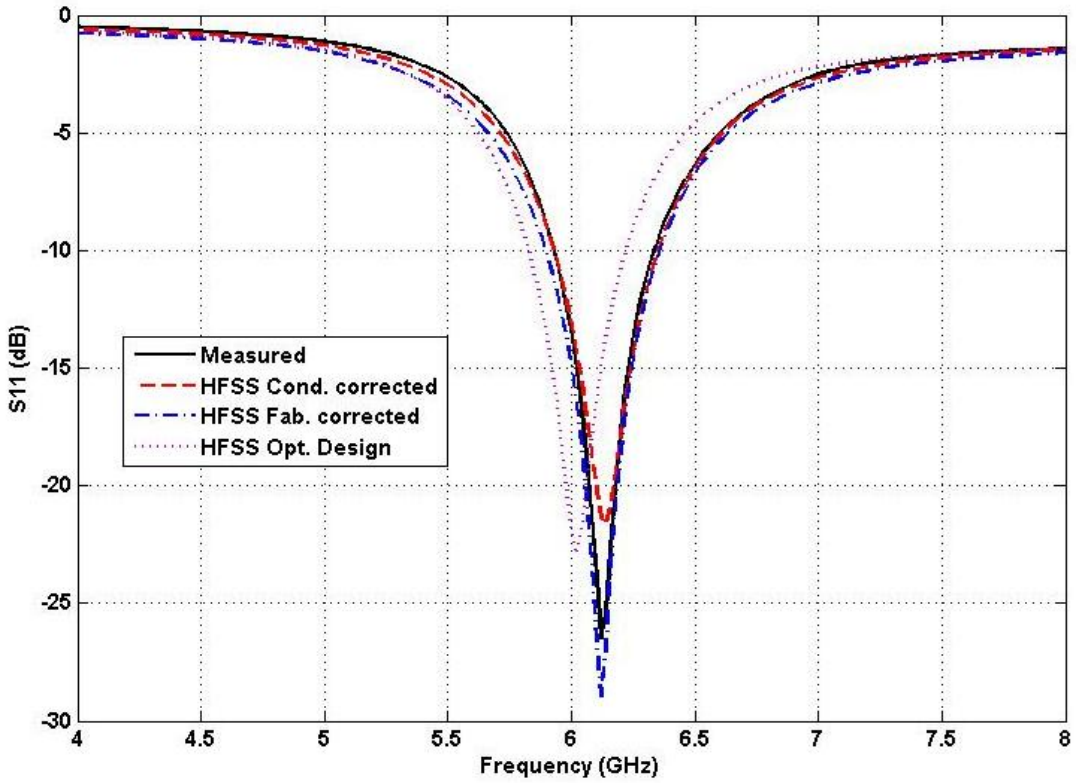

Figure D.2 : S11 measurement and simulation for 140 µm thick PPy patch antenna at 6 GHz

Figure D 1 and D 2 show the PPy antenna design optimisation process and also highlight how noticeable and measureable differences between the simulated patch antenna dimensions and actual antenna were accounted for and corrected. In addition it also shows how a perfect match between the actual measurement and simulation was obtained by adjusting the AC conductivity of the PPy patch.

D.2 Radiation Pattern Measurements

Cu-Patch antenna

Figure D.3 the E-plane Co-polarisation radiation measurements of copper patch antenna are presented along with its simulated measurements.

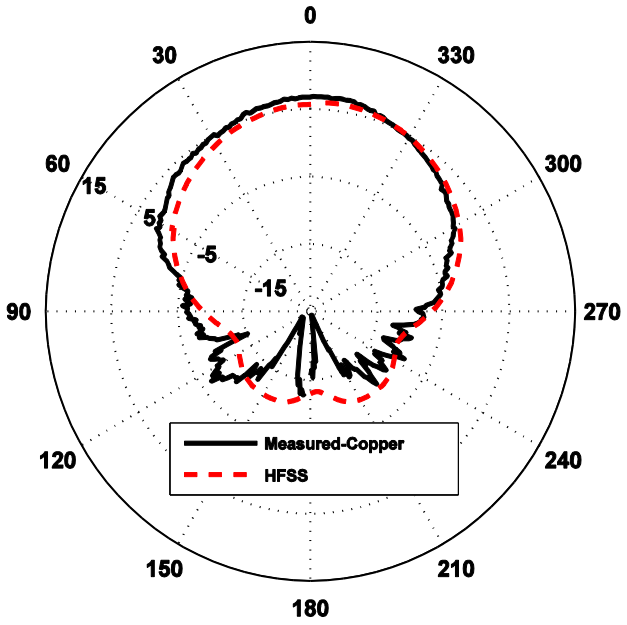

Figure D.3 : 6 GHz E Co-pol measurements and simulation of Copper patch antenna

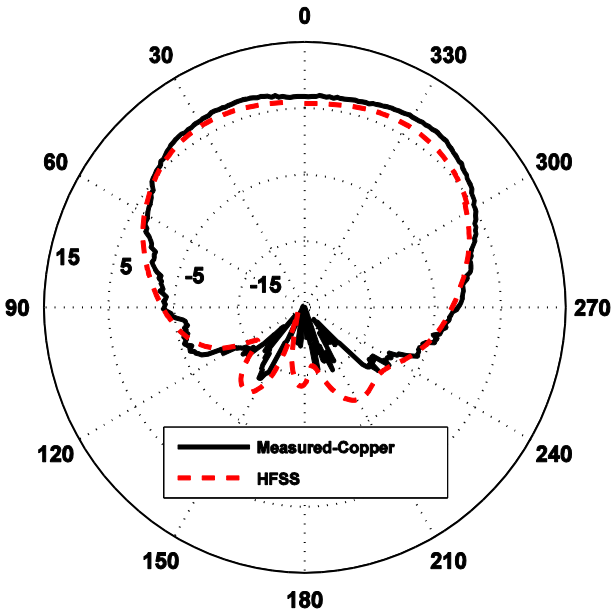

Figure D. 4 : 6 GHz H Co-pol measurements and simulation of Copper patch antenna

Similarly Figure D.4 presents the H-plane Co-polarisation measurements and simulation results of the copper patch antenna.

PPy-Patch Antennas

Figure D.5 indicates the E-plane Co-polarisation radiation measurements and simulation results of PPy patch antenna with patch thickness of 50 µm. Similarly Figure D.6 presents the H-plane Co-polarisation measurements and simulation results of the PPy patch antenna (50 µm). Similar radiation plots are shown in subsequent Figures for different thicknesses of the PPy patches.

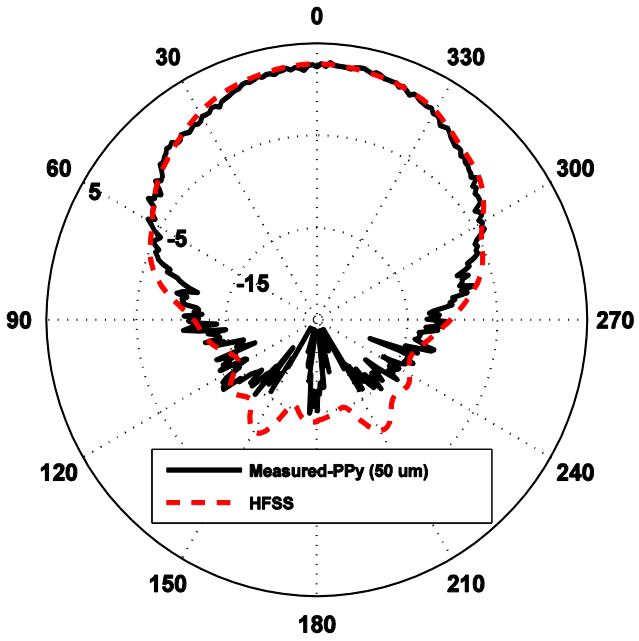

Figure D.5 : 6 GHz E Co-pol measurements and simulation of PPy patch (50 µm thick) antenna

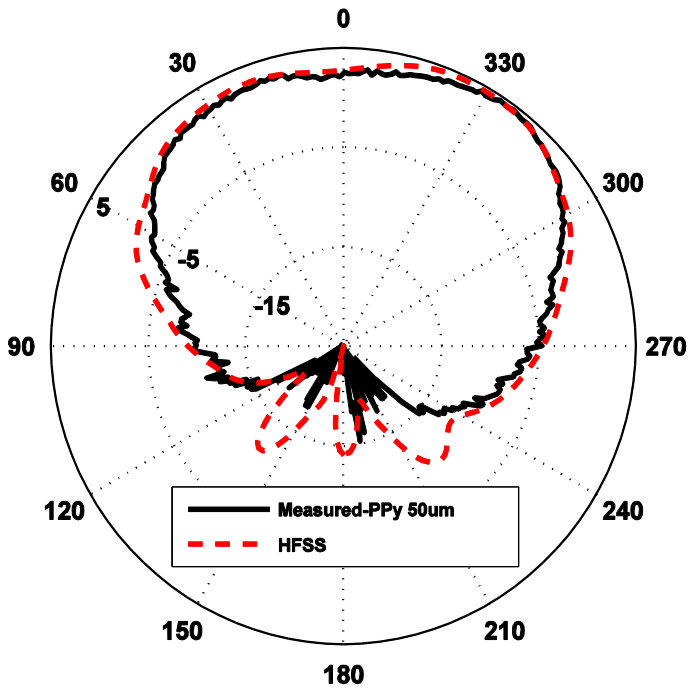

Figure D.6 : 6 GHz H Co-pol measurements and simulation of PPy patch (50 µm thick) antenna

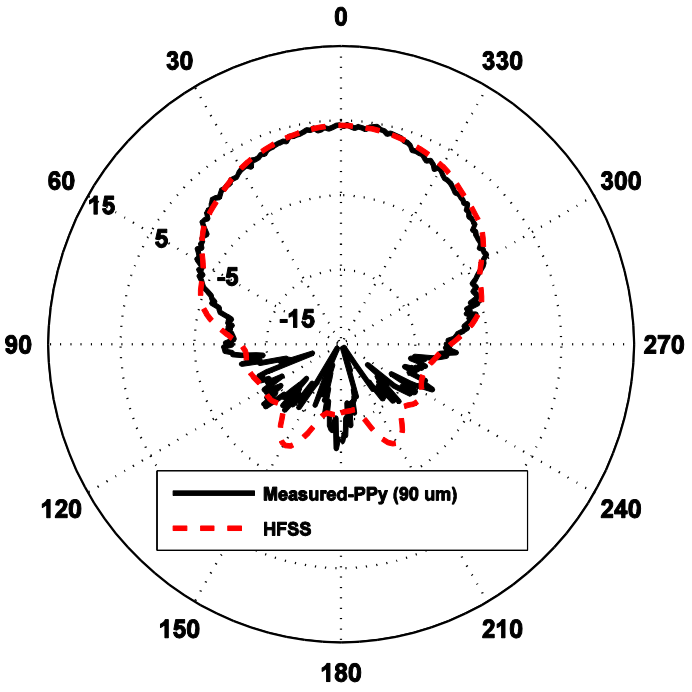

Figure D.7 : 6 GHz E Co-pol measurements and simulation of PPy patch (90 µm thick) antenna

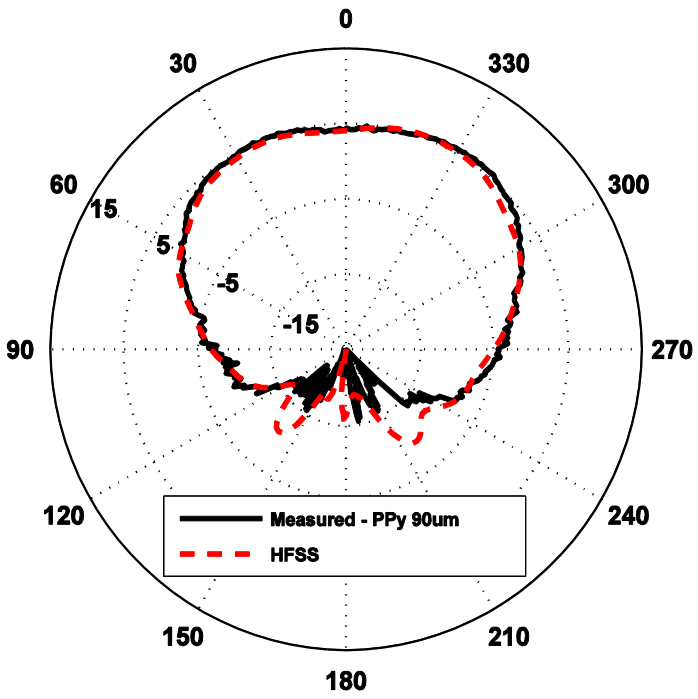

Figure D.8 : 6 GHz H Co-pol measurements and simulation of PPy patch (90 µm thick) antenna

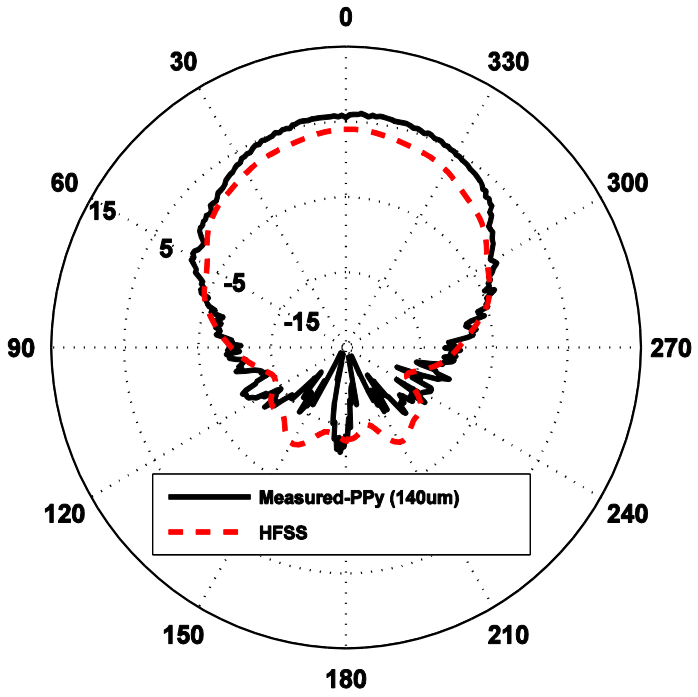

Figure D.9 : 6 GHz E Co-pol measurements and simulation of PPy patch (140 µm thick) antenna

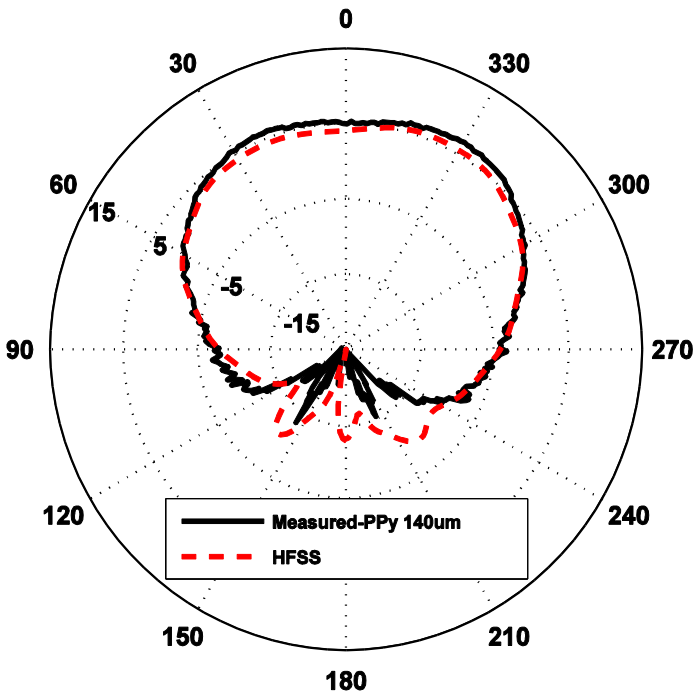

Figure D.10 : 6 GHz H Co-pol measurements and simulation of PPy patch (140 µm thick) antenna

PEDOT-Patch Antennas

Figure D.11 the E-plane Co-polarisation radiation measurements of the printed PEDOT patch antenna are presented along with its simulated measurements.

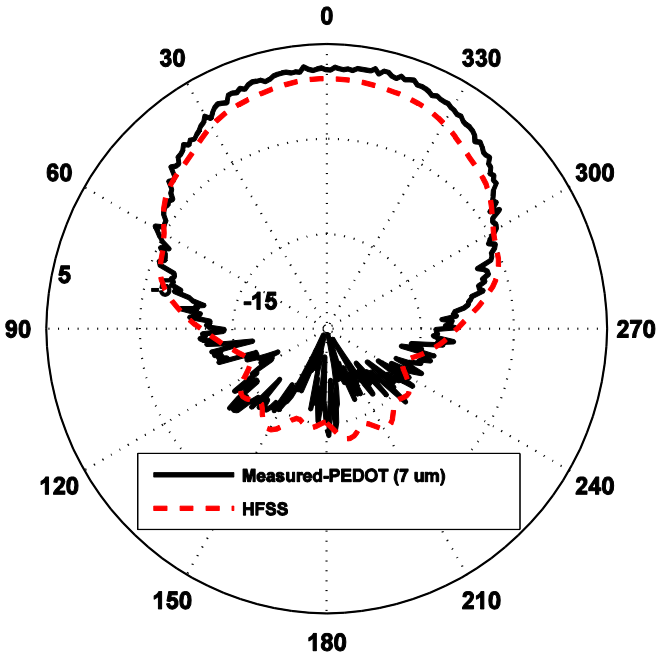

Figure D.11 : 6 GHz E Co-pol measurements and simulation of PEDOT patch antenna

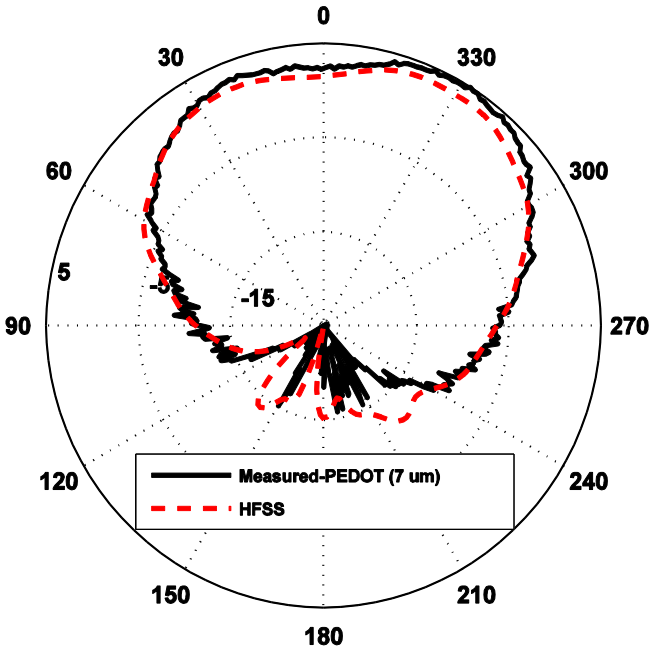

Figure D.12 : 6 GHz H Co-pol measurements and simulation of PEDOT patch antenna

Similarly Figure D.12 presents the H-plane Co-polarisation measurements and simulation results of the printed PEDOT patch antenna.